

UC Berkeley

UC Berkeley Electronic Theses and Dissertations

Title

The melanocortin 4 receptor functions at the neuronal primary cilium to control long-term energy homeostasis

Permalink

<https://escholarship.org/uc/item/2xj6330x>

Author

Bernard, Adélaïde

Publication Date

2021

Peer reviewed|Thesis/dissertation

“The melanocortin 4 receptor functions at the neuronal primary cilium
to control long-term energy homeostasis”

By

Adélaïde Bernard

A dissertation submitted in partial satisfaction of the
Requirements for the degree of
Doctor of Philosophy
in
Metabolic Biology
in the
Graduate Division
of the
University of California, Berkeley

Committee in Charge:

Professor Andreas Stahl, Chair
Professor Christian Vaisse, Co-chair
Professor Suneil Koliwad
Professor Kaoru Saijo
Professor Wally Wang

Spring 2021

Abstract

“The melanocortin 4 receptor functions at the neuronal primary cilium
to control long-term energy homeostasis”

by

Adélaïde Bernard

Doctor of Philosophy in Metabolic Biology

University of California, Berkeley

Professor Andreas Stahl, Chair

The melanocortin 4 Receptor (MC4R) is a central component of the leptin-melanocortin pathway in the hypothalamus. MC4R plays a critical role in the long-term regulation of energy homeostasis and mutations in MC4R are the most common cause of monogenic obesity. However, the precise molecular and cellular mechanisms underlying the maintenance of energy balance within MC4R expressing neurons are unknown. The expression of MC4R in neurons from the Paraventricular Nucleus of the hypothalamus (PVN) has been shown to be both necessary and sufficient to regulate food intake and body weight, and we discovered that MC4R localizes at the primary cilium of those neurons. Primary cilia are unique microtubule-based organelles that protrude from the cell membrane to sense and relay extracellular signals.

In Chapter one, we first mapped the expression of MC4R in the brain, to then determine the extent of MC4R localization at the primary cilia in some of the identified regions. We discovered that, in the PVN, MC4R localization at the primary cilium is dynamic and depends on age and physiological status relayed by MC4R ligands levels. Together, these results shed light on the complex regulation of MC4R bioavailability at the primary cilium.

In Chapter two, we found that cilia were required specifically on MC4R-expressing neurons for the control of energy homeostasis. Moreover, these cilia were critical for pharmacological activators of MC4R to exert an anorexigenic effect. Using a combination of mouse genetic approaches, we demonstrated that MC4R signals via cilia of PVN neurons to control food intake and body weight.

In Chapter three, we demonstrate that the Melanocortin Receptor Associated Protein 2 (MRAP2) is critical for the ciliary localization and weight-regulating function of MC4R.

These findings demonstrate that targeting of MC4R to neuronal primary cilia is essential for the control of long-term energy homeostasis and suggests that genetic disruption of MC4R ciliary localization may frequently underlie inherited forms of obesity.

Table of Contents

ABSTRACT	1
TABLE OF CONTENTS.....	I
TABLE OF FIGURES	IV
DEDICATION	VI
ACKNOWLEDGEMENTS.....	VIII
CHAPTER 0 : GENERAL INTRODUCTION.....	IX
HUMAN OBESITY AND GENETICS.....	IX
MAINTENANCE OF LONG-TERM ENERGY HOMEOSTASIS BY THE LEPTIN-MELANOCORTIN SYSTEM	IX
<i>Leptin and the leptin receptor</i>	<i>ix</i>
<i>Leptin action in the Central Nervous System</i>	<i>x</i>
<i>First order neurons: leptin-sensitive POMC and AgRP-expressing neurons</i>	<i>x</i>
<i>Second order neurons: MC4R-expressing neurons</i>	<i>xi</i>
REGULATION OF ENERGY HOMEOSTASIS BY NEURONAL PRIMARY CILIA.....	XIII
<i>Primary cilia architecture and maintenance</i>	<i>xiii</i>
<i>Examples of primary cilia-mediated functions</i>	<i>xiv</i>
<i>Linking neuronal primary cilia to obesity</i>	<i>xvi</i>
TRANSITION.....	XIX
CHAPTER 1 : MC4R LOCALIZES TO NEURONAL PRIMARY CILIA	1
SUMMARY	1
INTRODUCTION	2
RESULTS	3
<i>Ribosomal trapping of MC4R-GFP enhances signal and allows for neuronal expression mapping</i>	<i>3</i>
<i>Mapping of MC4R-expressing neurons</i>	<i>3</i>
<i>Trapping MC4R on the ribosome leads to obesity, mimicking a MC4R knockout phenotype</i>	<i>4</i>
<i>MC4R ciliary localization mapping</i>	<i>5</i>
<i>MC4R ciliary localization is dynamically regulated and responds to physiological status</i>	<i>5</i>
<i>MC4R ciliary localization depends on leptin and AgRP expression</i>	<i>6</i>
DISCUSSION AND FUTURE DIRECTIONS.....	7
FIGURES	9
METHODS.....	16
<i>Origin of the mouse lines used</i>	<i>16</i>
<i>Stereotaxic Surgeries for i.c.v cannula implantation</i>	<i>16</i>
<i>Mouse metabolism studies</i>	<i>16</i>
<i>Diphtheria toxin injections</i>	<i>16</i>
<i>Direct fluorescence and immunofluorescence studies of mouse hypothalamus</i>	<i>16</i>
<i>Image capture and processing</i>	<i>17</i>
<i>Statistical analysis</i>	<i>17</i>
TRANSITION.....	18
CHAPTER 2 : MELANOCORTIN-4 RECEPTOR SIGNALS AT THE NEURONAL PRIMARY CILIUM TO CONTROL FOOD INTAKE AND BODY WEIGHT	19
SUMMARY	19
INTRODUCTION	20
RESULTS	21

<i>Genetic ablation of primary cilia in MC4R-expressing neurons phenocopies MC4R deficiency.</i>	21
<i>Primary cilia are required for anorexigenic MC4R signaling</i>	22
<i>Adult PVN primary cilia are required for anorexigenic MC4R signaling</i>	23
<i>Adenylyl cyclase signaling in the primary cilia of MC4R-expressing neurons in the adult PVN is essential for controlling food intake and body weight</i>	24
DISCUSSION	24
FIGURES	26
METHODS	36
<i>Origin of the mouse lines used.</i>	36
<i>Generation of MC4R^{pt2aCre/t2aCre} mice.</i>	36
<i>Generation and injections of AAVs</i>	36
<i>Stereotaxic Surgeries.</i>	37
<i>Mouse metabolism studies.</i>	37
<i>Acute food intake studies</i>	37
<i>Direct fluorescence and immunofluorescence studies of mouse hypothalamus.</i>	38
<i>RNA scope</i>	38
<i>Image capture and processing.</i>	39
<i>Tamoxifen-induced recombination.</i>	39
<i>Osmotic stimulation.</i>	39
<i>Hypothalamic RNA and Protein quantification.</i>	39
<i>Statistical analysis</i>	39
TRANSITION	40
CHAPTER 3 MRAP2 REGULATES ENERGY HOMEOSTASIS BY PROMOTING PRIMARY CILIA LOCALIZATION OF MC4R	41
SUMMARY	41
INTRODUCTION	42
RESULTS	42
<i>MC4R neurons require MRAP2 to regulate energy homeostasis</i>	42
<i>MRAP2 promotes MC4R targeting to the primary cilium of IMCD3 cells</i>	43
<i>MRAP2 colocalizes with MC4R at the primary cilium of hypothalamic neurons in vivo</i>	44
<i>MC4R localization to primary cilia requires MRAP2</i>	44
DISCUSSION	45
FIGURES	47
METHODS	59
<i>Cell culture and Transfections</i>	59
<i>Expression plasmids</i>	59
<i>Ciliary expression of MCRs and MRAPs in cultured cells</i>	59
<i>Cell imaging</i>	59
<i>In vivo experiments</i>	59
<i>Animals</i>	59
<i>EUCOMM MRAP2 mice</i>	61
<i>Stereotaxic AAV-injection Surgeries.</i>	61
<i>Brain imaging</i>	61
<i>Microscopy</i>	62
<i>Image processing</i>	62
<i>Quantification of ciliary localization in cultured cells and hypothalamus sections</i>	62
<i>Mouse Metabolism Studies</i>	63
<i>Statistics</i>	63
<i>Data availability</i>	63
CHAPTER 4 : FINAL DISCUSSION AND CONCLUSIONS	64
CHALLENGES IN THE IDENTIFICATION OF PLAYERS IN PRIMARY-CILIA REGULATED ENERGY HOMEOSTASIS	64
TOWARDS UNDERSTANDING CILIARY MECHANISMS REGULATING ENERGY HOMEOSTASIS IN NEURONS	65

INTERACTION BETWEEN DIET, OBESITY AND PRIMARY CILIA HOMEOSTASIS	66
NEURONAL PRIMARY CILIA AND HUMAN OBESITY.....	67
FINAL CONCLUSION.....	68
CHAPTER 5 REFERENCES.....	70

Table of figures

Figure 0.1: The Leptin-Melanocortin System.	xx
Figure 0.2 Primary cilia components and main actors involved in ciliary homeostasis	xxi
Figure 1.1 Ribosomal trapping of MC4R-GFP stabilizes and enhances GFP signal, allowing for identification of MC4RGFP-expressing neurons at low magnification.	9
Figure 1.2: MC4R expression mapping.	10
Figure 1.3: Phenotypic characterization if the <i>NBL10 Mc4r^{gfp}</i> mice	11
Figure 1.4 Assessment of ciliary localization of MC4R localization in regions other than PVN.	12
Figure 1.5: Caloric restriction leads to increased MC4R ciliary enrichment.	13
Figure 1.6: MC4R ciliary enrichment depends on Leptin	13
Figure 1.7: MC4R ciliary enrichment depends on AGRP expression in adult mice and in pups.	14
Figure 1.8: Chronic AgRP infusion leads to increased MC4R ciliary localization	15
Figure 2.1 Developmental MC4R subcellular localization in the PVN at postnatal stage: P2 P6, P11, P15 and Adult.	26
Figure 2.2 Deletion of <i>Ift88</i> in MC4R-expressing neurons leads to obesity.	27
Figure 2.3: Time course of metabolic changes following ablation of primary cilia in adult mice. .	28
Figure 2.4: Primary cilia are essential for the response to the MC4R agonist MTII.	29
Figure 2.5: Primary cilia are required in PVN neurons for weight control and sensitivity to MC4R agonist	30
Figure 2.6: Inhibition of ciliary adenylyl cyclase causes hyperphagia and obesity.	31
Figure 2.7 - Supplementary figure 1: Characterization of <i>Mc4r^{t2aCre}</i> mouse model and central expression	32
Figure 2.8 - Supplementary Figure 2: Time course of IFT88 loss and cilia ablation following tamoxifen injection in <i>Ubc-Cre-Ert2 Ift88^{fl/fl}</i> mice.	33
Figure 2.9 - Supplementary Figure 3: Loss of the primary cilium abolishes THIQ activation of MC4R.	34
Figure 2.10 - Supplementary Figure 4: Complete loss of PVN cilia does not affect hypothalamic <i>Mc4r</i> expression or general PVN neuronal function.	35
Figure 3.1 MRAP2 functions in MC4R-expressing cells to regulate food intake and restrain body weight.	47
Figure 3.2 MRAP2 localizes MC4R to the IMCD3 primary cilium	48
Figure 3.3 MRAP2 colocalizes with MC4R at the primary cilia in vivo.	49
Figure 3.4 MRAP2 is required for MC4R localization to the primary cilia	50
Figure 3.5 MRAP2 is required in the adult PVN for MC4R ciliary localization	51
Figure 3.6 Figure S1: Phenotypical characterization of mice bearing EUCOMM MRAP2 tm1a and tm1c alleles.	52
Figure 3.7 Supplementary figure 2: Ciliary enrichment of Melanocortin receptors, MRAP1 and MRAP2.	53
Figure 3.8 Supplementary figure3: Specificity of MRAP2 antibody: no signal observed in MRAP2 knock-out hypothalamic sections.	54
Figure 3.9 Supplementary figure 4: MC4R localizes at the primary cilium in P6 pups.	55
Figure 3.10 Supplementary figure 5: MRAP2 co-localizes with SSTR3 and MC4R-GFP in a subset of neurons in the PVN.	56

Figure 3.11 Supplementary figure 6: MRAP2 deletion does not impact SSTR3 ciliary localization.
..... 57

Figure 3.12 Graphical abstract..... 58

Figure 4.1 The gut-fat-brain axis..... 69

Figure 4.2: Model for the integration of short- and long-term energy homeostasis signals in MC4R
neurons..... 69

Dedication

I don't think I will be able to find words to fully express all the gratitude I have for the extraordinary people I met and had in my life during my PhD journey, but here I go.

First, I want to thank the universe for making me land in Professor Christian Vaisse's lab for the first time for my master thesis internship. When I say the universe, I obviously mean luck, but I also mean Professor Maximiliano Figueroa, Professor Joseph Martial and Dr Anastasia Mavropoulos, who have been key factors in catalyzing my first internship at UCSF.

I want to thank Professor Christian Vaisse, for believing I could be a good fit in his lab, and for inviting me to come back to start my PhD. I could not have dreamed of a better lab to spend 6 years of my life. Christian: thank you for being the mentor I didn't know I needed, thank you for your encouragements, your trust, the amazing science, the freedom you gave me throughout my journey, and for simply being the coolest boss around.

I also want to thank the Berkeley Nutrition Sciences and Toxicology department for accepting me as the first UC Berkeley/UCSF student in the Metabolic Biology PhD program, I am very grateful to have been given this opportunity.

I want to acknowledge all my labmates, former and present. Thank you for making the lab a fun and comfortable place. For me, getting along with the people I work with is almost more important than the daily science, and you guys really made the Vaisse lab a perfect lab, I will miss you.

Special acknowledgments go to Chris and Florence, who, besides being the best lab managers a lab could hope for, are the definition of kindness and dedication. I feel so fortunate to call you my friends. Shout out to Chris for stimulating my handyman side (I made sure to pass the screwdrivers on to the new generation ;)), and for being such an amazing surgery trainer, who inspired me to become one myself. Thank you, Florence, for being always so positive, encouraging and caring and for inspiring me to have a better work/life balance.

I would like to thank Yi for the training I received during my first years in the lab, thank you for bearing with me when I didn't know anything, thank you for your patience. Thank you Sumei for your ever good mood and for being a PCR ninja and saving us so much time. I want to acknowledge the undergraduate and rotating students who taught me how to teach, and made the lab a very fun place. Special shout out to Annie and Abbey who decided to join the fun, I wish you all the best in your graduate journey. And another special shout out to Marine, I really wish you could have stayed longer with us, that semester was fire!

I want to thank all our collaborators, our joint meetings allowed me to think outside of the box, and I am very grateful for all the support I have had through the years. I especially want to thank Irene and Navneet who are two badass women who make excellent science and are extraordinary human beings.

I would like to thank my dear friends from other labs, thank you for making a fun community in the department. Special shout out to my best friend Caroline, thank you for being such an extraordinary person and sharing your passion for creative hobbies. Creating the photoclub with you was a blast, I learned so much, I am so glad we dived into this adventure together. Big up to Fred, for always being so calm and available for a cool chat after hours. Matt and María: I miss you so much! I wish I could have had you there for my whole thesis, we made an incredible team. Thank you for the laughs, the music, trips and so much more. I have so many other people to acknowledge. Thank you, Luz for being the best dancing buddy in the entire world, and Eleonora for being the brightest ray of sunshine, your friendship means a lot to me. Thank you, Gopika for being an example of determination, and Simone for your friendship and your passion for coaching, I learned a lot from you and I hope it's just the beginning, I wish you the best. Thank you to my best friends back home, Morgane, Jeremie and Jessica for their commitment to stay in touch through the distance and always being so supportive.

Finally, I want to thank my family, and especially my brother, for always being there and for being the best brother I could have wished for. I hope I made you proud.

A sincere gratitude to all of you for the laughs, the knowledge and reflections, and for making me the person I am today.

Acknowledgements

Chapter 2 adapted with permission from the journal of clinical investigation,

J Clin Invest 2021 May 3;131(9):e142064; doi: 10.1172/JCI142064.

Melanocortin-4 receptor signals at the neuronal primary cilium to control food intake and body weight.

Yi Wang*, Adelaide Bernard*, Fanny Comblain*, Xinyu Yue, Christophe Paillart, Sumei Zhang, Jeremy F. Reiter, Christian Vaisse

Chapter 3 adapted with permission from Biorxiv,

bioRxiv 2020.11.13.382325; doi: <https://doi.org/10.1101/2020.11.13.382325>

The single pass membrane protein MRAP2 regulates energy homeostasis by promoting primary cilia localization of the G protein-coupled receptor MC4R.

Adélaïde Bernard, Irene Ojeda Naharros, Florence Bourgain Guglielmetti, Jordi Ciprin, Xinyu Yue, Sumei Zhang, Erin McDad, Maxence Nachury, Jeremy F. Reiter, Christian Vaisse

Chapter 0 : General introduction

Human obesity and genetics

Obesity is a major contributor to chronic diseases including type 2 diabetes, hypertension, and heart disease, and presents a major public health challenge¹. While obesity rates increase worldwide, lifestyle interventions are hardly successful or maintained in the long-term, and available treatments remain limited. To date, bariatric surgery is the most effective treatment for body weight loss in patients with class 3 obesity (Body mass index >40 kg/m², “BMI”). This intervention is invasive and presents short-term risks as well as possible adverse effects in the long term¹.

Although it is clear that environment can influence BMI, genetic epidemiology studies such as familial aggregation, twin and adoption studies demonstrated that genetic predisposition accounts for 40 to 70% of susceptibility to obesity². “Drugging” obesity thus remains an open challenge and understanding the genetic and molecular basis of this pleiotropic pathology is a mandatory step in that direction.

While the study of monogenic forms of obesity have identified genes that individually have a strong impact on energy homeostasis, large genetic studies known as Genome-Wide Association Studies (GWAS) have identified variants that have small clinical effects, but that are strongly associated with obesity. The fat mass and obesity-associated (*FTO*) locus shows the strongest association with body mass index (BMI) and obesity risk, while the Melanocortin-4-Receptor locus, *MC4R*, is second³⁻⁶. Interestingly, most of the identified loci influencing body mass index (BMI) are located outside of coding regions, and most of the putative causal genes are highly expressed or known to act in the central nervous system (CNS)⁵. On the other hand, the study of rare monogenic forms of obesity has revealed the existence of two important functional sets of genes responsible for energy homeostasis. The first group of genes defines a neuroendocrine system in charge of relaying information from the adipose tissue to the CNS to adapt energy balance—the leptin-melanocortin system (Figure 1)—, and the second group of genes are involved in the structure and function of an organelle called the primary cilium (Figure 2), which will be extensively described in the following chapter of the introduction.

Maintenance of long-term energy homeostasis by the leptin-melanocortin system

Leptin and the leptin receptor

In 1950 and 1965, respectively, the *Ob/Ob* and *Db/Db* mice were discovered⁷. Both models were hyperphagic, obese and were used as a model for mild diabetes. Early parabiosis experiments suggested the *Ob* gene product was a “satiety factor” and the *Db* gene product was its receptor, as *Ob/Ob* mice responded to the factor produced by *Db/Db* and wild type mice, while the *Db/Db* mouse did not. Only in 1994 the product of the *Ob* gene was identified as a secreted hormone, and called leptin (*leptos*, “thin” in Greek)⁸. Shortly after, the Leptin Receptor, a member of class I cytokine receptor family, was identified as the product of the *Db* gene^{9,10}. Alternative splicing produces five different murine forms, of which only the “b” isoform possesses a long cytoplasmic region encoding all Jak-Stat motifs required for signal transduction, and is therefore crucial for leptin action¹¹.

Later studies showed that Leptin is an adipose tissue-derived hormone, which is released in the bloodstream in proportion to the amount of fat stored. Leptin then crosses the blood brain barrier and signals the amount of energy stored in the periphery to the brain in order to adapt food intake and energy expenditure to maintain body weight stable over time.

In 1997, homozygous mutations in the leptin gene were identified in two children with early-onset obesity. This congenital leptin deficiency was the first genetic evidence that leptin is an important regulator of energy balance in humans¹². Treatment with recombinant leptin completely reverted obesity and other leptin deficiency-associated symptoms¹³. However, while leptin replacement works in leptin-deficient patients, most patients with obesity present hyperleptinemia, as their leptin levels correlate with their fat mass. This observation leads to the concept of obesity leading to “leptin resistance”, as the endogenous leptin is not able to regulate metabolism accordingly.

Leptin action in the Central Nervous System

Screening for the expression of the leptin receptor isoform b (LepRb) mRNA revealed a high level of expression in the hypothalamus, midbrain and brainstem, structures previously known to play important roles in energy balance^{14,15}. The identification of Leptin-responsive neurons was also carried out by assessing JAK/STAT activation downstream of LepRb¹⁶. Janus Kinase 2 (JAK2) activation leads to the phosphorylation of a tyrosine in the leptin receptor, which serves as a binding site for STAT proteins. STAT3 (and other STATs) is recruited and phosphorylated by JAK2. This event leads to the dissociation of phospho-STAT3 from the receptor, followed by its dimerization and translocation to the nucleus where it acts as a transcription factor. Mapping the immunoreactivity of phospho-STAT3 revealed the existence of key leptin-responsive cells in the hypothalamus^{17,18}. These data showed that leptin acts via a broadly distributed network of LepRb-expressing neurons, the largest populations residing in hypothalamic nuclei as the Arcuate (ARC), Dorsomedial (DMH), ventromedial (VMH), lateral hypothalamic area (LHA), and ventral premammillary (PMv) nuclei¹⁹.

First order neurons: leptin-sensitive POMC and AgRP-expressing neurons

Among these nuclei, within the ARC, two types of neurons residing in close proximity have been identified as key regulators in energy homeostasis. A first anorexigenic population is activated by leptin and characterized by the expression of melanocortins, which are products of the pro-opiomelanocortin (POMC) propeptide²⁰. The second subset of neurons is inhibited by leptin, and expresses the Agouti-Related Protein (AgRP) and the Neuropeptide Y (NPY)²¹. These ARC neurons are located around the third ventricle, in a region characterized by a leaky blood-brain barrier²², which allows them to sense and adapt to small variations in circulating leptin²³.

In addition to being differentially regulated by leptin, the neuro-peptides produced by these neurons exert opposing effects on feeding and metabolism through their interaction with melanocortin receptors in second order neurons, triggering downstream responses designed to maintain fuel stores at a constant level^{24,25}.

In POMC neurons, the pro-hormone pro-opiomelanocortin is sequentially processed into the melanocortin peptides adrenocorticotrophin (ACTH), melanocyte-stimulating hormones (MSH) alpha, beta and gamma, as well as the opioid-receptor ligand beta-endorphin²⁶. POMC-deficiency leads to obesity both in mice and humans. Although very rare, patients with mutations in *POMC*

also display altered hair pigmentation, and, they are adreno-insufficient, as they do not produce ACTH^{26,27}. The central role of this neuronal subpopulation in the regulation of energy homeostasis is highlighted by the fact that deletion of *LepRb* specifically in POMC neurons leads to obesity and hyperleptinemia²⁸, and conversely, re-expression of *Pomc* only in *LepRb*-positive neurons is sufficient to rescue energy homeostasis in *Pomc* null animals²⁹. Additionally, central infusion of α -MSH reduces short term food intake in rodent models^{30,31}.

In the hypothalamus, the orexigenic neuropeptide AgRP is highly and specifically expressed in the ARC. The initial gene product is a 132 amino acid protein, that is processed intracellularly to generate AgRP[83-132] C-terminal fragment. A single dose of AgRP administered centrally increases food intake for up to one week³² and ubiquitous over-expression of AgRP leads to obesity. After fasting, leptin levels decrease, which leads to an increase in *Agrp* expression in order to stimulate hunger and reestablish energy balance. This increase of AgRP expression following fasting can be prevented by injecting leptin³³. Conversely, *Ob/Ob* and *Db/Db* animals present elevated expression of AgRP, which could explain part of their hyperphagia, as opposed to diet-induced obese wild type animals, which present normal AgRP levels. In the ARC, the expression of AgRP overlaps with Neuropeptide Y (NPY) expression. NPY is a 36 amino acid neuropeptide with powerful stimulatory effects on food intake when administered centrally. However, despite the considerable evidence that NPY and AgRP play a central role in stimulating appetite, NPY- and AgRP-deficient mice eat and grow normally, and refeed after a fast normally, showing very small phenotype alterations. To test whether this could be due to developmental adaptations allowed by the functional redundancy of these neuropeptides, double knockouts were created, but *Npy*^{-/-}/*AgRP*^{-/-} mice did not display any obvious feeding or body weight deficits and maintain a normal response to starvation. These findings suggested that other pathways can compensate to regulate energy homeostasis when these orexigenic peptides are missing^{25,34,35}. A more recent study showed that AgRP-deficient mice display an age-related lean phenotype, this is, they exhibit reduced body weight and adiposity after 6 months of age³⁶. Interestingly, neonatal ablation of NPY/AgRP neurons using a Diphtheria toxin receptor approach had minimal effects on feeding, whereas their ablation in adults lead to rapid starvation³⁷. These data further suggested that compensatory mechanisms can develop in early stages of development but do not occur once these neurons become essential in adults. Further studies demonstrated that this phenotype was independent of AgRP and NPY but rather depend on the fact these neurons also express the inhibitory neurotransmitter GABA, which also plays an important role in the orexigenic function of these neurons^{38,39}. Indeed, artificial activation of AgRP neurons using optogenetics or chemogenetics leads to voracious feeding⁴⁰.

Second order neurons: MC4R-expressing neurons

These first-order neurons expressing POMC and AgRP send axonal projections to second-order neurons in the Paraventricular Nucleus of the hypothalamus (PVN), that express the anorexigenic Melanocortin Receptor 4 (MC4R). Leptin promoted-POMC production and cleavage leads to the production of α -MSH, which is the endogenous agonist for MC4R. Conversely, in AgRP/NPY neurons, activation of *LepRb* represses AgRP production, which antagonizes MC4R. Together, these complementary circuits lead to a balance of extracellular α -MSH/AgRP concentrations that

are favorable to MC4R activation in the presence of higher concentrations of leptin, which acts as a feedback loop leading to satiety⁴¹.

MC4R is a member of a family of five melanocortin receptors, transcribed from different genes. MCRs are seven transmembrane domain G protein-coupled receptors (GPCRs), part of the subfamily of class A Gs-coupled receptors, signaling through the activation of the adenylyl cyclase to increase the level of intracellular cAMP^{42,43}. MCRs are activated by melanocortins, which are originated by the posttranslational processing of POMC. The receptors, jointly with their endogenous agonists (α -, β -, γ -MSH and ACTH), and the only two identified naturally occurring antagonists (AgRP and Agouti protein), represent the « melanocortin system »⁴⁴. This double input to modulate their activity makes these receptors totally unique among the extensive family of GPCRs⁴⁵. MCRs control a variety of physiologic responses depending on where they are expressed and respond to POMC-derived peptides with different affinity. MC1R is a key regulator of the pigmentation of the skin and is activated by α -MSH. MC2R is the ACTH receptor, and it is expressed primarily in the adrenal cortex where it mediates the effects of ACTH on steroidogenesis. MC3R is expressed in the CNS, the placenta and the gut and is involved in metabolism and nutrient partitioning. MC5R is involved in exocrine gland function and is widely expressed at low levels in numerous tissues^{44,46}.

MC4R is expressed mainly in the brain, and is involved in sexual and cardiovascular function, glucose and lipid homeostasis, and feeding behavior. MC4R is a key player in the central leptin-melanocortin system as it transduces anorexigenic signals in the long-term regulation of energy homeostasis⁴¹. More than 50 rare mutations in *MC4R* have been reported in patients with obesity⁴⁷⁻⁵¹, heterozygous mutations in *MC4R* are the most common cause of monogenic obesity in humans, and homozygous null mutations lead to severe, early-onset obesity^{47,52}. *Mc4r* knockout mice also develop severe obesity, with heterozygous mice displaying an intermediate phenotype⁵³.

The expression of MC4R in the PVN has been shown to be both necessary and sufficient to control food intake and body weight, as selective deletion of *Mc4r* in the PVN of *Mc4r* floxed animals leads to obesity, and rescue of *Mc4r* in the PVN of *Mc4r* null mice rescued their phenotype⁵⁴. Moreover, PVN MC4R neurons control real time feeding as their activation by chemogenetics and optogenetics leads to decreased food intake⁵⁵.

Understanding how MC4R signals is therefore of interest to design therapeutic approaches to treat obesity. A first step in this direction encompasses studying the subcellular dynamics on MC4R *in vivo*. Unfortunately, previous attempts to assess the subcellular localization of MC4R in brain slices have been unsuccessful due to its low levels of expression, the small number of neurons in which it is expressed, and the lack of working antibodies⁵⁶. We therefore created a mouse model expressing a GFP tag in frame with *Mc4r* endogenous locus, leading to the production of an MC4R-GFP fusion protein. Analyzing PVN sections of *Mc4r^{gfp}* mice, we discovered that MC4R colocalizes with adenylyl cyclase 3 (ADCY3) at the primary cilia of a subset of PVN neurons⁵⁶. Primary cilia are highly specialized signaling hubs that protrude from the cell membrane and act as cellular antennae, which will be extensively described hereafter.

Regulation of energy homeostasis by neuronal primary cilia

A number of pathways underlie long-term energy balance. At the crossroads between human genetics of obesity and the central control of energy homeostasis lies an underestimated organelle called the primary cilium. Most mammalian cells have a primary cilium, which is a non-motile solitary organelle projecting from the cell surface, that acts like an antenna sensing the extracellular environment. As such, they function as sensory units transmitting information to the cell. Primary cilia are critically involved in many different signaling pathways at every stage of life, from early development to adult tissue homeostasis regulation and control of long-term energy balance^{57,58}. Different cell-types and organs harbor primary cilia with distinct sets of molecules. Consequently, mutations affecting cilia-related genes can lead to a variety of symptoms depending on which components of cilia are affected. These symptoms range from developmental impairments to sensory deficiencies to obesity, and are associated with a wide range of disorders known as “ciliopathies”⁵⁹. Some ciliopathies have been linked to defects in body weight control, therefore highlighting the cilium as an important component of the intercellular communication necessary to achieve energy homeostasis.

Primary cilia architecture and maintenance

Primary cilia function as mechano-, osmo-, and chemosensory units that sense extracellular changes and transduce them to the cell⁶⁰. The sensory role of this organelle is facilitated by its unique structure and composition, together with the precise and timely organization of its components.

Primary cilia are microtubule-based structures that protrude from the plasma membrane into the extracellular space, with an average length that ranges from 1 to 15 microns⁶¹. Primary cilia can be divided in three main compartments: the basal body, the transition zone and the axoneme^{62,63} (Figure 2).

The cilium extends from the basal body. The basal body originates from a mother centriole and is made of nine triplets of microtubules. Anchored to the cell membrane through transition fibers, the basal body is the base structure and the nucleation site for the growth of the axoneme microtubules^{59,60}.

The axoneme is cilia’s cytoskeleton. It is made of nine pairs of microtubules, projecting from the basal body, and gives the organelle its characteristic elongated shape, allowing cilia to sense the extracellular environment. This 9 doublets (9+0) organization also differentiates primary cilia from other similar but motile structures such as airways epithelium cilia or flagella that have a 9 doublets + 2 central single microtubules (9+2) structure that gives them motile properties⁶³.

The area between the basal body and the axoneme is called the transition zone. It is a short (0,5 μm) but critical area for cilia function as it forms a diffusion barrier for membrane-associated and soluble proteins. Structurally, it is characterized by Y-shaped connectors between the axoneme microtubule doublets and the ciliary membrane⁶⁴.

Despite being continuous with the plasma membrane, ciliary membranes harbor a different composition of lipids and proteins, giving primary cilia their unique sensory properties. More specifically, ciliary membranes are enriched with various proteins, including signaling receptors, transcription factors and ion channels⁶⁵. Likewise, the cytoplasm composition inside primary cilia also differs from the rest of the cell. This difference allows cilia to function as a single unit⁶⁶. This compartmentalization is allowed by the transition zone, that functions as a barrier where many ciliary membrane-associated proteins accumulate. This suggests that it functions as check-point for proteins to enter or exit the cilium⁶⁷. Although Lipid contribution in ciliary signaling is still poorly understood, the distinct lipid composition of the ciliary membrane seems critical for creating a specialized environment for signaling^{68,69}. For example, compared to the cell plasma membrane, the ciliary membrane is enriched for the phosphoinositide PI(4)P and relatively poor in PI(4,5)P₂. Phosphoinositides are a class of membrane phospholipids that control a great diversity of cellular processes. This difference is due to the action of an enzyme, the inositol polyphosphate 5-phosphatase INPP5E that degrades PI(4,5)P₂ to form PI(4)P⁶⁸. Recent studies showed that proper phosphoinositide compartmentalization is essential for correct protein trafficking and hedgehog signaling in primary cilia⁷⁰.

Since cilia do not contain the machinery necessary for protein synthesis, all proteins functioning in cilia need to be imported in and exported out. In addition, cilia are dynamic structures, that are maintained by the activity of the intraflagellar transport machinery (IFT)⁷¹. IFT proteins facilitate the transport of cargo-proteins from the base to the top of the cilium and back in association with another complex called the BBSome^{59,65}. Recently, it was discovered that the BBSome is necessary for the exit of activated-G-protein-coupled Receptors (GPCR) out of the cilium, trafficking them across the transition zone^{72,73}. Hence, the IFT machinery also cooperates with the transition zone proteins to dynamically deliver or export ciliary components. Cilia cargo-proteins can migrate along the axoneme in two opposite directions: anterograde transport allows building blocks to migrate from the cytoplasm to the cilia tip, and retrograde transport brings back damaged proteins or activated receptors in the cytoplasm to be recycled⁷⁴. The IFT machinery requires the coordination of two complexes: IFT complex A (IFT-A) and IFT complex B (IFT-B). Historically, the anterograde transport of cargo proteins was thought to be achieved by IFT-B, which binds to a kinesin-2 that provides motility power. In the opposite direction, IFT-A, in association with another motor protein, dynein-2, was thought to be in charge of the retrograde transport from the cilia tip to its base⁶⁵. However, recent data indicate that these complexes may play multiple roles. IFTA, together with TUB/TULP proteins, were recently shown to mediate GPCR entry in the cilium, while IFTB appears to be necessary to retrieve activated GPCR from cilia⁷³. Recent data point at a model in which IFTB constitutes the trains on which proteins can be docked, while IFTA mediates their entry, and the BBSome their exit (for a detailed review refer to⁷³).

The coordination of all these different actors is essential to maintain cilia homeostasis and ensure the coordinated flow of all cilia signaling components.

Examples of primary cilia-mediated functions

While there are some generalities about the composition and structure of different kinds of primary cilia, the specific functions of some types of primary cilia are reflected in their peculiar shapes and specific components.

The ciliary membrane is highly enriched for receptors, ions channels and downstream effectors. Indeed, a number of signaling pathways rely on primary cilia. This concentrated microenvironment therefore requires a high level of regulation. Part of its efficiency relies on the organization of signaling components in supramolecular complexes, allowing for highly regulatable, sensitive, and fast signaling ⁷⁵.

G protein-coupled receptors (GPCR) form a large family of 7-transmembrane domain receptors. GPCRs are widely studied as they constitute more than 50% of all therapeutic drug targets ⁷⁵. Interestingly, a large number of GPCRs localize to primary cilia. Out of six major classes, ciliary GPCRs belong to classes A, B, and F ⁷⁶. A growing number of class A GPCRs have been found enriched in neuronal primary cilia both *in vivo* and *in vitro* : the Melanin-concentrating hormone receptor 1 (MCHR1), the somatostatin receptor 3 (SSTR3), the serotonin receptor 6 (5HT6), the neuropeptide Y receptor 2 (NPY2), the kisspeptin receptor (KISS1R), and more recently identified, the melanocortin-4-receptor (MC4R) ⁷⁶⁻⁷⁸. Furthermore, a component of the cAMP-dependent, G protein-coupled signaling cascade, the adenylyl cyclase 3 (ADCY3), also very specifically localizes to neuronal primary cilia.

Examples of well-described primary cilia sensory functions include their role in vision and olfaction. In the retina, light is detected by photosensory GPCRs called rhodopsin receptors, which exhibit the highest receptor concentration at the ciliary membrane (27 000 receptors/ μm^2) ^{74,79}. Activated rhodopsin receptors trafficking out through the transition zone are replaced at rates estimated to be about a 1000 molecules per second ⁸⁰. This illustrates the efficiency and speed at which primary cilia can operate. Olfaction also relies on primary cilia, that constitute a chemo-sensory interface that detects and transmits odorant information to the brain ⁸¹. In the nasal epithelium, cilia of olfactory sensory neurons (OSNs) harbor olfactory GPCRs on their surface. Their activation by volatile olfactory ligands activates canonical signaling cascades leading to neuronal depolarization, consequently sending olfactory information to the brain ^{82,83}.

In addition to their chemo-sensory role, the shape and structure of primary cilia provide them with mechano- and osmo-sensory abilities. In the kidneys, for example, cilia can detect urine flow and composition. This ability relies on highly regulated ciliary calcium concentration, which is 7 fold higher than in the cytoplasm ⁶⁶. This difference is maintained through the work of mechanosensory units of the ion channels Polycystic Kidney Disease-like proteins PKD1L1 and PKD2L2, associated with Polycistins PC1 and PC2, and held through a diffusion barrier isolating the ciliary compartment from the rest of the cell ^{84,85}. Liquid flow over primary cilia modifies the forces applied by the ciliary membrane over the axoneme and its base, facilitating the extracellular calcium influx through PC2. This in turn can regulate intra-cellular calcium signaling by stimulating the release of calcium from intra-cellular stores ^{60,86-88}. Of note, Calcium is also an important second messenger to different receptors, like GPCRs ²⁵⁸⁹.

Lastly, it is worth noting that the Sonic-hedgehog pathway was one of the first described to rely on primary cilia for signal transduction. This pathway is highly conserved and it is essential for the regulation of cell differentiation during embryonic development, regulation of adult stem cells and maintenance of tissue homeostasis ^{57,90}. Notably, this pathway relies on the timely translocation

of a GPCR (the Smoothed receptor) to the cilium, emphasizing how dynamic regulation of ciliary elements is essential for ciliary function and signal transduction.

Linking neuronal primary cilia to obesity

Mutations in cilia-related genes can lead to an array of symptoms depending on which ciliary process or component and which organ are affected. Indeed, ciliopathies can present with developmental impairments, sensory deficiencies and/or obesity⁵⁹. While integrity, formation and maintenance of cilia are obviously key to ciliary function, timely trafficking and targeting of its building blocks and signaling machinery are also essential^{59,91}. Historically, mutations in genes responsible for some of those tasks have been linked to defects in body weight control, bringing interest in understanding the involvement of primary cilia in the control of energy homeostasis.

Evidence for a role of primary cilia in obesity

Bardet-Biedl syndrome (BBS) was the first human ciliary disorder discovered, with cardinal features of polydactyly, retinal degeneration, cystic kidney, cognitive impairment and obesity⁵⁹. Twenty-two BBS proteins have been identified so far. Molecularly, BBS gene products assemble or regulate the BBSome, an octameric protein complex (BBS1, BBS2, BBS4, BBS5, BBS7, BBS8, BBS9 and BBS18) part of the basal body⁶⁵. Most *Bbs* mutant mouse models (except *Bbs3*, also called *Arl6*) present hyperphagia-induced obesity and recapitulate several clinical features seen in patients, although with variable penetrance and expressivity⁹². While most BBS gene products localize to the basal body or cilia, mutations in *BBS* genes in most cases do not affect ciliogenesis^{73,93}.

Alstrom syndrome (ALMS) is the second most studied ciliopathy after BBS. It was first described in 1959 by Carl-Henry Alstrom⁹⁴. ALMS and BBS share common symptoms such as retinal degeneration, early onset obesity and type II diabetes but patient with ALMS do not suffer from mental retardation, polydactyly or hypogonadism. Mutations observed in ALMS are all associated to *ALMS1* gene⁹². *In vitro* studies specifically localized *ALMS1* protein to the basal body of primary cilia, but its deletion, likewise *Bbs* mutations, does not affect ciliogenesis⁹³. The role of *ALMS1* in ciliary homeostasis is not yet fully understood. *foz/foz* mice produce a truncated *ALMS1* protein and develop both obesity and diabetes⁹². Unlike *Bbs* mutants, *foz/foz* mice present fewer ciliated neurons in their hypothalamus, but don't fail to localize GPCRs to cilia⁹⁵.

The Joubert syndrome (JS) is another ciliopathy that presents, amongst numerous other symptoms, with obesity. Thus far, Twenty-two causative JS genes have been identified, all encoding proteins localized within or near the primary cilium. Molecularly, *ARL13B* variants were reported in patients with JS presenting with obesity. *ARL13B* is a small ciliary GTPase, found within the primary cilia of hypothalamic neurons. In mouse, loss of *Arl13b* function results in disrupted cilia and defective SHH signaling, leading to embryonic lethality⁹⁶. Mutations in the inositol polyphosphate 5-phosphatase E (INPP5E) have also been linked to JS⁶⁸. INPP5E mutations cause primary cilium signaling defects and ciliary instability both in human and mouse. These studies highlighted that specific distribution of phosphoinositide in the ciliary membrane is important for proper protein trafficking in cilia^{68,69,93}.

Other mouse models of ciliopathy include the *Tubby* mouse, and mutants for RAB23 and CEP19. The *tubby* mouse displays retinal degeneration, hearing loss and maturity-onset obesity. While TUB is expressed mainly in the brain, it is part of a more widely expressed family that includes tubby-like protein 1, 2 and 3 (TULP1, 2 and 3), that share a phosphodiesterase binding C-terminal tubby domain⁹³. Although *Tulp3* knockout mice are embryonic lethal, it has been shown that TULP3 facilitates the import of specific GPCR to cilia through its interaction with the IFT-A complex^{73,75,93}. CEP19 is a novel centrosomal protein, therefore localized to the cilia basal body. Albeit not altering cilia morphology, *Cep19* deletion leads to hyperphagia, obesity, glucose intolerance and insulin resistance but no other features of ciliopathy in mice⁹³. Humans with *CEP19* mutations also display other symptoms like intellectual disability, and cardiovascular problems. RAB23 is another GTP-binding protein that promotes ciliary localization of GPCRs⁷⁶. Mutations in *RAB23* in humans lead to Carpenter Syndrome (CS), which is characterized by obesity and defects in hedgehog signaling⁹⁷. This mutation leads to the development of an open brain in mice and is embryonic lethal⁹³.

Progress towards identifying molecular actors regulating energy homeostasis through primary cilia

After highlighting how endogenous mutations in different ciliary components compromise energy homeostasis, tools had to be designed to more precisely dissect the tissue- and cell-specificity of these phenotypes. Since developmental deletion of cilia is embryonic lethal, conditional ciliary mutants were created, including floxed alleles for IFT88 (a component of IFT-B) and Kif3a (a subunit of kinesin-2). The disruption of these genes leads to the complete structural loss of the cilium in most cells. Interestingly, induction of cilia loss using ubiquitous inducible CRE-recombinase in adult mice resulted mainly in an obese phenotype with increased leptin, glucose and insulin levels⁹⁸. Pair-feeding to control littermates normalized body weight and leptin, insulin and glucose levels, indicating that the disruption of metabolic parameters was caused by hyperphagia. Interestingly, removal of cilia exclusively in neurons using a *Synapsin-Cre* driver led to a similar phenotype, demonstrating the importance of neuronal primary cilia in the regulation of energy homeostasis⁹⁸.

The hypothalamus is a brain region responsible for homeostatic control of appetite and body weight. Genetic deletion of *Ift88* in the ventromedial hypothalamus (VMH), by SF1-CRE recombination or by injecting a CRE recombinase-expressing adeno-associated virus (AAV) in the VMH of *Ift88^{fl/fl}* mice, leads to increased body weight, bone density accrual and leptin resistance⁹⁹. The injection of small inhibitory (siRNA) specific to *Kif3a* and *Ift88* specifically into the ARC, where POMC- and AgRP-expressing neurons lie, led to an increased food intake but decreased energy expenditure, resulting in weight gain⁶¹. In line with these results, deletion of *Ift88* from ARC POMC-expressing neurons also lead to obesity, confirming the importance of this nucleus for cilia-dependent regulation of energy expenditure. However, a recent study has demonstrated that adult-onset ciliary dysgenesis in POMC neurons does not have an impact on energy homeostasis, and shows that POMC neurons primary cilia are rather required during early postnatal life to extend their projections to second order nuclei¹⁰⁰.

Interestingly, attempts to link ciliopathies to leptin signaling in the hypothalamus have led to some controversial results. Indeed, some BBS mutants are resistant to the anorexigenic effect of

exogenously administered leptin, even after body weight normalization by caloric restriction¹⁰¹. Furthermore, deletion of *Bbs1* gene from the nervous system, or more selectively from the arcuate nucleus or from LepR-expressing cells lead to both an increase in food intake and a decrease in energy expenditure, leading to obesity¹⁰². Mechanistically, POMC expression was decreased in these models, which could explain the hyperphagia caused by decreased MC4R activity¹⁰². However, when pre-obese *Bbs4*^{-/-} mice were injected with leptin, they presented a normal anorectic response to leptin both in terms of feeding and activation of STAT3 downstream signaling of the leptin receptor¹⁰³. Consistently, studies on *Ift88* conditional knock-out mice revealed that leptin effect was also preserved after deletion of primary cilia when tested in pre-obese state. These experiments indicated that leptin resistance was a consequence of body weight gain, and not the cause of the hyperphagia and obesity observed in mice with ciliary dysfunction¹⁰³.

Since deletion of BBS genes only from the hypothalamus lead to obesity, a combination of *in vivo* and *in vitro* experiments studied the role of the BBSome in the trafficking of hypothalamic GPCRs to primary cilia. On one hand, the BBSome was first thought to be required for the localization of GPCRs to primary cilia, since the Somatostatin Receptor 3 (SSTR3) or the Melanin Concentrating Hormone Receptor 1 (MCHR1), for example, are not detected in neuronal primary cilia of *Bbs* mutants¹⁰⁴. However, a recent model proposes that the BBSome removes activated GPCRs, like SSTR3 or Smoothed, from cilia by enabling their passage through the transition zone^{72,73}. In addition, BBS proteins have also been implicated in the regulation of the actin cytoskeleton, which can affect cilia length and other processes^{105,106}. The BBSome is therefore believed to ensure proper signal onset and termination by both sorting trafficking vesicles to the primary cilium and removing activated GPCRs from cilia^{65,72}. Notably, although MCHR1 is an important regulator of feeding and energy balance¹⁰⁴, MCHR1 activation has orexigenic effects, and therefore its exclusion from cilia and probable loss of function in *Bbs* mutants cannot explain their obese phenotype.

LepRb-expressing neurons in the ARC relay information about global energetic status to neurons expressing MC4R. Mutations in *MC4R* are the most common monogenic cause of severe human obesity, and the expression of MC4R specifically in the PVN was shown to be both necessary and sufficient to control food intake and body weight¹⁰⁷. Activation of MC4R by α -MSH leads to G α s protein coupling that in turn increases the local concentration of cAMP through adenylyl-cyclase. In neurons, the adenylyl cyclase 3 (ADCY3) very specifically localizes to primary cilia. ADCY3 fails to localize to cilia in *Alms1* mutant mice¹⁰⁸, and loss-of-function variants in *ADCY3* were recently found to cause monogenic severe obesity in humans^{109,110}. Consistently, adult *Adcy3* knockout mice are obese, and restricted ablation of *Adcy3* in the hypothalamus is sufficient to cause obesity^{111,112}. Since ADCY3 is downstream Gs-coupled receptors, the upstream receptor responsible for the obesogenic effect was yet to be identified. Remarkably, we recently demonstrated that MC4R co-localizes with ADCY3 at the neuronal primary cilia in a subset of neurons in the PVN⁷⁸. We discovered that some human mutations that don't impact MC4R activity nor trafficking to the plasma membrane, may cause obesity by impairing MC4R localization to primary cilia. Furthermore, we showed that inhibiting adenylyl cyclase signaling at the cilium of PVN neurons leads to hyperphagia and obesity⁷⁸. Together, these results suggest an essential role of MC4R and

ADCY3 at the neuronal primary cilia to regulate food intake and body weight in adult mice, providing an additional link between ciliopathies and the melanocortin system.

While the study of monogenic forms of obesity identified genes that individually have a strong impact on energy homeostasis—Like *MC4R*, *POMC*, *LEP* or *LEPR*—, large genetic studies known as Genome-Wide Association Studies (GWAS) have identified variants that have small clinical effects, but that are strongly associated with obesity. The fat mass and obesity-associated (*FTO*) locus shows the strongest association with body mass index (BMI) and obesity risk, while the *MC4R* locus is second ⁶. Interestingly, recent studies have suggested that a regulatory element within the first intron of the *FTO* gene may impact the expression of a nearby ciliary gene, *RPGRIP1L* (Retinitis Pigmentosa GTPase Regulator-Interacting Protein-1 Like). *RPGRIP1L* encodes a critical component of the primary cilia, and mice with hypomorphic *RPGRIP1L* display hyperphagia-induced obesity and leptin resistance. This could be caused by decreased trafficking of the leptin receptor in the vicinity of primary cilia, or the decreased number of ADCY3-positive cilia in the their hypothalamus

113.

Transition

From studying rare monogenic forms of obesity to identifying rare variants through GWAS studies, and from modeling ciliopathies both *in vitro* and *in vivo*, there is growing evidence linking primary cilia to the regulation of energy homeostasis. However, many ciliary actors remain to be identified, and molecular mechanisms enabling primary cilia to exert such control remain to be elucidated.

My PhD work was focused on further studying the implications of *MC4R* localization at the primary cilium for the control of long-term energy homeostasis. The first chapter is dedicated to descriptive studies in which we mapped *MC4R* expression throughout the CNS to then analyze *MC4R* subcellular localization in different regions of the brain. We then focused on the population of *MC4R* neurons in the PVN to try to understand *MC4R* subcellular dynamics by assessing its ciliary localization in different genetic models and physiological conditions. In the second chapter, we performed a series of experiments to demonstrate that *MC4R* ciliary localization is necessary to exert its role as key regulator of energy homeostasis. Following these studies, we hypothesized that any molecule necessary for *MC4R*'s trafficking to the primary cilium could be a candidate gene for obesity. In the last chapter, we focused on an accessory protein called *MRAP2*, and demonstrated that *MRAP2* colocalizes with *MC4R* at the neuronal primary cilium and enhances *MC4R* localization to primary cilium *in vivo*.

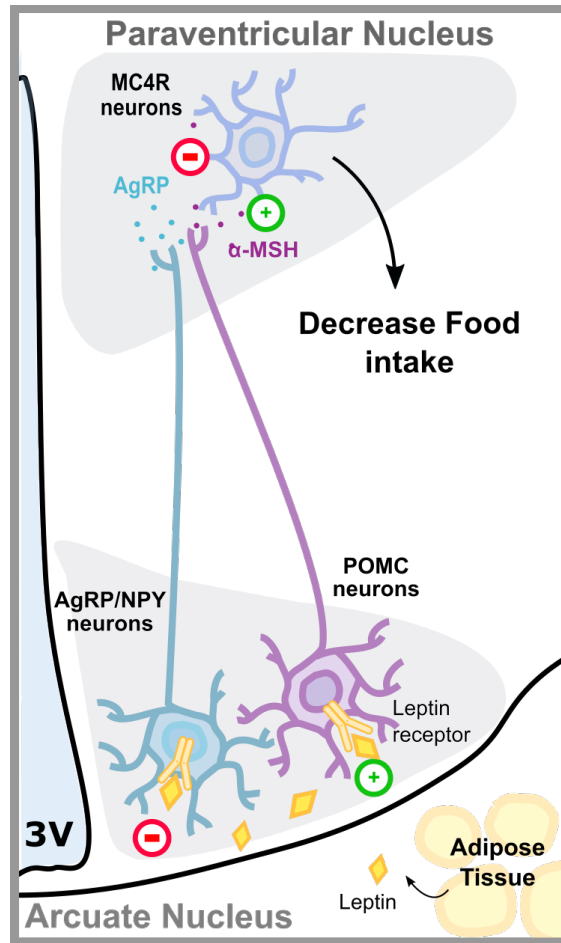


FIGURE 0.1: THE LEPTIN-MELANOCORTIN SYSTEM.

Leptin is secreted by adipocytes into the blood. When it reaches the Arcuate Nucleus of the Hypothalamus (ARC), it binds to its receptor (LepR) in two adjacent but distinct population of neurons, in which it inhibits the production of the Agouti-Related Peptide (AgRP), while activating the transcription of the Pro-opiomelanocortin gene (POMC) and its processing into the alpha-Melanocyte Stimulating Hormone (α -MSH). α -MSH is the agonist, and AgRP is the antagonist for the MC4R. These ARC neurons project to MC4R neurons in the PVN. There, an increase in the balance α -MSH/AgRP activates MC4R and decreases food intake.

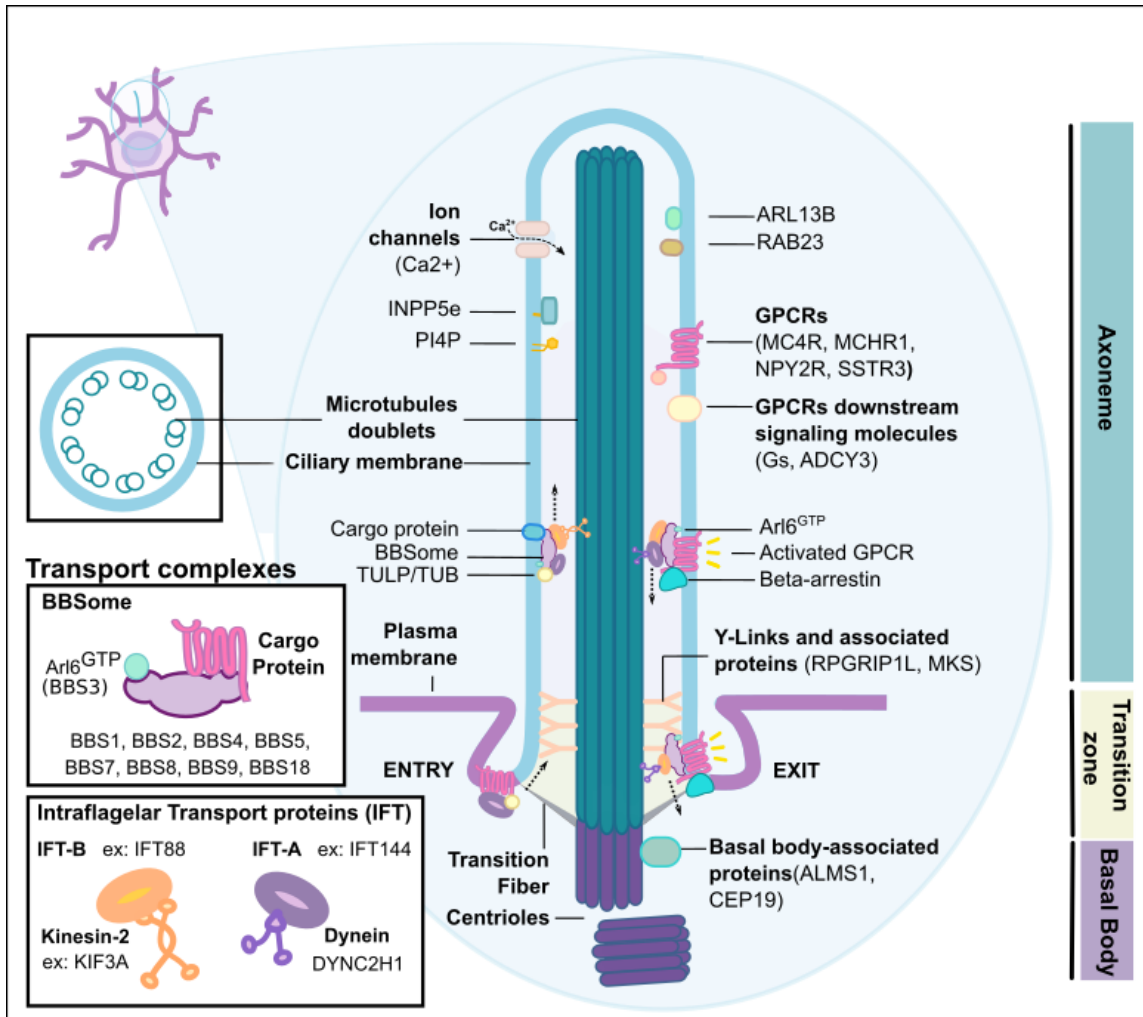


FIGURE 0.2 PRIMARY CILIA COMPONENTS AND MAIN ACTORS INVOLVED IN CILIARY HOMEOSTASIS

Structure: the basal body originates from a mother centriole made of 9 triplets of microtubules. The axonem is made of 9 doublets of microtubules and covered by a specialized ciliary membrane. The transition zone forms a diffusion barrier for membrane-associated and soluble proteins and is anchored to the membrane through Y-Links connectors and associated proteins.

Homeostasis: IFTA associates to TUB/TULP proteins to allow GPCR entry. Anterograde transport of cargo proteins involves the IFT-B complex, powered by Kinesin 2. Retrograde Transport involves the IFT-A complex, powered by Dynein. The exit of activated GPCRs is a complicated process that requires passage through the transition zone, which involves the formation of a complex comprising the activated GPCR, the BBSome, beta arrestin and IFT-B.

Signaling: Primary cilia unique composition and high density of effectors such as ions channels or receptors, like GPCRs, which allows cilia to sense and transduce signals from the extra-cellular environment to the cell. Ciliary localization of GPCR is facilitated by RAB23 and tubby-like protein 1, 2 and 3 (TULP1, 2 and 3). INPP5E enriches ciliary membrane in PI(4)P, helping creating a specialized environment for signaling.

Ciliopathies associated with obesity: Bardet-Biedl Syndrome: BBS gene products assemble or regulate the BBSome, a protein complex that facilitates the transit of cargo-proteins (like for example GPCRs) to and from cilia. **Almstrom Syndrome:** mutations in *Alms1* impair cilia signaling but not its structure. **Joubert Syndrome :** *ARL13b* malfunction results in disrupted cilia and defective SHH signaling.

Chapter 1 : MC4R localizes to neuronal primary cilia

Summary

The melanocortin 4 Receptor (MC4R) is a central component of the leptin-melanocortin pathway in the hypothalamus. We have recently reported that inserting a GFP tag in frame at the C-terminus of the endogenous mouse *Mc4r* allowed for sub-cellular localization of MC4R at neuronal primary cilia in the paraventricular nucleus (PVN) of the hypothalamus. However, the very low levels of expression of this receptor became a limiting factor when using this tool to extensively map its expression and sub-cellular localization. Here, we show that ribosomal trapping of the GFP tag by a nanobody allowed for stabilization and enhancement of the GFP signal, making MC4R-GFP-expressing neurons detectable under a widefield microscope. We used this approach to extensively map the expression of MC4R in the CNS, to then determine the extent of MC4R localization at the primary cilia in some of the identified regions. We propose that this approach could be used to map and study the subcellular localization of other GPCRs expressed at low levels. We show that ribosomal trapping allows for complete functional sequestration of MC4R, making the homozygous *Mc4r^{gfp/gfp}* mice phenocopy the *Mc4r* null mouse model. Finally, we discovered that, in the PVN, MC4R localization at the primary cilium is dynamic and depends on age and physiological status relayed by MC4R ligands levels. Together, these results shed light on the complex regulation of MC4R bioavailability at the primary cilium.

Introduction

Mapping the expression and assessing the subcellular localization of neuronal G protein-coupled receptors (GPCRs) is essential to understand their physiology. Unfortunately, raising antibodies against GPCRs can be challenging, as their relatively low expression and hydrophobicity can lead to scarce exposure of antigens when membrane-embedded, and instability when purified. GPCRs are also dynamic structures, which increases the challenge to produce conformational binders¹¹⁴. Additionally, some GPCRs, like the melanocortin receptor 4 (MC4R), are expressed in a small number of neurons.

MC4R is a Gs-coupled GPCR that transduces anorexigenic signals in the long-term regulation of energy homeostasis⁴¹. Heterozygous mutations in *MC4R* are the most common monogenic cause of severe obesity in humans and homozygous null mutations cause severe, early-onset obesity^{47,48,52}. *Mc4r* knockout mice also develop severe obesity, with heterozygous mice having an intermediate phenotype⁵³. Of the multiple nuclei where MC4R is expressed in the central nervous system, its expression in the paraventricular nucleus of the hypothalamus (PVN) has been shown to be both necessary and sufficient to control food intake and body weight⁵⁴.

To gain insight into MC4R subcellular localization, we previously reported a knock-in mouse model that expresses a GFP tag in frame at the C terminus of the endogenous mouse *Mc4r*⁵⁶, which revealed that, in the PVN, MC4R co-localizes with adenylyl cyclase 3 (ADCY3) at the neuronal primary cilia⁵⁶.

Primary cilia are unique organelles that protrude from the cellular membrane sensing the extracellular environment. Disruption of the structure or function of this organelle leads to pleiotropic conditions collectively referred to as ciliopathies, of which obesity can be one of the symptoms. Measuring approximately 0.25 μm in diameter and up to 15 μm in length^{115,116}, these structures require high magnification confocal microscopy imaging. Whole-brain expression mapping of GPCRs localizing to specific compartments of the cell can therefore become a tedious process.

Besides protein direct visualization, widespread techniques to assess protein expression include the use of cell-specific CRE-recombinase-expressing lines, in-situ hybridization or transgenic reporter lines. However, they all present limitations. Conventional CRE lines allow for tracing the developmental expression of a protein, but using this technology can lead to technical problems including transient CRE expression and adverse recombination events. In order to visualize the expression pattern of a protein in a time-sensitive manner, inducible CRE-lines have been engineered. However, few lines are available compared to the amount of conventional CRE lines. While *in situ* hybridization are time-sensitive, their low signal-to-noise ratio can lead to false negatives for lowly expressed proteins. Lastly, the use of transgenic reporter constructs leads to a better sensitivity and are CRE-independent, but the inability to capture the complete endogenous promoter environment of a gene sometimes leads to ectopic or reduced expression of the reporter, leading to false positives/negatives and therefore inaccurate expression mapping.

MC4R is a unique GPCR as it possesses both an endogenous agonist (α -MSH) and an endogenous antagonist (AgRP). These neuropeptides are expressed in the arcuate nucleus of the hypothalamus

(ARC) and their expression is regulated by the levels of circulating leptin, a bloodborne hormone secreted by the adipose tissue that conveys information about energy stores in the periphery to the CNS^{41,42}. High leptin levels reflecting high adiposity, promote *Pomc* expression while repressing *Agrp* expression to activate MC4R to reduce food intake and re-establish energy balance. After fasting and caloric restriction, leptin levels decrease, releasing the break on *Agrp* transcription³³ to increase food intake. Conversely, total α -MSH levels are low in *Ob/Ob* hypothalami and exogenous leptin administration rescues this phenotype¹¹⁷. While the expression of AgRP and α -MSH can be surveyed at the mRNA or total protein level, little is known about how the concentrations of these peptides fluctuate over time in the extracellular medium, to in term, affect MC4R activity. Additionally, despite being a major target for the pharmacotherapy of obesity, the sub-cellular dynamics of MC4R has not yet been investigated *in vivo*. While we recently showed that, in ad-libitum fed mice, MC4R localizes to neuronal primary cilia in the PVN, MC4R subcellular localization in other brain regions remains to be investigated, as well as how this localization is affected by different physiological conditions. While a previously published transgenic MC4R::GFP model expressing a GFP reporter under the control on *Mc4r* promoter aimed at revealing the distribution of MC4R throughout the CNS, this model did not allow for tracking the subcellular localization of the receptor, since it does not express a fusion protein¹¹⁸.

This chapter describes a new approach based on nanobody technology that allowed for the mapping of MC4R expression, and further characterization of its subcellular localization throughout the brain. furthermore, we describe how this tool can also be used to create functional knockout models, allowing for functional studies of GFP-tagged neuronal receptors. Finally, we discovered that MC4R localization to primary cilia is affected by different physiological conditions through the action of leptin and AgRP.

Results

Ribosomal trapping of MC4R-GFP enhances signal and allows for neuronal expression mapping

We recently reported a mouse model expressing a GFP-tagged MC4R, that allowed for the study of MC4R subcellular localization. Confocal images at high magnification of the PVN of these mice revealed that MC4R localizes to neuronal primary cilia. Primary cilia are 0.25 micron thick and up to 15-micron long structures, which makes MC4R-GFP detection at low magnification impossible, and the expression mapping of MC4R throughout the brain challenging (Figure 1C). In order to stabilize MC4R-GFP in neuronal somas, we used a strategy developed by Ekstrand *et al.* in which ribosomes are tagged with a camelid nanobody raised against GFP. These transgenic mice express an N-terminal fusion protein consisting of the V_HH fragment of the nanobody, fused to large ribosomal subunit protein Rpl10a under the control of the synapsin promoter (hereinafter denoted as SYN-NBL10). When crossing *Mc4r^{gfp}* mice with SYN-NBL10 mice, MC4R-GFP binds to NBL10, and thus, to the ribosome, which stabilizes MC4R-GFP, allowing for the visualization of MC4R-GFP-expressing neurons with a widefield microscope (Figure 1B,D,F).

Mapping of MC4R-expressing neurons

In *Mc4r^{gfp} hSyn-NBL10^{tg}* brain slices, MC4R-GFP signal is very bright, allowing for expression mapping of MC4R throughout the mouse brain. Although GFP⁺ cells can clearly be identified without antibody staining, immunofluorescence staining against GFP was performed to increase

the signal and decrease the effect of photobleaching after scanning the slides for subsequent stitching of the images. The Online Allen brain atlas and the Paxinos brain atlas were used as a reference to map GFP⁺ cells. Some representative sections are shown in figure 2 and discussed below.

MC4R-GFP SYN-NBL10 positive cells recapitulated previously published mappings of MC4R expression. More precisely, the *MC4R^{tdaCre} tdTomato* knock-in mouse reported by Garfield *et al.*⁵⁵ and the BAC *MC4R::GFP* transgenic mouse line reported by Hongyan Liu *et al.*¹¹⁸.

Regarding the main nuclei implicated in the leptin melanocortin pathway, MC4R is expressed in a great number of neurons in the PVN, Ventromedial nucleus (VMH) and Dorsomedial nucleus (DMH), but in very few neurons in the Arcuate nucleus (ARC). Other hypothalamic nuclei where MC4R is expressed in adult mice are: the preoptic area (PO), the anterior hypothalamic nucleus (AHN), and in a small number of cells in the Lateral hypothalamus (LH).

From rostral to caudal, MC4R expression appears to be scattered but very consistent at different levels of the olfactory system. It is abundantly expressed in the olfactory bulb, the olfactory piriform cortex, the tenia tecta (TTd). Interestingly, the GFP signal was most intense in the L2 of the nucleus of the lateral olfactory tract (nLOT).

In the rest of the cortex, MC4R is expressed preferentially in layer 5, including the orbital area (ORB), the motor cortex (Mo) and the gustatory area (GU5). MC4R is also expressed in the Peduncular Cortex (DP), the dorsal part of the anterior cingulate area (ACAd), and infralimbic and prelimbic areas.

In the amygdala, the nuclei with higher number of cells are the medial amygdalar nucleus (MeA), the basomedial amygdalar nucleus (BMA), and the medial subdivision of the central amygdala (CeM)

In the striatum, MC4R expression was detected in the ventral pallidum.

Sparse expression of Mc4r was found in the Hippocampus, contrasting with the intense expression detected previously by transgenic approach¹¹⁸ or CRE-mediated recombination¹¹⁹, although the level of expression varied depending on the analyzed bregma.

In the caudal part of the brain, MC4R was expressed in the midbrain, in the pons and the medulla, but not in the cerebellum.

In the midbrain, MC4R is expressed in the red nucleus (RN). In the pons and medulla, MC4R is expressed in the Lateral parabrachial nucleus (LPBN), the magnocellular reticular nucleus (MARN).

Trapping MC4R on the ribosome leads to obesity, mimicking a *MC4R* knockout phenotype

Since we established that some MC4R mutations found in patients with obesity reduced MC4R enrichment to cilia without affecting its activity⁵⁶, we sought to investigate whether preventing MC4R from localizing to the primary cilium, by trapping it onto ribosome in *Mc4r^{gfp} SYN-NBL10*-expressing mice, would lead to obesity.

Body weight and fat mass assessment revealed that the insertion of a GFP tag at the C-terminus of MC4R does not have a statistically significant effect on the phenotype of these mice. Similarly, the expression of a neuronal nanobody did not have an effect on the body weight and fat mass of the *SYN-NBL10* mice compared to their wild type littermates (Figure 3C,D). Notably, co-expression of MC4R-GFP and NBL10 lead to severe obesity (Figure 3B-E), with a higher fat mass (Figure 3D) both in males and females. Notably, the heterozygous *Mc4r^{gfp/+} SYN-NBL10* mice displayed an intermediate body weight and fat mass, phenocopying mice carrier of *Mc4r* heterozygous mutation, accounting for the haploinsufficiency of this gene⁵³. Together, these results show that excluding MC4R from the primary cilia by ribosome trapping prevents this receptor from exerting its function as a principal regulator of body weight and energy homeostasis.

MC4R ciliary localization mapping.

After mapping the expression of MC4R in the brain of the *Mc4r^{gfp} hSyn-NBL10^{Tg}* mouse, we sought to investigate whether MC4R also localizes to the primary cilia in regions other than the PVN. To this end, we analyzed coronal brain sections from the *Mc4r^{gfp}* mouse, focusing on some of the regions where MC4R expression was mapped, and assessed the co-localization of MC4R-GFP with ADCY3 (Figure 4).

Our data showed that in ad-libitum fed adults, MC4R localizes to primary cilia in most regions (yellow arrows in Figure 4), including the BNST, medial preoptic area, LOT, ARC, DMH and VMH, RN (“RMC”), SNR, PIF and solitary nucleus. However, in some nuclei like the ARC, VMH, DMH, RN (“RMC”), SNR and solitary nucleus (NTS), MC4R-GFP signal also intensely labels the neuronal soma and projections. Labelling of the soma can also be seen in other nuclei, but less intensely (nLOT, medial preoptic area, BNST, PVN). Analysis of confocal sections reveals that the signals is not specifically located at the cell membrane, but rather fills the cell body (not shown).

Interestingly, in the cortex, MC4R-expressing neurons appear to have a round morphology and larger size, and no ciliary-expressed MC4Rs could be identified (Figure 4A,B).

Together, these results show that while MC4R is expressed in different regions throughout the brain, its subcellular localization likely depends on the neuronal type it is expressed in, and it is therefore, region-dependent.

MC4R ciliary localization is dynamically regulated and responds to physiological status.

MC4R expression in the PVN is essential to regulate food intake and body weight⁵⁴. During development, there is a positive energy imbalance reflected by growth and increasing body weight¹²⁰. Since MC4R activity encodes anorexigenic signals, we sought to analyze whether MC4R ciliary localization would be altered in early stages of development. To this end, we assessed ciliary localization of MC4R in early postnatal mouse pups at age P2, P6, P11 and P15. Interestingly, we found that MC4R is highly enriched at the primary cilium of PVN neurons in early postnatal days compared to adults (Figure 2.1, Chapter 2 [published]).

Since adult mice housed in regular conditions have *ad libitum* access to food and are therefore never calory deprived, we sought to investigate whether disrupting energy balance by subjecting mice to caloric restriction would have an impact on MC4R ciliary enrichment. For this pilot

experiment, baseline food intake of *Mc4r^{gfp/gfp}* adult littermates was measured for 4 days, and they were subsequently divided into two groups that were either fed ad libitum or at 75% caloric restriction (CR) on low fat diet for a week. These mice were subjected to a final 48h fast before sacrifice in order to maximize the potential effects. Strikingly, we observed a drastic increase in MC4R ciliary enrichment and MC4R-positive cilia in the PVN of CR mice compared to ad-libitum littermates (Figure 5c). These results demonstrate that MC4R localization is also dynamic in adult mice and represent changes in physiological state.

MC4R ciliary localization depends on leptin and AgRP expression.

Since Leptin levels decrease with fasting and caloric restriction¹²¹, we hypothesized that MC4R ciliary enrichment would be maximal in Leptin knock-out animals. We generated *Mc4r^{gfp/gfp} Lep^{Ob/Ob}* mice from which we collected hypothalamic sections that we compared to their *Mc4r^{gfp/gfp} Lep^{+/+}* littermates. As predicted, MC4R localization was dramatically increased in the PVN of *Mc4r^{gfp/gfp} Lep^{Ob/Ob}* mice compared to their wild-type littermates (Figure 6).

Leptin conveys information about fat storage to the ARC POMC- and AgRP-expressing neurons, that further relay this information to MC4R neurons. In order to ensure long-term energy homeostasis, leptin activates *Pomc* expression while simultaneously repressing *Agrp* expression. During fasting, circulating leptin levels drop and AgRP expression is increased. The same is observed in *Ob/Ob* mice, in which AgRP levels are higher compared to their wild type littermates¹²². We therefore sought to investigate whether MC4R ciliary enrichment in *Ob/Ob* mice was dependent on AgRP. To this end, we generated mice knock-out for *Agrp* in the *Mc4r^{gfp/gfp} Lep^{Ob/Ob}* background. Two different AgRP null stains were used for the following experiments. We used previously characterized AgRP knock out mouse model expressing an allele obtained by targeting a diphtheria toxin receptor (DTR) cassette in the *Agrp* locus. The *AgRP^{DTR}* allele is a knock-out allele that enables temporal ablation of AgRP neurons after diphtheria toxin (DT) inoculation³⁷. Homozygote *Agrp^{DTR/DTR}* animals therefore do not express AgRP, and AgRP neurons integrity is preserved unless DT is injected. In order to study whether AgRP is necessary for MC4R ciliary enrichment observed in *Ob/Ob* mice, we first generated *Mc4r^{gfp/gfp} Lep^{Ob/Ob} AgRP^{DTR/DTR}* mice, and compared them to *Agrp* wild type littermates, without DT administration. Interestingly, we observed that, in the PVN of *Mc4r^{gfp/gfp} Lep^{Ob/Ob} AgRP^{DTR/DTR}* mice, MC4R did not localize to primary cilia, and filled the neuronal soma, demonstrating that AgRP expression is necessary for MC4R ciliary enrichment in absence of leptin (Figure 7A,B). Since *Agrp^{DTR/DTR}* mice are developmental homozygote null, we sought to investigate whether we would observe similar results if AgRP neurons were ablated in adult mice. Deletion of AgRP neurons in this model has previously been shown to lead to decreased food intake that could lead to dramatic weight loss³⁷. *Mc4r^{gfp/gfp} Lep^{Ob/Ob} AgRP^{DTR/+}* mice and their *Mc4r^{gfp/gfp} Lep^{Ob/Ob} AgRP^{+/+}* littermates were injected with DT at 7 weeks of age, and were perfused one week later (Figure 6C). While DTR-expressing mice lost on average 20% of their body weight, their wild-type littermates gained 20% weight in the same period of time (n=2 per group, not shown). In line with the previous results, deletion of AGRP neurons in adult mice lead to a decrease in MC4R ciliary localization after injecting DT into *Mc4r^{gfp/gfp} Lep^{Ob/Ob} AgRP^{DTR/+}* mice, compared to the mice that did not express the DTR (Figure 6D).

Since MC4R ciliary localization is increased in pups, we sought to determine whether knocking out *Agrp* would have an effect on ciliary enrichment of MC4R in this model. We generated *Mc4r^{gfp/gfp}*

AgRP^{-/-} P6 pups (An *Agrp* null model was used in this experiment), and we assessed MC4R ciliary localization (n=4 per group). Strikingly, in this model, almost no MC4R could be detected in the PVN of *Mc4r*^{gfp/gfp} *AgRP*^{-/-} pups, while we observed high enrichment in wild type littermates (Figure 6F).

Collectively, these data demonstrate that MC4R ciliary localization is AgRP-dependent.

We therefore hypothesized that chronic infusion of exogenous AgRP into the brain of *Mc4r*^{gfp/gfp} mice would lead to the enrichment of MC4R at the primary cilia. *Mc4r*^{gfp/gfp} female littermates were divided into two groups (n=4) and were either implanted with an intracerebroventricular (i.c.v) cannula connected to a subcutaneous micro-osmotic pump filled with AgRP, or received a Sham surgery. After 10 days of infusion, the AgRP-infused mice had gained significantly more weight than their control littermates, and MC4R ciliary localization was dramatically increased (Figure 8).

Together, these results demonstrate that higher AgRP levels lead to increased MC4R localization at the cilium.

Discussion and future directions

This chapter describes new insights into MC4R ciliary localization throughout the brain and how it is subject to changes depending on the physiological status and MC4R ligands levels.

We report a strategy to map the expression of GFP-tagged GPCRs in neurons, using our MC4R-GFP knock-in mouse model, that is specific, sensitive, and CRE-independent. We show that ribosomal trapping of GFP stabilizes and enhances the fluorescent signal allowing for extensive mapping of neuronal MC4R expression, by making the MC4RGFP-expressing neurons easily detectable with a widefield microscope. Using this information, we then determined the extent of MC4R localization to the primary cilia in some of the identified regions. Interestingly, in an ad lib fed mouse, MC4R subcellular localization does not seem to be uniform across the brain. As we show that caloric restriction and increase in AgRP concentration lead to increased MC4R ciliary localization, it will be interesting to analyze other brain regions in these conditions so assess whether changes in ligand balance affect MC4R in the same way outside of the PVN. While MC4R expression in the PVN is critical for the control of food intake and body weight but not energy expenditure, its function in other nuclei inside and outside of the hypothalamus is not clear. Other hypothalamic regions like the lateral hypothalamus (LHA), the ventromedial (VMH) and dorsomedial (DMH) nuclei have been previously implicated in different aspects of energy balance, like regulation of energy expenditure, glucose tolerance, hedonic feeding or food preference and reward pathways^{41,123}. However, rescued *Mc4r* expression in null animals specifically in the lateral parabrachial nucleus (LPBN), the nucleus of the solitary tract (NTS) and dorsomedial nucleus of the vagus (DMV), or the lateral hypothalamus do not affect food intake⁴¹. It will be interesting to determine whether MC4R preferential localization to cilia is specific neuronal populations that regulate energy balance, and if those regions are specifically innervated by projections from AGRP and/ or POMC neurons.

Interestingly, ribosomal trapping of MC4R led to obesity resembling *Mc4r* mutation phenotype, demonstrating that ribosomal trapping of GFP-tagged GPCRs can be used to link expression of a

neuronal GPCR of interest to their function. It is important to note that trapping MC4R on ribosomes could also impair MC4R transport to the cell membrane, and therefore cannot be considered as an evidence that MC4R function at the primary cilia is essential for the regulation of body weight. Complementary experiments specifically targeting the primary cilia of MC4R neurons are required to test this hypothesis, and are described in chapter 2.

Lastly, we further characterized the dynamics of MC4R subcellular localization in the PVN in different physiological conditions, including calory-restriction and leptin deficiency-associated obesity. Our preliminary data indicate that MC4R enrichment at the primary cilium is increased in conditions where AgRP levels are high, suggesting that MC4R ciliary localization is dependent on its ligand concentrations and therefore its activity. These observations lead to the concept that MC4R ciliary localization could be inversely correlated with its activity, since AgRP is MC4R's endogenous antagonist. This hypothesis is counterintuitive since, as described in chapter 2, we demonstrated that MC4R ciliary localization is necessary for MC4R to control food intake and body weight. However, it is well known that activated GPCRs are retrieved from the primary cilium, either by BBS-mediated retrieval from cilia back into the cell or by a process called ectocytosis, by which cilia shed vesicles called ectosomes, containing activated GPCRs, into the extracellular environment¹²⁴. Therefore, one hypothesis could be that the lifetime of activated MC4R in cilia is short, leading to a smaller number of molecules in primary cilia at any given time, hindering its visualization, while inhibited MC4R cannot exit the cilium until it is activated, consequently increasing the signal to be detected.

Technically speaking, it will be imperative to development automated methods to consistently quantify the ciliary enrichment of MC4R and its downstream effector ADCY3 in different physiological and pharmacological conditions, which will allow to perform dose-response analyses of their ciliary enrichment against infused ligand concentrations.

Future experiments will be geared towards mechanistic studies aimed at understanding the relationship between ciliary dynamics and MC4R signaling *in vivo*.

Figures

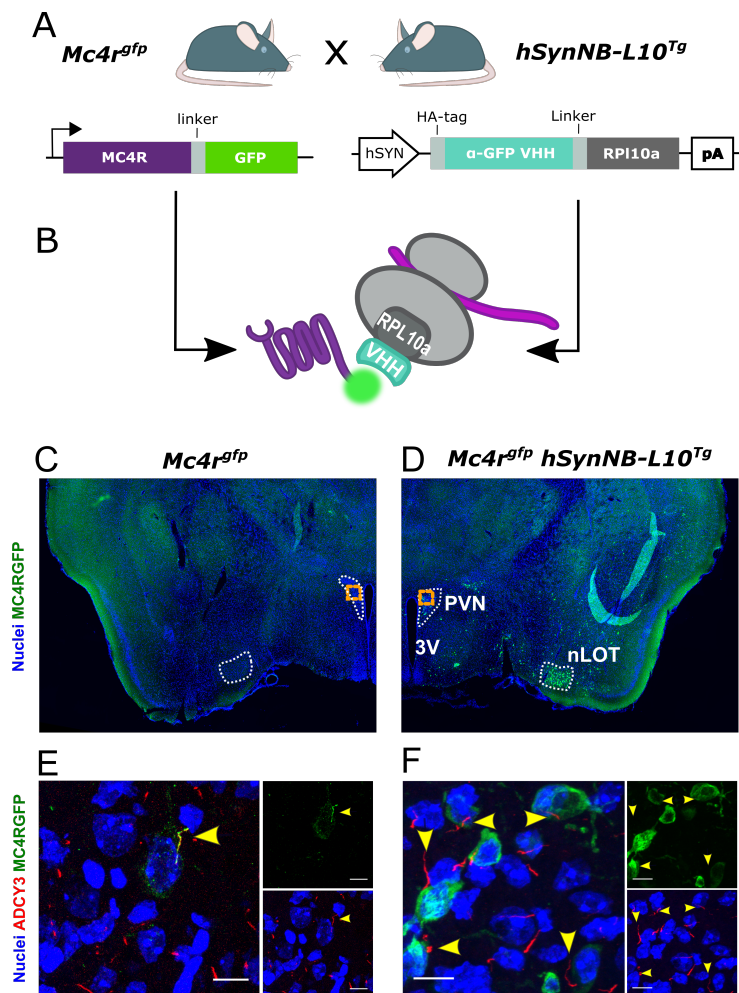


FIGURE 1.1 RIBOSOMAL TRAPPING OF MC4R-GFP STABILIZES AND ENHANCES GFP SIGNAL, ALLOWING FOR IDENTIFICATION OF MC4RGFP-EXPRESSING NEURONS AT LOW MAGNIFICATION.

A) Breeding strategy for the obtention of *Mc4r^{gfp} hSynNB-L10^{tg}* mice. Left: the *Mc4r^{gfp}* knock-in mouse expresses the endogenous MC4R fused to GFP; Right: *hSynNB-L10^{tg}* transgenic mice express an anti-GFP nanobody (α -GFP VHH) fused to the N terminus of the ribosomal subunit protein RPL10a, under the control of the neuron-specific human synapsin promoter (hSyn). B) Graphic representation of the interaction between MC4R-GFP and NBL10. When both constructs are expressed, the anti-GFP nanobody fused to a ribosomal subunit binds MC4R-GFP. C. Coronal section of the brain of the *Mc4r^{gfp}* knock-in mouse compared to the same bregma (B=-0.9) in a *Mc4r^{gfp} Syn-NBL10^{tg}* mouse. MC4R-expressing neurons can be observed in the PVN and the LOT. Scale bar, 1mm. E-F) Confocal images representing orange inserts from (C) and (D). E) Ciliary localization of MC4R in the PVN of the *Mc4r^{gfp}* knock-in mouse. F) Soma sequestration of MC4R-GFP when NBL10 is co-expressed. Nuclei (blue), ADCY3 (red), MC4R-GFP (green). Scale bar, 10um. PVN: paraventricular nucleus of the hypothalamus, nLOT: nucleus of the lateral olfactory tract.

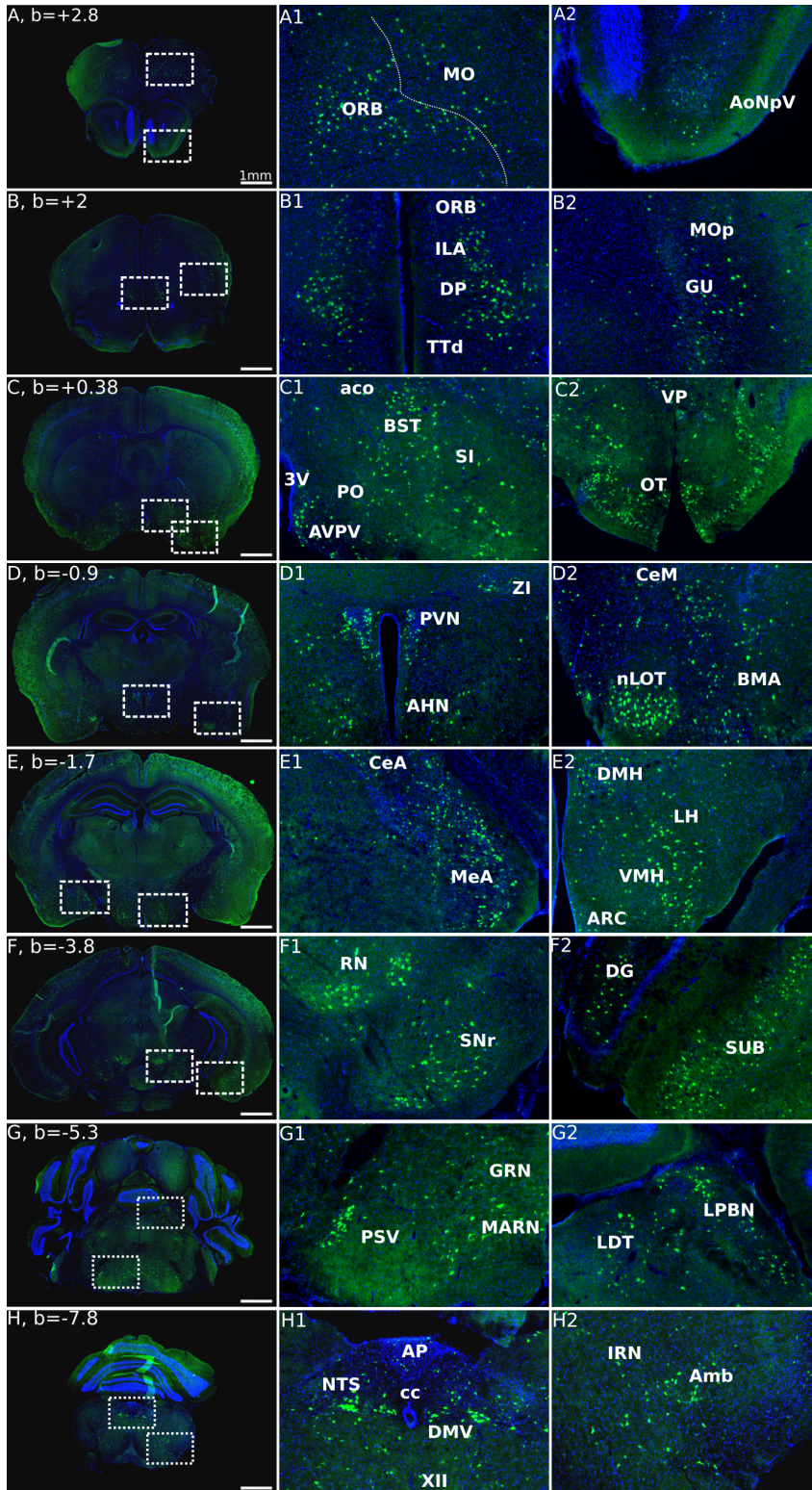


FIGURE 1.2: MC4R EXPRESSION MAPPING.

Brain sections of *Mc4r^{gfp} hSynNB-L10^{tg}* mice are arranged in a rostral-to-caudal manner. Second and third columns are inserts from the first column. ACAd, dorsal part of the anterior cingulate area; aco, anterior commissure, olfactory limb; AHN, anterior hypothalamus nucleus; Amb, nucleus ambiguus AONPV, anterior olfactory nucleus posteroventral part; AP, area postrema; ARC, arcuate nucleus; AVPV, anteroventralperiventricular nucleus; BMA, basomedial amygdalar nucleus; BST, bed nuclei of the stria terminalis; Cc, central canal; CeA, central nucleus of the amygdala; CeM, central medial amygdala; CeM, medial subdivision of the central amygdala; DG, dentate gyrus; DMH, dorsomedial Hypothalamus; DMV, dorsal motor nucleus of the vagus nerve; DP, dorsal peduncular cortex; GRN, gigantocellular reticular nucleus; GU, gustatory area; IC, inferior colliculus; ILA, infralimbic area; IRN, intermediate reticular nucleus; LDT, laterodorsal tegmental nucleus; LH, lateral hypothalamus; LPBN, lateral parabrachial nucleus; MARN, magnocellular reticular nucleus; MARN, magnocellular reticular nucleus; MeA, medial amygdalar nucleus; MO, motor area; MO, motor area; MOp; primary motor area; nLoT, nucleus of lateral olfactory tract; NTS, nucleus of the solitary tract; ORB, orbital cortex; OT, olfactory tubercle; PO, preoptic area (PO); PSV, principal sensory nucleus of the trigeminal; PVN, paraventricular Nucleus of the hypothalamus; RN, red nucleus; SI, substantia innominata; SNr, substantia nigra; SUB, subiculum; TTd, taenia tecta; VMH, ventromedial hypothalamus; VP, ventral pallidum; XII, hypoglossal nucleus; ZI, zona incerta.

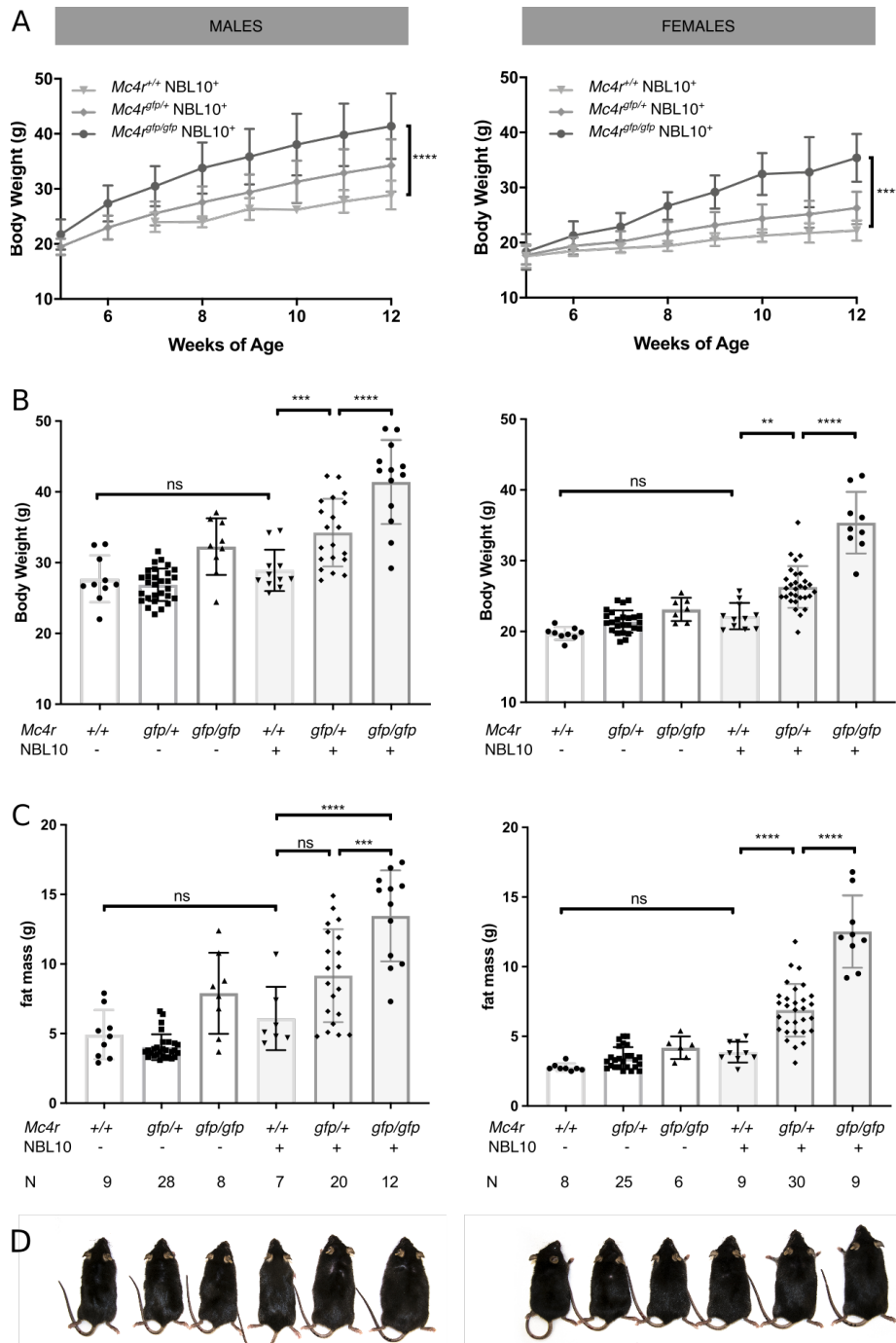


FIGURE 1.3: PHENOTYPIC CHARACTERIZATION OF THE *NBL10* *Mc4R*^{GFP} MICE

Trapping MC4R at the ribosome by NBL10 leads to obesity.

A) Body weight curves of NBL10+ mice (left, males; right, females), co-expressing the wild type allele of *Mc4r* compared to heterozygous and homozygous expression of the *Mc4r*^{gfp} allele. Body weight (B), fat mass (C), and phenotype (D) of mice wild type, heterozygous or homozygous for the *Mc4rgfp* allele, co-expressing NBL10 or not (left, males; right, females). 2way (A) and One way Anova with Tukey's multiple comparison test (B,C). **p≤ 0.01; ***p≤0.001; ****p≤0.0001.

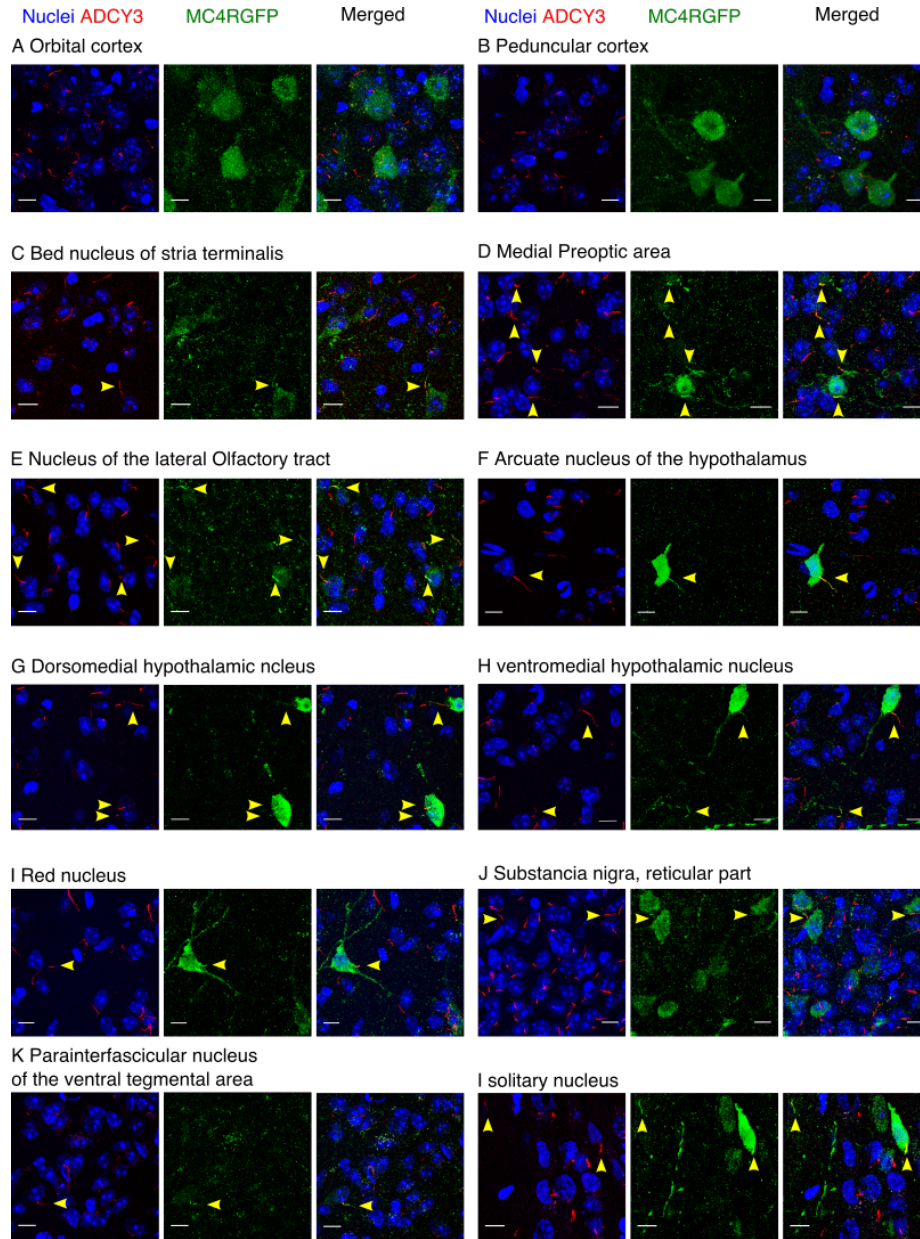


FIGURE 1.4 ASSESSMENT OF CILIARY LOCALIZATION OF MC4R LOCALIZATION IN REGIONS OTHER THAN PVN.

Representative confocal images of different brain regions where MC4R is expressed in an *Mc4r^{gfp}* mouse. Immunofluorescent imaging of primary cilia (ADCY3, red) and GFP (MC4R-GFP, Green), nuclei (blue). A) ORB, Orbital Cortex; B) DP, Peduncular cortex; C) BNST, Bed nucleus of the stria Terminalis; D) MPO, Medial Preoptic Area; E) nLOT, Nucleus of the lateral Olfactory Tract F) ARC, Arcuate Nucleus; G) DMH, Dorsomedial Hypothalamus; H) VMH, Ventromedial Hypothalamus; I) RMC=RN (Change!), Red Nucleus ; J) SNR, Substantia Nigra, Reticular Part ; K) PIF, Parainterfascicular nucleus of the Ventral Tegmental Area ; L) NTS, Nucleus of solitary tract. Scale bar, 10um.

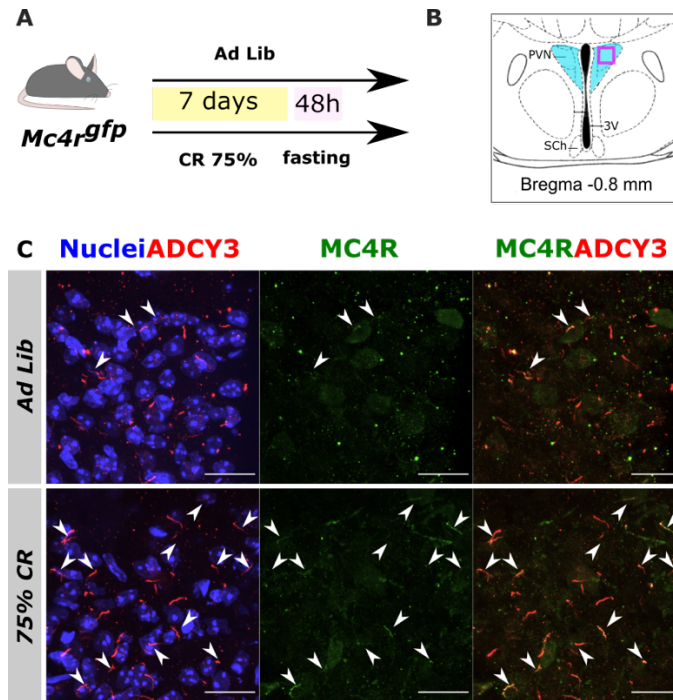


FIGURE 1.5: CALORIC RESTRICTION LEADS TO INCREASED MC4R CILIARY ENRICHMENT.

A) Experimental protocol schematic. *Mc4r^{gfp/gfp}* littermates (n=2 per group) were fed low fat diet from weaning, then continued on the diet ad libitum or at 75% for a week, followed by a 48h fast prior to perfusion. B) Schematic representation of hypothalamic region studied. C) Representative images of PVN sections of *Mc4r^{gfp/gfp}* mice after Ad Libitum feeding (top) or 75% Calor restriction (bottom). Immunofluorescent imaging of primary cilia (ADCY3, red) and MC4R-GFP (Green), nuclei (blue). Arrows indicate MC4R-GFP⁺ cilia. Scale bar, 20 μm. PVN: paraventricular nucleus; 3V: third ventricle; Sch: Suprachiasmatic nucleus.

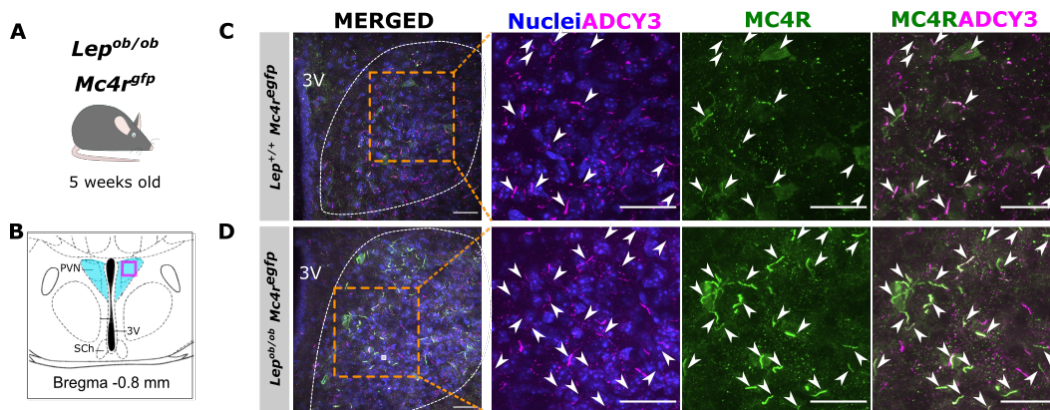


FIGURE 1.6: MC4R CILIARY ENRICHMENT DEPENDS ON LEPTIN

A) Mouse model: *Lep^{ob/ob} Mc4r^{gfp/gfp}* and their *Lep^{+/+} Mc4r^{gfp/gfp}* littermate mice were perfused at 5 weeks old. At least 5 animals were assessed per genotype. B) Schematic representation of hypothalamic region studied. C-D) Representative images of PVN sections of *Lep^{+/+} Mc4r^{gfp/gfp}* (C) and *Lep^{ob/ob} Mc4r^{gfp/gfp}* littermates (D). Immunofluorescent imaging of primary cilia (ADCY3, magenta) and MC4R-GFP (Green), nuclei (blue). Arrows indicate MC4R-GFP⁺ cilia. Scale bar, 20 μm. PVN: paraventricular nucleus; 3V: third ventricle; Sch: Suprachiasmatic nucleus.

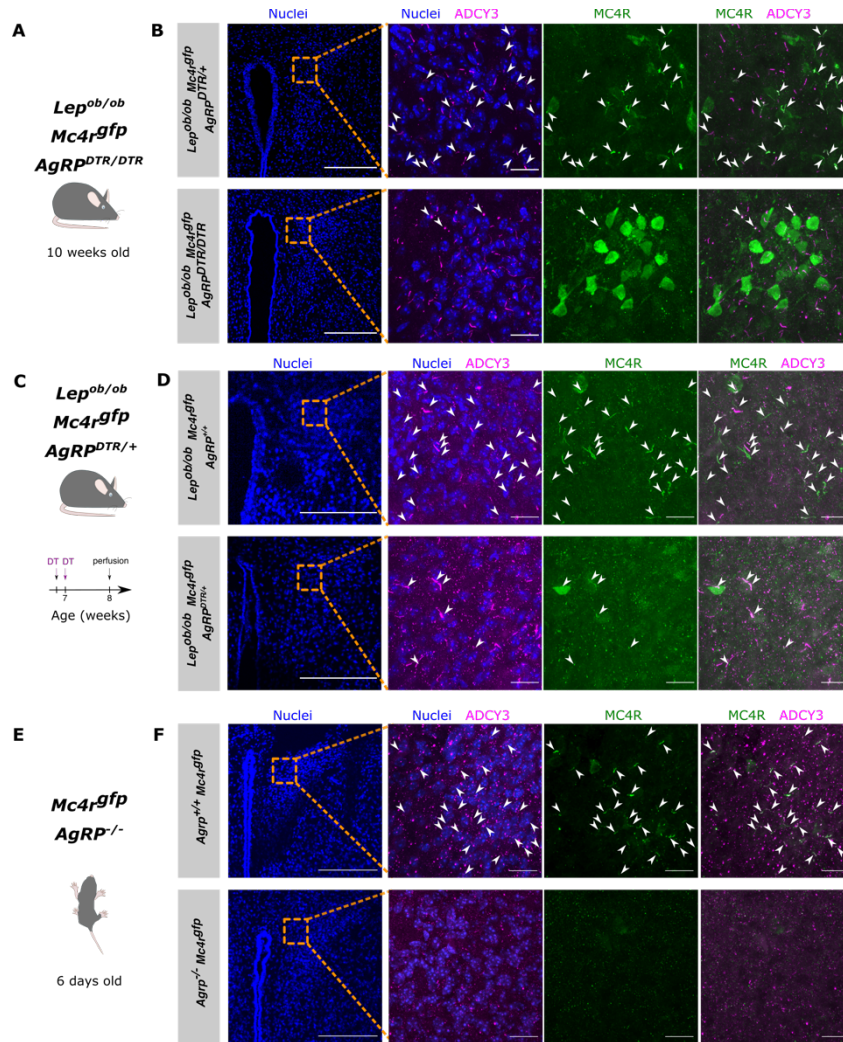


FIGURE 1.7: MC4R CILIARY ENRICHMENT DEPENDS ON AGRP EXPRESSION IN ADULT MICE AND IN PUPS.

A-D) MC4R ciliary enrichment is dependent on AgRP expression in adult mice. A) Mouse model: *Lep^{Ob/Ob} Mc4r^{gfp} AgRP^{DTR/DTR}* mice and their *Lep^{Ob/Ob} Mc4r^{gfp} AgRP^{DTR/+}* littermates were perfused at 10 weeks old. Two animals were analyzed per genotype. B) Representative images of PVN sections of a *Lep^{Ob/Ob} Mc4r^{gfp} AgRP^{DTR/+}* mouse (top) and a *Lep^{Ob/Ob} Mc4r^{gfp} AgRP^{DTR/DTR}* littermate (bottom). C-D) Deletion of AgRP neurons in adult mice leads to decreased MC4R ciliary enrichment in *Ob/Ob* mice. C) Mouse model and experimental design: *Lep^{Ob/Ob} Mc4r^{gfp} AgRP^{DTR/+}* mice and their *Lep^{Ob/Ob} Mc4r^{gfp} AgRP^{+/+}* littermates were injected with DT at 7 weeks of age and perfused at 8 weeks old. Two animals were analyzed per genotype. D) Representative images of PVN sections of a *Lep^{Ob/Ob} Mc4r^{gfp} AgRP^{+/+}* mouse (top) and a *Lep^{Ob/Ob} Mc4r^{gfp} AgRP^{DTR/+}* littermate (bottom) one week following DT injection. E-F) MC4R ciliary enrichment is dependent on AgRP expression in P6 pups. E) Mouse model: *Mc4r^{gfp} AgRP^{+/+}* mice and their *Mc4r^{gfp} AgRP^{-/-}* littermates were perfused at 6 days old. At least 4 animals were analyzed per genotype. F) Representative images of PVN sections of a *Mc4r^{gfp} AgRP^{+/+}* mouse (top) and a *Mc4r^{gfp} AgRP^{-/-}* littermate (bottom). Immunofluorescent imaging of primary cilia (ADCY3, magenta) and GFP (MC4R-GFP, Green), nuclei (blue). Arrows indicate MC4R-GFP⁺ cilia. Scale bars, 200 (left panel) and 20 μ m (insets). PVN: paraventricular nucleus; 3V: third ventricle; Sch: Suprachiasmatic nucleus; DT: Diphtheria toxin.

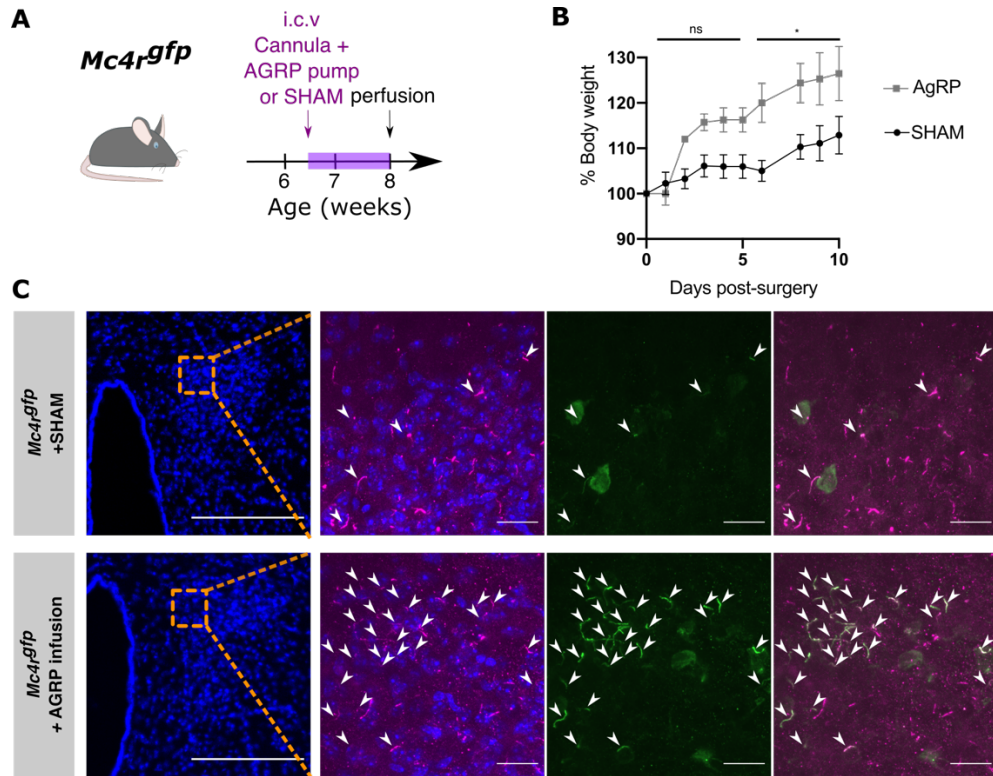


FIGURE 1.8: CHRONIC AGRP INFUSION LEADS TO INCREASED MC4R CILIARY LOCALIZATION

A) Mouse model and experimental design: *Mc4r^{gfp}* female littermates (n=4 per group) were either implanted with an intracerebroventricular (i.c.v.) cannula connected to a subcutaneous micro-osmotic pump filled with AgRP, or received a Sham surgery. The mice were perfused 10 days after 10 days after surgery. B) Body weight curve following surgery. C) Representative images of PVN sections of a *Mc4r^{gfp}* infused with AgRP (bottom) and controls (top). Left panel represent lower magnification depicting the PVN and third ventricle of which right panels are insets. Immunofluorescent imaging of primary cilia (ADCY3, magenta) and GFP (MC4R-GFP, Green), nuclei (blue). Arrows indicate MC4R-GFP⁺ cilia. Scale bars, 200 (left panel) and 20 μ m (insets). i.c.v., intracerebroventricular.

Methods

Origin of the mouse lines used.

Mice were housed (with enrichment) in a barrier facility and maintained on a 12:12 light cycle (on: 0700-1900) at an ambient temperature of $23\pm 2^{\circ}\text{C}$ and relative humidity 50-70 %. Mice were fed with rodent diet 5058 (Lab Diet) and group-housed up to 5 or single housed after surgery. Experiments were performed with weight and sex-matched littermates. *Mc4r*^{tm1(egfp)Vai} mice express an EGFP tag inserted in frame at the C-terminus of the endogenous *Mc4r* locus (Vaisse lab⁵⁶); hSyn-NBL10^{Tg} mice express a transgene encoding an anti-GFP single-chain antibody (Nanobody) expressed under the control of human synapsin promoter, and were obtained from Dr Zachary Knight (UCSF)¹²⁵. B6.129S4-Agrp^{tm2(DTR)Rpa/J} (Agrp^{DTR}) and B6.Cg-*Lep*^{ob/J} mice were obtained from the Jackson Laboratory. *Agrp* null mice¹²⁶ were obtained from Dr Allison Xu, UCSF.

Stereotaxic Surgeries for i.c.v cannula implantation.

Animals were anesthetized with an initial flow of 4% isoflurane, maintained under anesthesia using 2% isoflurane and kept at 30-37°C using a custom heating pad. The surgery was performed using aseptic and stereotaxic techniques. Briefly, the animals were put into a stereotaxic frame (KOPF Model 1900, USA), the scalp was opened, the planarity of the skull was adjusted and holes were drilled (coordinates: lateral ventricle for cannula implantation [AP=-0.3, ML=1.0, DV=-2.5]). The cannulas (Alzet brain infusion kit, 2.5mm) were implanted and secured to the skull using a tissue bonding glue (Loctite 454) and dental acrylic. The cannulas were connected to the micro-osmotic pumps (Alzet, model 1002, 0.25µl/h, 1.5µg AgRP/day in aCSF) through a catheter filled with artificial cerebrospinal fluid (aCSF) and implanted subcutaneously. Animals were given pre-operative analgesic (buprenorphine, 0.3 mg/kg) and post-operative anti-inflammatory Meloxicam (5mg/Kg). Animals were singly-housed until the end of the experiment.

Mouse metabolism studies.

Weight was measured weekly, or as mentioned in figures. Fat mass and lean mass were measured using Dual Energy X-ray Absorptiometry (DEXA, Piximus). Food intake was assessed by hand by measuring food intake every 24h. Caloric restriction was done manually, by delivering 75% of baseline food intake every day before 7PM.

Diphtheria toxin injections

Diphtheria toxin (1µg in 200µl PBS) was injected twice 2 days apart at age 7weeks.

Direct fluorescence and immunofluorescence studies of mouse hypothalamus.

Mice were perfused trans-cardially with PBS followed by 4% paraformaldehyde fixation solution. Brains were dissected and post-fixed in fixation solution at 4°C overnight, soaked in 30% sucrose solution overnight, embedded in O.C.T. (Tissue-Tek, Sakura Finetek USA, INC., Torrance, CA), frozen, and cut into 20-35 µm coronal sections, then stored at -80°C until staining.

After washing, sections were blocked for 1 hr in 50% serum 50% antibody buffer (1.125, %NaCl, 0.75%Tris base, 1%BSA, 1.8 %L-Lysine, 0.04% azide), followed by incubation with primary antibody overnight at 4°C. After washing, sections were incubated with secondary antibodies for an hour at

room temperature, washed and stained with Hoechst (1:5000), washed and mounted with Prolong™ Diamond antifade Mountant. Primary antibodies used: Chicken anti-GFP (Abcam, ab13970), 1:250; Rabbit anti-Adcy3 (Santa Cruz Biotechnology, sc-588). Secondary antibodies used: Goat anti-chicken Alexa fluor 488 (Invitrogen, A11039), 1:500; Goat anti-rabbit Alexa fluor 633 or 555 (Invitrogen, A21070, A21429), 1:500.

Image capture and processing.

Confocal images were generated using a Zeiss LSM 780 confocal microscope (Figure 1E,F and 4) or a Nikon W1 spinning disk confocal (Figures 5-7). Images were processed with Fiji. Maximal intensity Z projections are from at least 20 slices over 10-20 μm . Widefield Images of coronal sections of *hSyn-NBL10^{Tg} Mc4r^{gfp}* mouse brains (Figure 1C,D and Figure 2) were generated using an Keyence B7-X710. 10x images were stitched with the Keyence BZ analysis software to cover entire coronal sections.

Statistical analysis

Sample sizes were chosen based upon the estimated effect size drawn from previous publications (Siljee et al., 2018) and from the performed experiments. Data distribution was assumed to be normal, but this was not formally tested. Statistical analysis was performed using unpaired Student t test or repeated measures of two-way ANOVA followed by Sidak's multiple comparisons test, as indicated. All data were expressed as mean \pm SEM. A p-value ≤ 0.05 was considered as statistically significant. All data were analyzed using Prism 8.0 (GraphPad Software).

Transition

In the previous chapter we established that MC4R is enriched at the neuronal primary cilia in the PVN of adult mice, and that it is subject to changes depending on physiological conditions and ligand availability.

Although a number of GPCRs have been recently been identified to localize to primary cilia, the importance of this localization for their function is not clear.

Since MC4R expression in the PVN has been shown to be both necessary and sufficient for the control of food intake and body weight, we next sought to investigate whether this specific localization is strictly necessary for MC4R to signal satiety.

Chapter 2 : Melanocortin-4 receptor signals at the neuronal primary cilium to control food intake and body weight

Yi Wang*, Adelaide Bernard*, Fanny Comblain, Xinyu Yue, Christophe Paillart, Sumei Zhang, Jeremy F. Reiter, Christian Vaisse

Published in the Journal of Clinical investigation, 10.1172/JCI142064¹¹⁹

Summary

The Melanocortin-4 Receptor (MC4R) plays a critical role in the long-term regulation of energy homeostasis and mutations in MC4R are the most common cause of monogenic obesity. However, the precise molecular and cellular mechanisms underlying the maintenance of energy balance within MC4R expressing neurons are unknown. We recently reported that MC4R localizes to primary cilia, a cellular organelle that allows for partitioning of incoming cellular signals, raising the question of whether MC4R functions there. Here, using mouse genetic approaches, we found that cilia were required specifically on MC4R-expressing neurons for control of energy homeostasis. Moreover, these cilia were critical for pharmacological activators of MC4R to exert an anorexigenic effect. MC4R is expressed in multiple brain regions. Using targeted deletion of primary cilia, we found that cilia in the paraventricular nucleus (PVN) of the hypothalamus were essential to restrict food intake. MC4R activation increases adenylyl cyclase activity. Like removing cilia, inhibiting adenylyl cyclase activity in the cilia of MC4R-expressing neurons of the PVN caused hyperphagia and obesity. Thus, MC4R signals via cilia of PVN neurons to control food intake and body weight. We propose that defects in ciliary localization of MC4R cause obesity in human inherited obesity syndromes and ciliopathies.

Introduction

Most mammalian cells, including neurons, possess a single, immotile primary cilium, an organelle that transduces select signals¹²⁷. Defects in the genesis or function of primary cilia cause a range of overlapping human diseases, collectively termed ciliopathies¹²⁸. Several ciliopathies, such as Bardet-Biedl syndrome and Alström syndrome, cause obesity, and mutations in genes encoding ciliary proteins, such as *CEP19*, *ANKRD26* and *ADCY3*, cause non-syndromic obesity in mice and humans^{129–132}. While the mechanisms underlying a number of cilia-associated phenotypes, such as polycystic kidney disease or retinal degeneration, have been at least partly elucidated, how ciliary dysfunction leads to obesity remains poorly understood^{133,134}. Since primary cilia are essential for embryonic development, in particular through their critical role in Hedgehog signaling^{135,136}, one hypothesis is that obesity could result from perturbations in the development of cells and pathways implicated in the regulation of energy homeostasis. However, ubiquitous ablation of the primary cilia in adult mice or from neurons also leads to obesity¹³⁷. This finding indicates that neuronal primary cilia are post-developmentally required for the function of one or more signaling pathway implicated in the regulation of energy homeostasis.

We recently demonstrated that the melanocortin-4 receptor (MC4R) localizes to the neuronal primary cilia in vivo¹³⁸. MC4R is a G protein-coupled receptor (GPCR) essential for long-term regulation of energy homeostasis⁴¹. In humans, polymorphisms at the *MC4R* locus are tightly associated with obesity in genome wide association studies¹³⁹, heterozygous mutations in the *MC4R* coding sequence are the most common monogenic cause of severe obesity, and individuals with homozygous null mutations display severe, early-onset obesity^{140–142}. In mice, deletion of *Mc4r* causes hyperphagia and severe obesity¹⁴³. MC4R is found in a number of neuronal populations but its expression in the para-ventricular nucleus of the hypothalamus (PVN) is both necessary and sufficient for regulation of food intake and body weight¹⁴⁴.

MC4R activity is regulated by two endogenous ligands, an anorexigenic agonist, alpha melanocyte-stimulating hormone (α -MSH), and an orexigenic antagonist/inverse agonist, Agouti-Related Peptide (AgRP). These neuropeptides are produced by neurons of the arcuate nucleus of the hypothalamus (ARC) under the control of the adipocyte-secreted hormone leptin⁴¹. As leptin levels are proportional to fat mass¹⁴⁵, the observation that MC4R can localize to neuronal primary cilia suggests that signaling from the primary cilia of MC4R expressing neurons is a rate-limiting step in the sensing of energy stores and conditional modulation of energy intake.

Here, we use a combination of genetic and pharmacological approaches to demonstrate that primary cilia are required for ligand dependent activation of MC4R and long-term regulation of energy homeostasis by MC4R-expressing PVN neurons, and that altered MC4R ciliary function can underlie ciliopathy-associated obesity.

Results

Genetic ablation of primary cilia in MC4R-expressing neurons phenocopies MC4R deficiency.

By engineering mice in which GFP is inserted in frame with MC4R we have previously shown that MC4R co-localizes with the adenylyl cyclase type 3 (ADCY3) at the neuronal primary cilia¹³⁸. This co-localization can also be observed early in post-natal development (Figure 1). We then determined whether MC4R-expressing neurons require primary cilia to regulate body weight. Primary cilia can be specifically eliminated without affecting cell viability by inactivating *Ift88*, a gene encoding an intra-flagellar transport protein specifically required for ciliogenesis and ciliary maintenance¹⁴⁶. To inactivate *Ift88* in MC4R neurons, we first generated an *Mc4r*^{t2aCre} allele by CRISPR/Cas9-mediated zygotic recombination (Supplementary Figure 1A). We inserted a T2A sequence and Cre recombinase open reading frame at the terminator codon of *Mc4r* so that the endogenous promoter/enhancer elements direct Cre expression to MC4R-expressing cells. Accurate insertion at the *Mc4r* locus was verified by long-range PCR and sequencing. Recombinase activity, assessed in *Mc4r*^{t2aCre/t2aCre} *Rosa26*^{Ai14/Ai14} mice which express a red fluorescent protein in a Cre-dependent fashion, recapitulated the endogenous MC4R expression in particular in the PVN¹⁴⁷ (Supplementary Figure 1C). Importantly, the weight curves of mice homozygous for the insertion (*Mc4r*^{t2aCre/t2aCre}) did not differ from those of wild type littermates, indicating that the *Mc4r*^{t2aCre} allele preserves MC4R function (Supplementary Figure 1B).

We crossed *Mc4r*^{t2aCre} mice to *Ift88*^{fl/fl} mice¹⁴⁶ to generate mice with specific deletion of *Ift88* in MC4R-expressing cells. To determine the effect of primary cilia deletion in MC4R neurons, we compared *Mc4r*^{t2aCre/t2aCre} *Ift88*^{fl/fl} mice to *Mc4r*^{t2aCre/t2aCre} *Ift88*^{+/+} littermates. *Mc4r*^{t2aCre/t2aCre} *Ift88*^{fl/fl} mice were born at a Mendelian ratio and develop a severe obesity phenotype (Figure 2A-J) that mimics germline loss of MC4R¹⁴³. Specifically, body weight curves of *Mc4r*^{t2aCre/t2aCre} *Ift88*^{fl/fl} and *Mc4r*^{t2aCre/t2aCre} *Ift88*^{+/+} mice diverged after weaning (Figure 2A,F). This difference in body weight was characterized by a large increase in fat mass (Figure 2B,G), an increase in lean mass (Figure 2C,H) and length (Figure 2D,I) as well as an increase in food intake (Figure 1E,J). We observed the same effect in males (Figure 2A-E) and females (Figure 2F-J).

To confirm that loss of primary cilia in MC4R neurons did not affect neuronal survival, we generated triple knock-in *Mc4r*^{t2aCre/t2aCre} *Ift88*^{fl/fl} *Rosa26*^{Ai14/Ai14} mice. We found no difference in the number of MC4R-expressing neurons in the PVNs of *Mc4r*^{t2aCre/t2aCre} *Ift88*^{fl/fl} *Rosa26*^{Ai14/Ai14} mice when compared to those of *Mc4r*^{t2aCre/t2aCre} *Ift88*^{+/+} *Rosa26*^{Ai14/Ai14} control mice (Figure 2K,L). We also determine whether loss of cilia affected the capacity of MC4R neurons to decrease food intake when activated. A CRE-dependent adeno-associated virus (AAV) encoding a GqDREADD-mCherry was stereotaxically injected bilaterally in the PVN of *Mc4r*^{t2aCre/t2aCre} *Ift88*^{fl/fl} and control *Mc4r*^{t2aCre/t2aCre} *Ift88*^{+/+} or *Ift88*^{fl/+} mice. A negative control group was injected with AAV DIO-mCherry (Figure 2M-O). All three groups were fasted for 24h and challenged with saline and CNO with a randomized crossover experiment design, and their 3-hour refeeding food intake was measured (Figure 2O). Activation of MC4R neurons by CNO lead to a significant decrease in food intake in both groups that expressed the GqDREADD, while the control AAV-mCherry group did not respond to CNO. This result demonstrates that loss of cilia does not impair the capacity of MC4R neurons to generate an anorexigenic response upon activation.

Together these results indicate that primary cilia are critically and cell autonomously required for MC4R neurons to control long term-energy homeostasis.

Primary cilia are required for anorexigenic MC4R signaling

Since loss of primary cilia does not appear to affect the survival of MC4R-expressing neurons (Figure 2K,L) or their capacity to be artificially stimulated by DREADDs (Figure 2M-O), we hypothesized that the obesity observed in *Mc4r^{t2aCre/t2aCre} Ift88^{fl/fl}* mice was due to impaired MC4R function in differentiated neurons. To test this hypothesis, we determined whether primary cilia are required for the anorexigenic agonist-dependent function of MC4R in adult mice.

As opposed to ubiquitous germline ablation of primary cilia, which is embryonic lethal, ubiquitous adult conditional ablation of primary cilia, achieved by deleting *Ift88* using a tamoxifen-inducible Cre (*Ubc-Cre-Ert2 Ift88^{fl/fl}*), results in obesity¹³⁷.

To determine whether loss of primary cilia affects MC4R signaling, we assessed whether the timeline of primary cilia ablation and onset of the metabolic phenotype in this model is compatible with a dysfunction of the central melanocortin system. Adult *Ubc-Cre-Ert2 Ift88^{fl/fl}* mice injected with tamoxifen were compared to *Ift88^{fl/fl}* mice injected with tamoxifen controls (Figure 3A). Tamoxifen led to neuronal ablation of the primary cilia specifically within *Ubc-Cre-Ert2 Ift88^{fl/fl}* mice within two weeks, as assessed by ciliary ADCY3 staining, a delay consistent with the half-life of IFT88 (Supplementary Figure 2). Body weight, body composition, food intake and energy expenditure were assessed repeatedly over 4 weeks (Figure 3A,B). Concurrent with neuronal cilia loss, tamoxifen-injected *Ubc-Cre-Ert2 Ift88^{fl/fl}* mice developed obesity characterized by increased fat mass and a slight increase in lean mass (Figure 3B-E). This accumulation of fat mass was associated with hyperphagia, rather than changes in energy expenditure (Figure 3F,G), which would be consistent with loss of MC4R function in the PVN¹⁴⁸.

To more specifically determine whether MC4R activity was impaired following ablation of primary cilia in this model, we evaluated the anorexigenic effect of pharmacological stimulation of MC4R before and after tamoxifen-induced ablation of primary cilia, but prior to weight divergence (Figure 4A-C). Specifically, *Ubc-Cre-Ert2 Ift88^{fl/fl}* and control *Ift88^{fl/fl}* mice were injected intracerebroventricularly (ICV) with Melanotan-II (MTII), an MC4R agonist, before and after tamoxifen-mediated cilia loss (Figure 4B). Mice were fasted for 24 hours prior to ICV injection, and their food intake was measured over a 4-hour period following injection. As expected, prior to tamoxifen-mediated cilia loss, MTII induced a drastic reduction of food intake in both groups compared to injection of the control solution, artificial cerebrospinal fluid (aCSF, Figure 4D). After tamoxifen injection, the anorexigenic effect of MTII gradually diminished specifically in *Ubc-Cre-Ert2 Ift88^{fl/fl}* mice (Figure 4D). Thus, primary cilia are necessary for MC4R-mediated effects on food intake.

As an additional test of whether cilia are required for MC4R signaling, we tested the effects of deleting cilia on the activity of THIQ, another specific agonist of MC4R that inhibits food intake. Similar to MTII, the anorexigenic response to ICV administration of THIQ was abolished specifically following removal of primary cilia specifically in *Ubc-Cre-Ert2 Ift88^{fl/fl}* mice (Supplementary Figure 3).

As observed when specifically removing primary cilia from MC4R neurons developmentally, deletion of *Ift88* from adult hypothalamus did not alter neuron number (Supplementary Figure 4). Deletion of *Ift88* also did not alter expression levels of *Sim1* or *Mc4r* in the adult hypothalamus (Supplementary Figure 4D). These results indicate that the loss of responsiveness to MC4R stimulation upon removal of primary cilia was not due to loss of MC4R-expressing cells or decreased *Mc4r* expression.

In addition to regulating feeding behavior, PVN neurons respond to osmotic stimulation, for example, by phosphorylating the ribosomal protein S6¹⁴⁹. pS6 activation by osmotic stimulation in PVN neurons was preserved in tamoxifen-treated *Ubc-Cre-Ert2 Ift88^{fl/fl}* mice following cilia loss, indicating that primary cilia are not required for all functions of these neurons (Supplementary Figure 4E-F).

Adult PVN primary cilia are required for anorexigenic MC4R signaling

MC4R is expressed in a number of brain regions, including multiple hypothalamic nuclei¹⁵⁰. However, much of the anorexigenic activity of MC4R is due to its function in PVN neurons of the hypothalamus, where MC4R activity is both necessary and sufficient to inhibit food intake and control body weight^{144,148}. In *Mc4r^{t2aCre/t2aCre Ift88^{fl/fl}}* mice, primary cilia were ablated from all MC4R expressing cells, including those of the PVN. In *Ubc-Cre-Ert2 Ift88^{fl/fl}* mice, treatment with tamoxifen removed cilia globally. Therefore, to test whether primary cilia are specifically required in the PVN for regulation of body weight through MC4R activation, we deleted *Ift88* by bilateral stereotaxic injection of an AAV expressing GFP-tagged Cre recombinase (AAV-creGFP) into the PVN of adult *Ift88^{fl/fl}* mice (Figure 5A). Mice injected with adeno-associated virus expressing a GFP-tagged functionally impaired Cre recombinase (AAV-nGFP) served as controls. GFP expression indicated infected cells and allowed for post-hoc confirmation of PVN injection (Figure 5C, D). Injection of Cre-producing virus, but not control virus, lead to the ablation of primary cilia in the PVN (Figure 5C,D inserts).

Following ablation of the primary cilia in the PVN, AAV-creGFP-injected *Ift88^{fl/fl}* mice gained weight (Figure 5E,F). Thus, cilia are critical for the regulation of energy homeostasis in the PVN and account, in full or in part, for the obesity observed after ubiquitous disruption of primary cilia in adult mice. As MC4R localizes to primary cilia of neurons in the PVN¹³⁸, these data further suggest that MC4R could function at PVN cilia to control body weight.

To determine whether MC4R activation requires PVN primary cilia, we implanted an ICV cannula in the lateral ventricle at the time of AAV injection (Figure 5G,H) and measured changes in the anorectic effect of MTII after PVN primary cilia loss as described above. Mice were injected with MTII (0.05 nmol) or vehicle (aCSF) after a 24 hour fast, and their food intake was consequently measured over 4 hours. (Figure 5I). While control AAV-nGFP-injected mice decreased their food intake by sixty percent on average after MTII injection as compared to after aCSF injection, this response was blunted in AAV-CreGFP-injected mice lacking primary cilia in the PVN (Figure 5I,J). Together, these results demonstrate that the anorexigenic function of MC4R requires primary cilia in the PVN.

Adenylyl cyclase signaling in the primary cilia of MC4R-expressing neurons in the adult PVN is essential for controlling food intake and body weight

We reasoned that if MC4R functions at the primary cilia of PVN neurons, then inhibiting MC4R signaling specifically in these primary cilia would increase food intake and cause obesity. Activation of MC4R stimulates G α s to increase adenylyl cyclase (AC) activity¹⁵¹. Inhibition of adenylyl cyclase specifically at the primary cilia can be achieved by expression of a constitutively active version of the cilium-localized, G α i-coupled receptor, GPR88 (GPR88(G283H) or GPR88*)¹⁵².

To target MC4R neurons of the PVN, we stereotaxically injected a Cre-dependent AAV encoding a FLAG-tagged version of GPR88* (AAV DIO Flag-GPR88*) into the PVNs of 20 week-old *Mc4r^{t2aCre/t2aCre}* male mice (coordinates: AP=-0.8, ML=0.0, DV=-5.2). To verify injection accuracy, PVN transduction, and Cre activity, we co-injected AAV expressing mCherry in a Cre-dependent manner (AAV DIO-mCherry). Control mice included *Mc4r^{t2aCre/t2aCre}* mice injected only with AAV DIO-mCherry as well as *Mc4r^{+/+}* littermates injected with AAV DIO-GPR88* and AAV DIO-mCherry (to control for Cre-independent effects of AAV DIO-GPR88*). Body weight was measured weekly and body composition was assessed by Echo-MRI 3, 6 and 9 weeks post AAV injections. Food intake and energy expenditure were assessed at 3 weeks post AAV injections by CLAMS.

Mc4r^{t2aCre/t2aCre} mice injected with AAV DIO-GPR88* into the PVNs increased their body weight (Figure 6E,F) and fat mass (Figure 6H). Food intake and Energy expenditure were higher in AAV DIO-GPR88*-injected *Mc4r^{t2aCre/t2aCre}* mice 3 weeks post AAV injection (Figure 6I, J). Thus, GPR88*-mediated obesity was attributable to hyperphagia.

We then determined whether MC4R activation requires AC signaling at the primary cilium of MC4R neurons. We implanted an ICV cannula in the lateral ventricle (coordinates: AP=-0.3, ML=+1, DV=-2.5) at the time of AAV injection (coordinates: AP=-0.8, ML=±0.2, DV=-5.2) and measured changes in the anorectic effect of MTII after GPR88* expression at the cilium of PVN MC4R neurons, as described above (Figure 6K-M). Mice were randomly assigned to two groups that were injected with MTII (0.5nmoles) or vehicle (aCSF) after a 24 hour fast, and their food intake was consequently measured over 4 hours; the reverse treatment was completed 5 days later (Figure 6L). While control AAV DIO-mCherry mice significantly decreased their food intake after MTII injection as compared to after aCSF injection, this response was blunted in AAV GPR88*-injected mice (Figure 6M).

These results demonstrate that reducing adenylyl cyclase activity specifically at the primary cilia of adult MC4R PVN neurons is sufficient to increase food intake and disrupt regulation of body weight, and that the anorexigenic function of MC4R requires AC signaling at the primary cilium of PVN MC4R neurons.

Discussion

Obesity is a hallmark of several human ciliopathies, including Bardet-Biedl syndrome, MORM syndrome and Carpenter syndrome. As the major physiological pathway implicated in the regulation of long-term energy homeostasis, the central leptin-melanocortin system may link

human ciliopathies and obesity. Since deletion of primary cilia in adult mice causes leptin resistance, the initial hypothesis was that dysfunction of central leptin signaling could play a role in the observed associated obesity^{101,137,153,154}. However, leptin resistance was subsequently found to be a consequence, rather than a cause, of obesity in this model¹⁵⁵, suggesting that dysfunction of a downstream effector of leptin may account for ciliopathy-associated obesity.

Here, we used several complementary genetic and pharmacological approaches to demonstrate that MC4R, a GPCR critically required for maintenance of body weight, not only localizes to primary cilia, but also operates at primary cilia of PVN neurons to control energy homeostasis in adult mice. Removing primary cilia specifically from MC4R-expressing cells (in *Mc4r^{t2aCre/t2aCre} lft88^{fl/fl}* mice) phenocopies the obesity phenotype caused by germline loss of MC4R¹⁴³, demonstrating that primary cilia are essential for the function of MC4R-expressing neurons.

As this requirement of primary cilia in MC4R-expressing neurons could reflect a developmental role for cilia caused by removing cilia, we investigated whether primary cilia are required for the production of MC4R-expressing neurons and found that removing cilia does not affect the number of MC4R-expressing neurons nor expression of MC4R. Furthermore, MC4R neurons that lost their cilia can still be chemogenetically activated and lead to anorexigenic response. Therefore, primary cilia are dispensable for the production of MC4R-expressing neurons.

Moreover, three additional lines demonstrate that MC4R functions at primary cilia. First, cilia are essential for the anorexigenic effects of MC4R agonists such as MTII and THIQ. Second, cilia are required specifically in MC4R-expressing neurons for the regulation of feeding behavior. Third, inhibiting the MC4R signaling pathway by inhibiting adenylyl cyclase specifically in the primary cilia of MC4R expressing PVN neurons is sufficient to induce hyperphagia and obesity, as well as resistance to MTII. Since obesity is the most striking phenotype resulting from ubiquitous ablation of primary cilia in adult mice, our data suggest that a major function of adult primary cilia is to regulate long-term energy homeostasis by transducing MC4R signaling in PVN neurons.

Since partial loss of MC4R activity, as caused by heterozygous *MC4R* mutations, is sufficient to cause severe obesity in mice and humans¹⁴², a parsimonious model for ciliopathy-associated obesity is that it results from decreased localization of MC4R to the primary cilia of PVN neurons. This model also implies that partial attenuation of the ciliary localization of MC4R is sufficient to cause obesity and that genetic variation decreasing primary cilia localization of MC4R could predispose to weight gain. It will be interesting to assess to what extent obesity-associated variants detected in GWAS studies are involved in primary ciliary function. In this respect, it is interesting to note that obesity-associated variants are located within the MC4R and ADCY3 genomic regions¹⁵⁶ and that variants in the FTO region (the strongest obesity associated signal in GWAS) could affect the primary cilia transition zone component RPRGRIP1L¹⁵⁷.

Coordinated feeding behavior results from adapting short-term feeding behavior to immediate food availability and long-term caloric needs to maintain body weight stable over time. While MC4R integrates neuro-endocrine signals provided by α -MSH and AgRP, MC4R-expressing neurons in the PVN are also sensitive to neural afferent inputs that communicate short-term energy status from arcuate nucleus glutamatergic neurons and GABAergic AgRP-expressing neurons^{158,159}. Our findings suggest that primary cilia could be a mean for MC4R neurons to

compartmentalize long-term energy state signaling resulting from MC4R activity modulation⁴¹. This subcellular compartmentalization of signaling may explain how MC4R neurons are able to integrate different timescales afferent information to coordinate feeding behavior. Future studies will address how MC4R neurons integrate ciliary and synaptic communication.

Figures

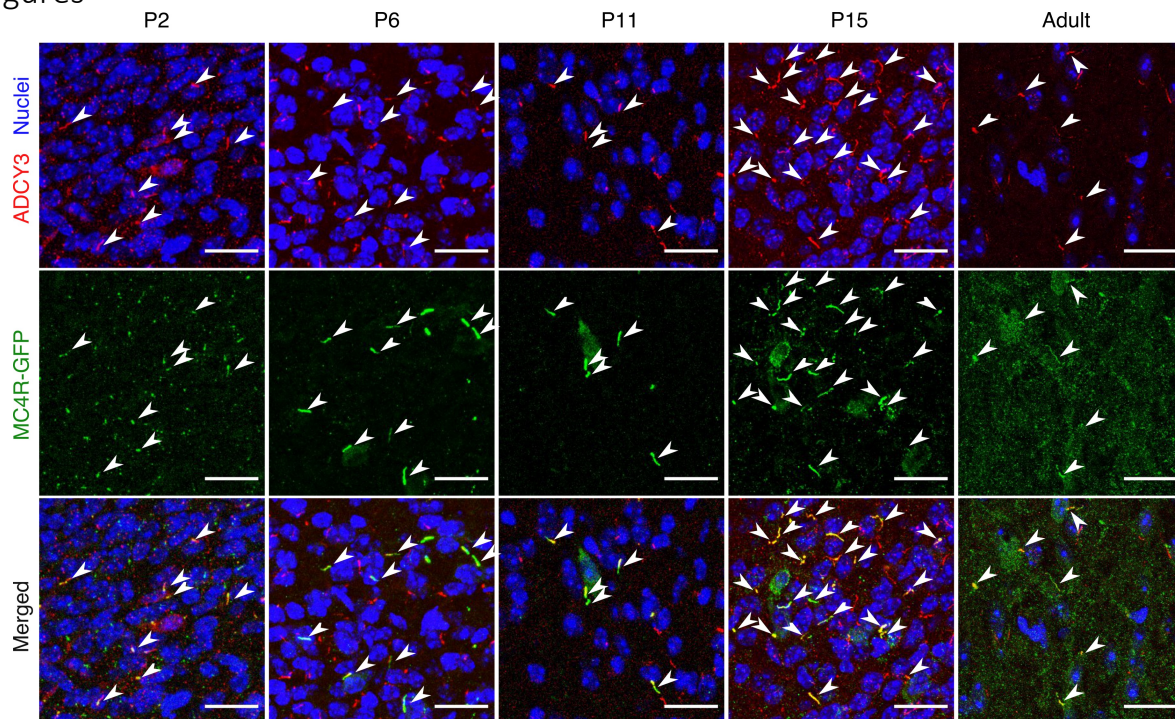


FIGURE 2.1 DEVELOPMENTAL MC4R SUBCELLULAR LOCALIZATION IN THE PVN AT POSTNATAL STAGE: P2 P6, P11, P15 AND ADULT.

Representative immunofluorescence staining of MC4R-GFP (green) and ADCY3 (red) in brains sections of *Mc4rgfp/gfp* mice during the post-natal period and in adults. Nuclei are stained with Hoescht (blue). Arrows indicate primary cilia expressing MC4R. A minimum of 3 mice were imaged per age. Scale bar, 20 μ m.

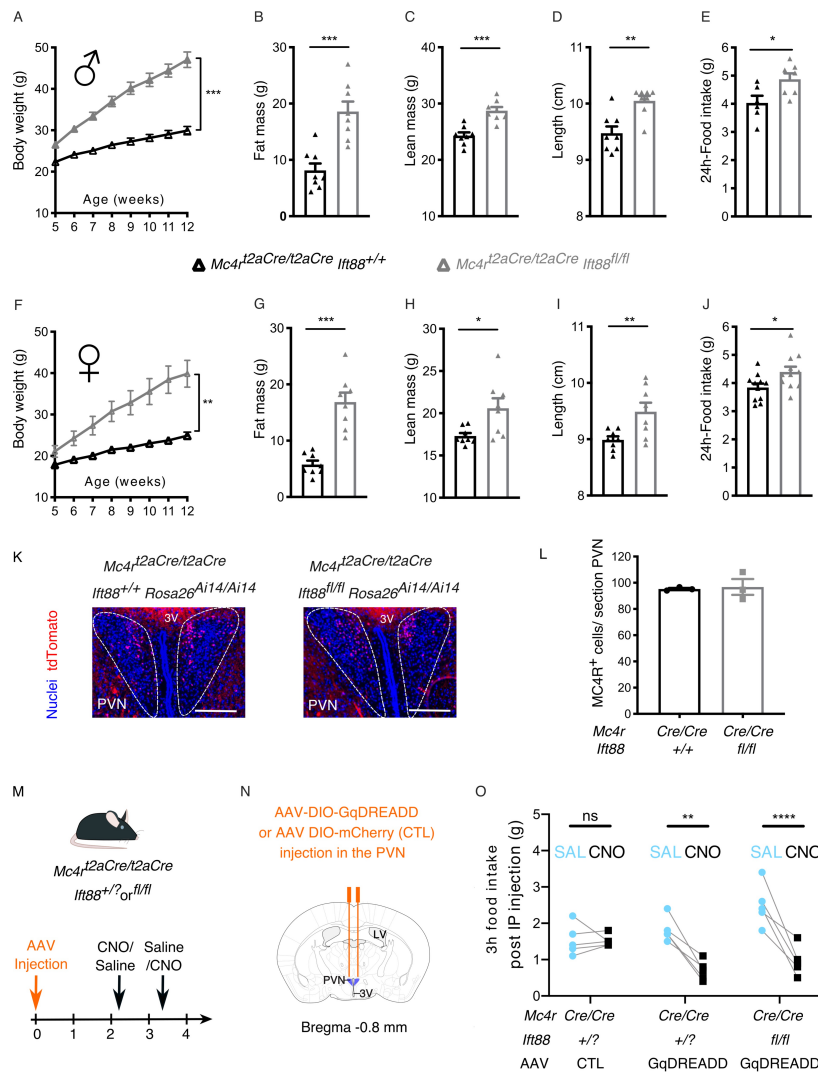


FIGURE 2.2 DELETION OF *IFT88* IN MC4R-EXPRESSING NEURONS LEADS TO OBESITY.

(A-J) Phenotyping of control *Mc4rt2aCre/ t2aCre Ift88+/+* and *Mc4rt2aCre/ t2aCre Ift88fl/fl* male (A-E) and female (F-J) mice. Body weights were measured weekly from 5 to 12 weeks of age (A,F). Fat mass (B,G) and lean mass (C,H) (measured by echoMRI), and length (D,I) were assessed at 12 weeks of age. n=8 mice per group. E,J) 24-hour food intake at 12 weeks of age (females n=11 control and 11 experimental; males n=6 control and 7 experimental). K) Representative images of the PVN in which MC4R-expressing neurons express a red fluorescent protein (tdTomato) in both *Mc4rt2aCre/t2aCre Ift88+/+* (left) and *Mc4rt2aCre/t2aCre Ift88fl/fl* (right) mice, Scale bar, 200 μm. L) Quantification of the number of MC4R-expressing neurons in *Mc4rt2aCre/t2aCre Ift88+/+* and *Mc4rt2aCre/t2aCre Ift88fl/fl* mice (n=3 PVN sections per group, ns). M-O: Chemogenetic activation of MC4R neurons in *Mc4rt2aCre/t2aCre Ift88+/+* and *Mc4rt2aCre/t2aCre Ift88fl/fl* mice. M) Schematic of the experimental timeline: 7-14 week-old male mice were stereotaxically injected with an AAV DIO-GqDREADD or DIO-mCherry and then tested either for CNO or saline 2 weeks and 3 weeks post injection, with a randomized crossover design. N) Schematic of bilateral stereotaxic injections (coordinates: AP=-0.8, ML=±0.25, DV=-5.2) of AAV DIO-GqDREADD or AAV DIO-mCherry (CTL). O) 3h food intake following injection of saline or CNO in three groups of mice (n=5 per group): *Mc4rt2aCre/t2aCre Ift88+/?* injected with AAV DIO-mCherry (negative control), *Mc4rt2aCre/t2aCre Ift88+/?* mice injected with AAV DIO-GqDREADD (positive control), and *Mc4rt2aCre/t2aCre Ift88fl/fl* mice injected with AAV DIO-GqDREADD. Mice were

fasted for 24h prior to injection. Statistics: t-test or Repeated measures of two-way ANOVA followed by Sidak's multiple comparisons test were performed. All values are displayed as mean \pm SEM. * $p < 0.05$, ** $p < 0.01$, *** $p < 0.001$. PVN: paraventricular nucleus of the hypothalamus; 3V: third ventricle; LV: lateral ventricle.

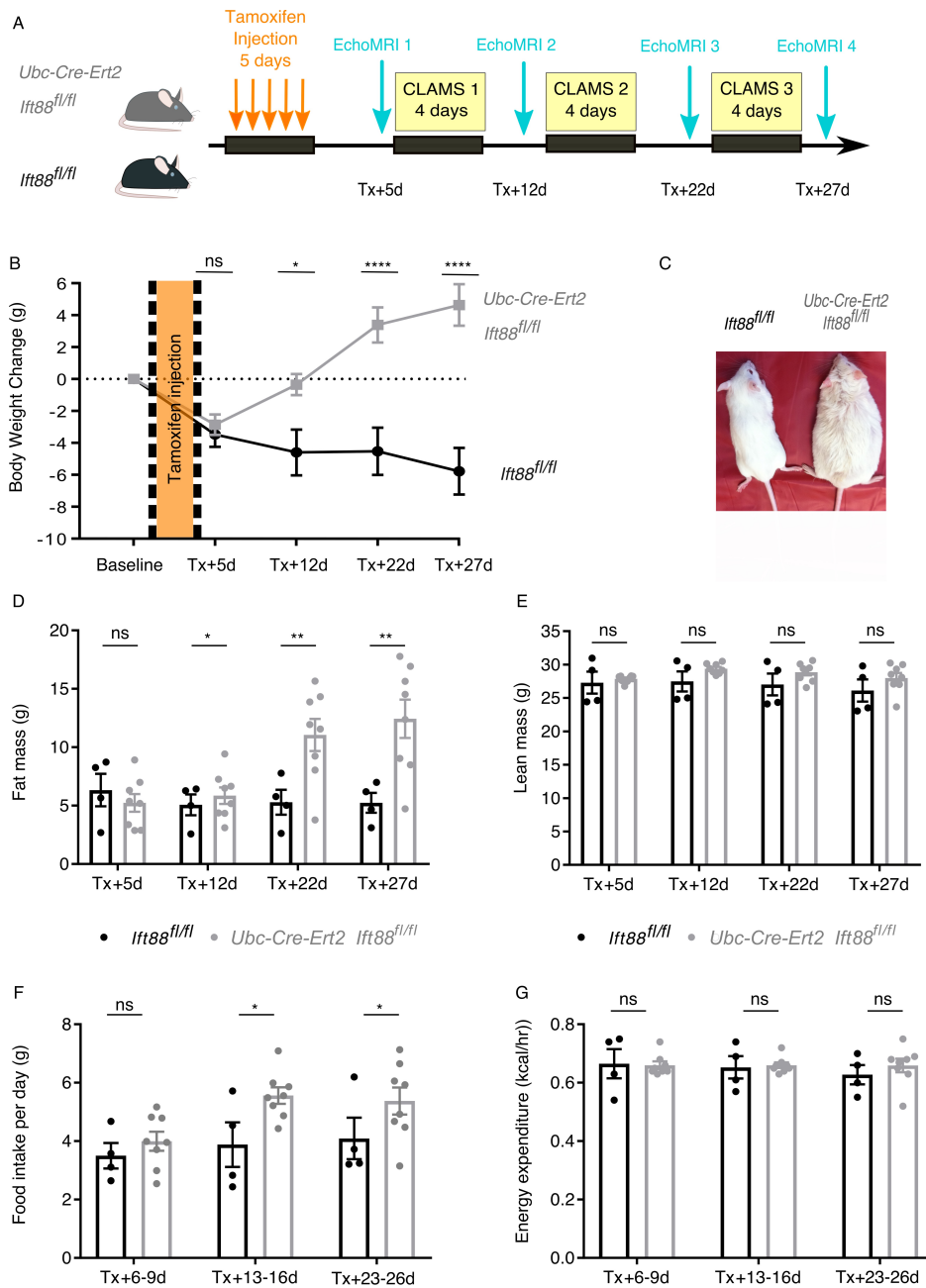


FIGURE 2.3: TIME COURSE OF METABOLIC CHANGES FOLLOWING ABLATION OF PRIMARY CILIA IN ADULT MICE.

A) Schematic of the experimental protocol. B) Time course of body weight changes of *Ubc-Cre-Ert2 Ift88fl/fl* (n=8) and *Ift88fl/fl* (n=4) 20 week-old male mice at baseline and at the indicated times after tamoxifen (Tx) injection. C) Male control (*Ift88fl/fl*) and *Ubc-Cre-Ert2 Ift88fl/fl* mice 4 weeks following tamoxifen injection. D) Fat mass, E) lean mass as measured by EchoMRI, F) food intake and G) energy expenditure as measured in CLAMS, of *Ubc-Cre-Ert2 Ift88fl/fl* compared to *Ift88fl/fl* male mice at the indicated times after tamoxifen injection. Error bars represent SEM. * $p < 0.05$; ** $p < 0.01$; **** $p < 0.0001$. Energy expenditure was analyzed using CalR app ANCOVA, with body weight included as a covariate.

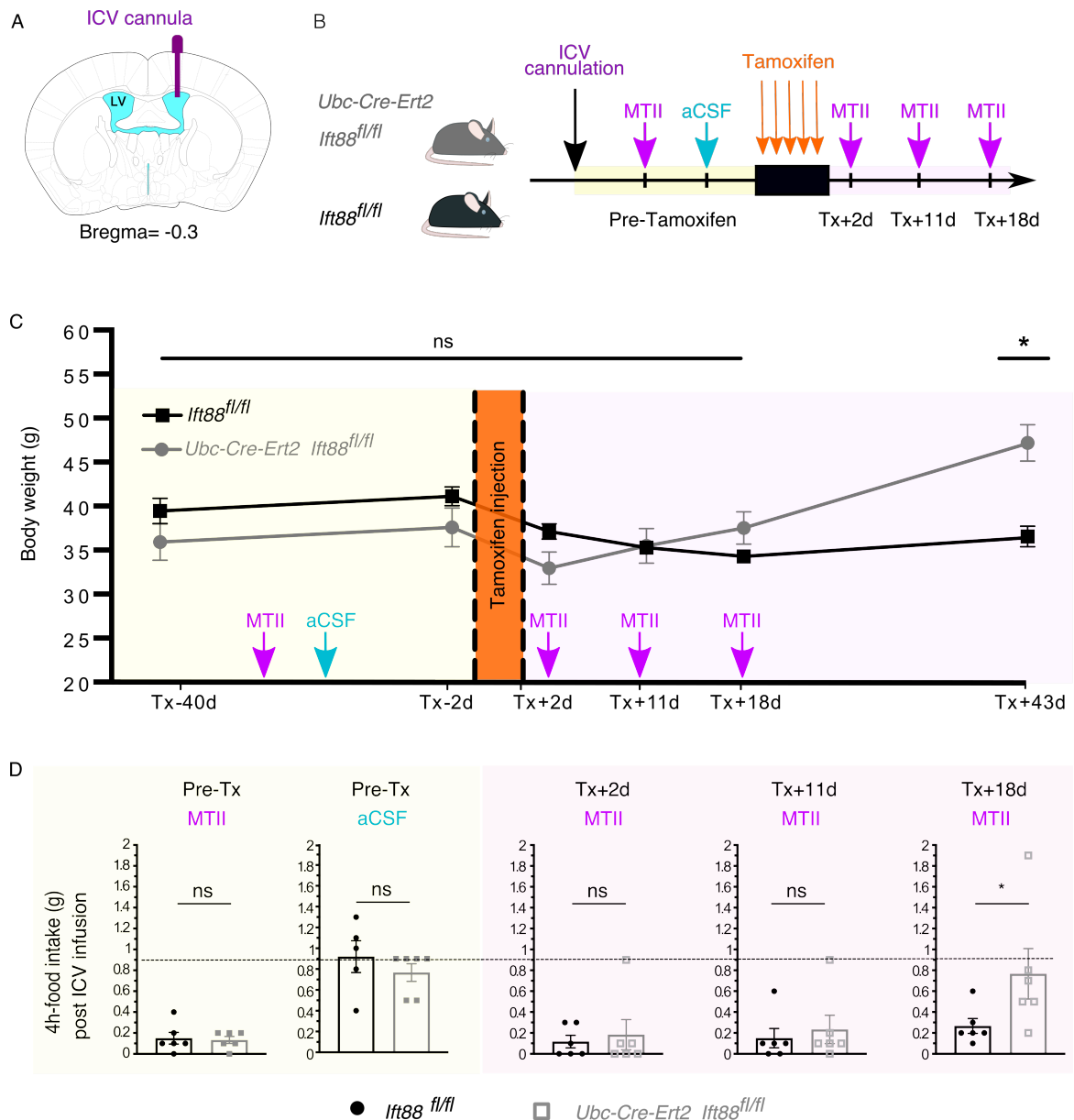


FIGURE 2.4: PRIMARY CILIA ARE ESSENTIAL FOR THE RESPONSE TO THE MC4R AGONIST MTII.

A) Schematic of the placement of an ICV cannula in the lateral ventricle (coordinates: AP=-0.3, ML=+1, DV=-2.5) B) Schematic of the experimental protocol: over 20 week-old male control (*lft88^{fl/fl}*) and *Ubc-Cre-Ert2 lft88^{fl/fl}* littermates (n=6 per group) were implanted with an ICV cannula in the lateral ventricle. After recovery, food intake was measured following ICV delivery of MTII and vehicle control (aCSF). Mice were then injected with tamoxifen (Tx) for 5 days and the response to ICV-delivered MTII was measured again 2, 11, and 18 days after the last Tx injection. C) Weights of *lft88^{fl/fl}* control and *Ubc-Cre-Ert2 lft88^{fl/fl}* littermate mice during the experiment. D) Assessment of anorectic effect of MTII (0.5 nmol) on short-term food intake (4 hours) compared to vehicle (aCSF) before and after primary cilia loss. Mice were fasted for 24h prior to injection. ICV: intracerebroventricular; LV: lateral ventricle. Two-way Anova (C), unpaired t-test (D). Error bars represent SEM. * indicates p<0.05.

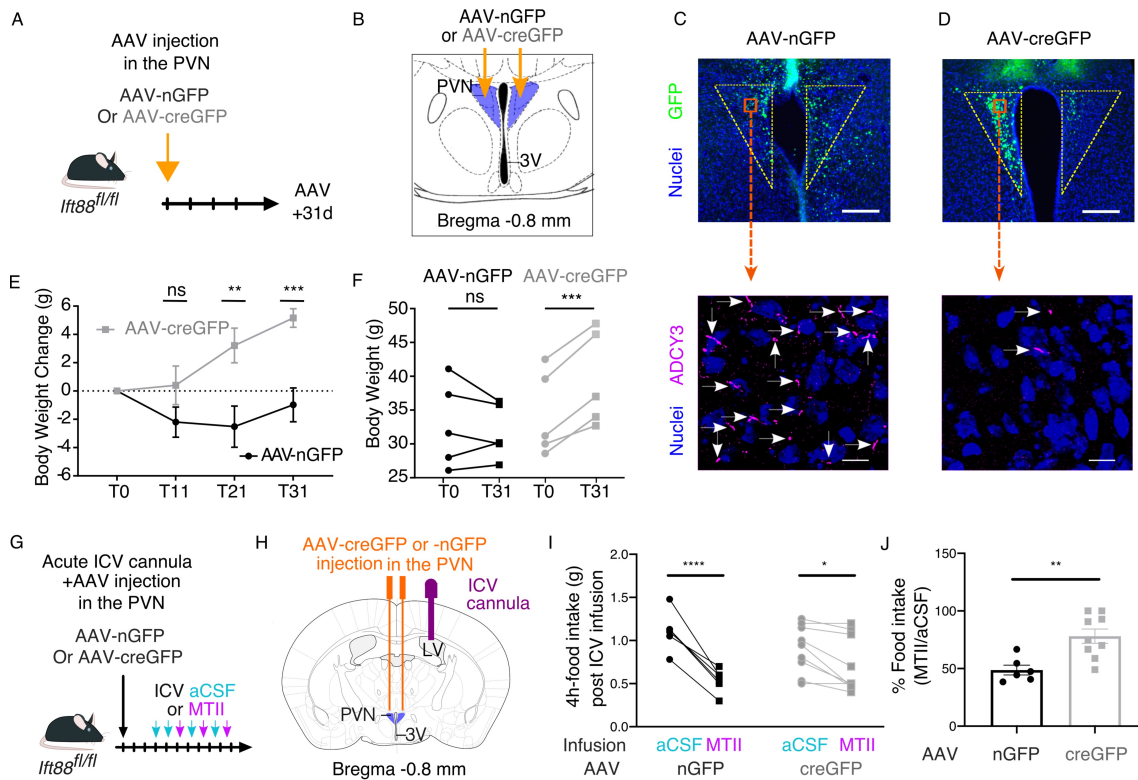


FIGURE 2.5: PRIMARY CILIA ARE REQUIRED IN PVN NEURONS FOR WEIGHT CONTROL AND SENSITIVITY TO MC4R AGONIST

A) Experimental protocol schematic. Bilateral stereotaxic injections (coordinates: AP=-0.8, ML=±0.2, DV=-5.2) of AAV-creGFP or AAV-nGFP were performed on 20 week-old *Ift88^{fl/fl}* mice B) Schematic representation of hypothalamic region studied. C,D) Representative images of PVN sections of AAV-creGFP- or AAV-nGFP-injected mice showing AAV-infected cells in green, and nuclei in blue. Scale bar, 200 μ m. Inserts: immunofluorescent imaging of primary cilia (ADCY3, magenta) of PVN regions denoted in C and D. Arrows indicate cilia. Scale bar, 10 μ m. E) Body weights of *Ift88^{fl/fl}* mice following bilateral PVN injection of AAV-creGFP (n=5) or AAV-nGFP (n=5). F) Body weights at time of AAV injection and one month afterwards. Individual mice are indicated by lines. G) Schematic of the experimental protocol for testing the anorexigenic effects of the MC4R agonist MTII. 3 weeks following AAV injection and cannulation, 20 week-old *Ift88^{fl/fl}* mice were alternately treated with vehicle (aCSF) or Melanotan II (MTII) by ICV infusion after fasting for 24 hours, with a 4-day recovery in between infusions. Food intake during 4h re-feeding was then averaged for aCSF and MTII (values in I and J). H) Schematic of bilateral stereotaxic injections (coordinates: AP=-0.8, ML=±0.2, DV=-5.5) of AAV-creGFP (n=9) or AAV-nGFP (n=6), and placement of an ICV cannula in the lateral ventricle (coordinates: AP=-0.3, ML=+1, DV=-2.5). I) 4h food intake following injection of aCSF or MTII in AAV-creGFP- and control AAV-nGFP-injected *Ift88^{fl/fl}* mice (Repeated measures averaged). J) Percentage of food ingested in 4h following ICV administration of MTII normalized to administration of aCSF. T=days following AAV injection. Error bars represent SEM. Statistics: t-test (J) or repeated measures of two-way ANOVA followed by Sidak's multiple comparisons test. * p <0.05, ** p <0.01, *** p <0.001, **** p <0.0001. PVN: paraventricular nucleus; 3V: third ventricle; ICV: intracerebroventricular; LV: lateral ventricle.

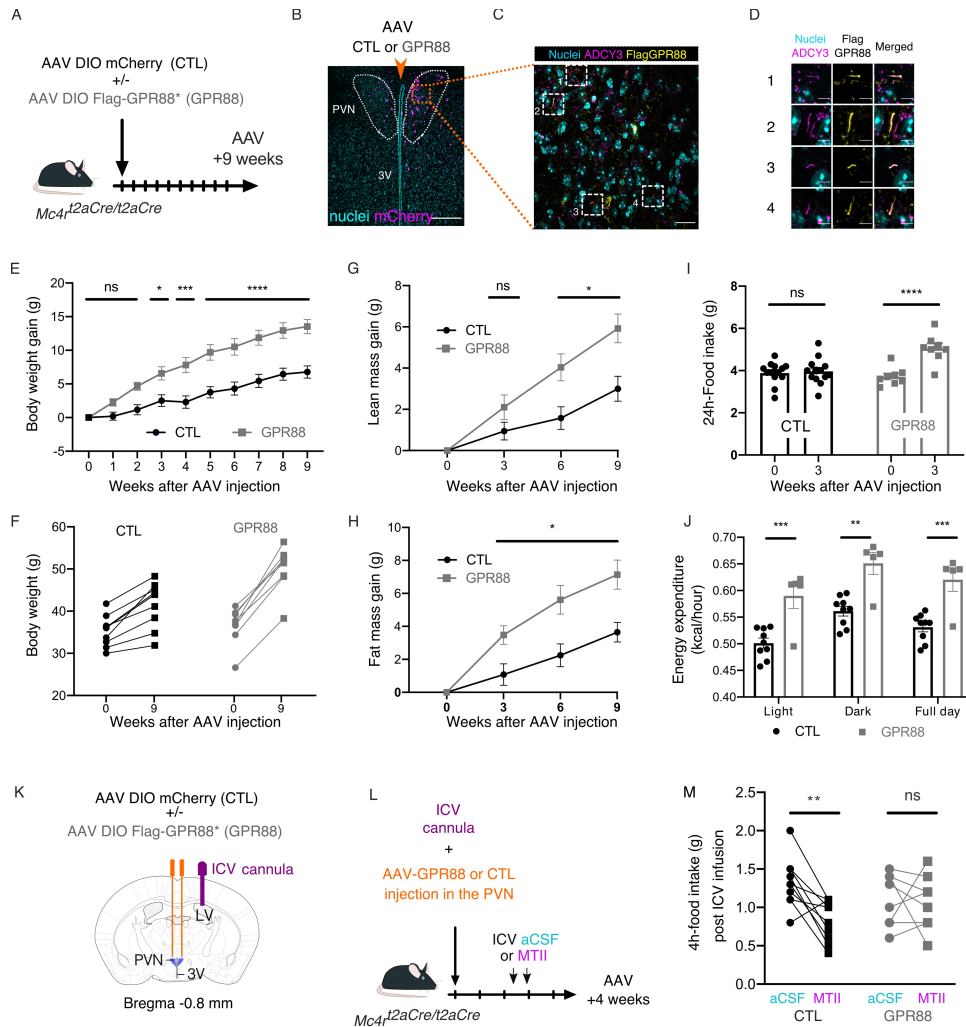


FIGURE 2.6: INHIBITION OF CILIARY ADENYLYL CYCLASE CAUSES HYPERPHAGIA AND OBESITY.

A) Experimental protocol schematic. Midline stereotaxic injections of AAV DIO-FlagGPR88* (“GPR88”) and AAV DIO-mCherry (“CTL”) in 18 weeks old *Mc4rt2aCre/t2aCre* male mice. B) PVN sections of GPR88 mice showing nuclei (cyan) and mCherry (magenta) indicating region of viral transfection. Scale bar, 200 μm . C) Inset from B. Immunofluorescence imaging of cilia (ADCY3, magenta), FLAG-GPR88* (yellow) and nuclei (cyan). Scale bar, 20 μm . D) Magnified insets from C depicting GPR88 localization to individual cilia. Scale bar, 5 μm . E) Body weight change of GPR88 (n=8) and control (n=13) mice over nine weeks following AAV injection. F) Weights at time of AAV injection and 9 weeks afterwards. Lines connect individual mice. Lean mass (G) and fat mass (H) gain over the nine weeks following AAV injection. I) 24h food intake at time of AAV injection and 3 weeks afterwards. J) Average hourly energy expenditure during light phase, dark phase and full day of GPR88 (n=5) and control (n=9) mice 3 weeks following AAV injection. K) Schematic of bilateral injections of AAV-DIO GPR88 (n=8) or control-AAV (n=10), and placement of an ICV cannula in 8-11 week-old *Mc4rt2aCre/t2aCre* male mice. L) Schematic of the experimental protocol for testing the anorexigenic effect of Melanotan II (MTII): mice were fasted for 24h and infused ICV with vehicle (aCSF) or MTII (randomized crossover design, 2 and 3 weeks following surgery). M) 4h-food intake following infusion of aCSF or MTII in AAV-GPR88- and control AAV-injected mice. All values are displayed as mean \pm SEM. Statistics: repeated measures of two-way ANOVA followed by Sidak’s multiple comparisons test. * $p < 0.05$, ** $p < 0.01$, *** $p < 0.001$, **** $p < 0.0001$. Energy expenditure was analyzed by ANCOVA, with body weight included as a covariate. 3V: third ventricle, ICV: intracerebroventricular, PVN: paraventricular nucleus of the hypothalamus.

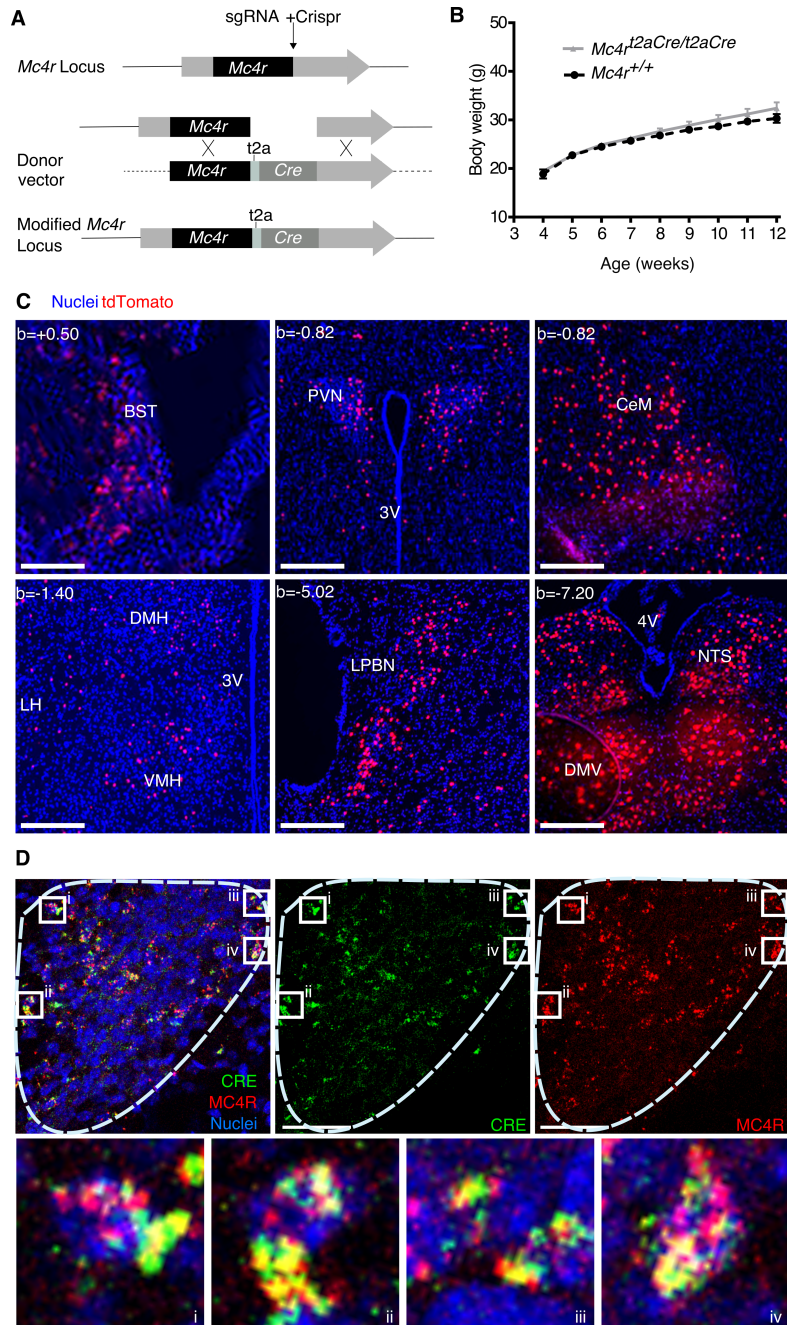


FIGURE 2.7 - SUPPLEMENTARY FIGURE 1: CHARACTERIZATION OF $Mc4R^{T2ACRE}$ MOUSE MODEL AND CENTRAL EXPRESSION

A) Strategy used to target the mouse *Mc4r* locus by CRISPR/Cas9 to insert a *T2A* and *Cre* open reading frame in frame with *MC4R*. B) Body weights of *Mc4r^{t2aCre/t2aCre}* (n=7) mice and their *Mc4r^{+/+}* littermates (n=6). C) The expression of the *Mc4r-t2a-Cre* allele was surveyed in the brain of an *Mc4r^{t2aCre/t2aCre} Rosa^{Ai75}* mouse on the rostral-caudal axis. Scale bar, 250 μ m. D) *Mc4r* (red) and *Cre* (green) mRNA transcripts in the PVN of a *Mc4r^{t2aCre/t2aCre}* P6 mouse pup, detected using RNAScope Multiplex Fluorescent V2 Assay, colocalize in the same cells. Each punctum represents one mRNA transcript. Scale bar, 50 μ m. BST, bed nucleus of the stria terminalis; CeM, central amygdaloid nucleus; DMH, dorsal medial hypothalamus; DMV, dorsal motor nucleus; LH, lateral hypothalamus; LPBN, lateral parabrachial nucleus; PVN, paraventricular nucleus; NTS, nucleus of the solitary tract; VMH, ventromedial hypothalamus.

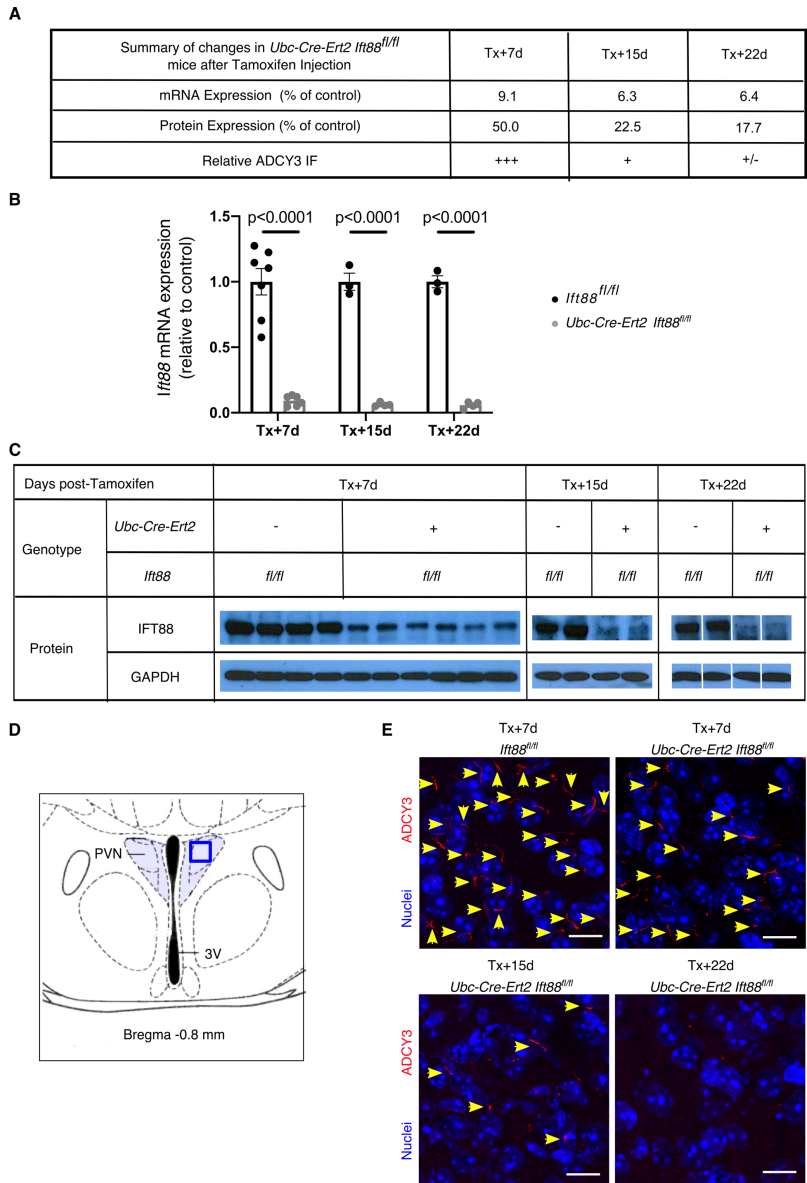


FIGURE 2.8 - SUPPLEMENTARY FIGURE 2: TIME COURSE OF IFT88 LOSS AND CILIA ABLATION FOLLOWING TAMOXIFEN INJECTION IN *UBC-CRE-ERT2 IFT88^{FL/FL}* MICE.

A) Summary of time dependent changes in mRNA expression, protein expression and cilia ablation. B) Time course of hypothalamic *Ift88* mRNA expression measured by qPCR following tamoxifen injection in *Ift88^{fl/fl}* and *Ubc-Cre-Ert2 Ift88^{fl/fl}* mice. (n=7 at Tx+7d, n=3 at Tx+15d and Tx+22d, in duplicate) and *Ift88^{fl/fl}* mice (n=7 at Tx+7d, n=4 at Tx+15d and Tx+22d, in duplicate) (mean \pm SEM; 2way ANOVA, sidak's multiple comparison test, *Ift88^{fl/fl}* vs. *Ubc-Cre-Ert2 Ift88^{fl/fl}* ; p values are shown in the figure) C) Time course of hypothalamic IFT88 protein expression measured by western blots following tamoxifen injection in *Ift88^{fl/fl}* and *Ubc-Cre-Ert2 Ift88^{fl/fl}* mice. For Tx+22d the lanes were run on the same gel but were non-contiguous. D) Schematic representation of hypothalamic region studied E) Immunofluorescence of ADCY3 (red), a neuronal primary cilia specific protein, allows for the time course of cilia loss (arrows) in the hypothalamus of *Ubc-Cre-Ert2 Ift88^{fl/fl}* mice following tamoxifen injection (repeated in at least 4 mice in each group at each timepoint). Scale bar, 10 μ m.

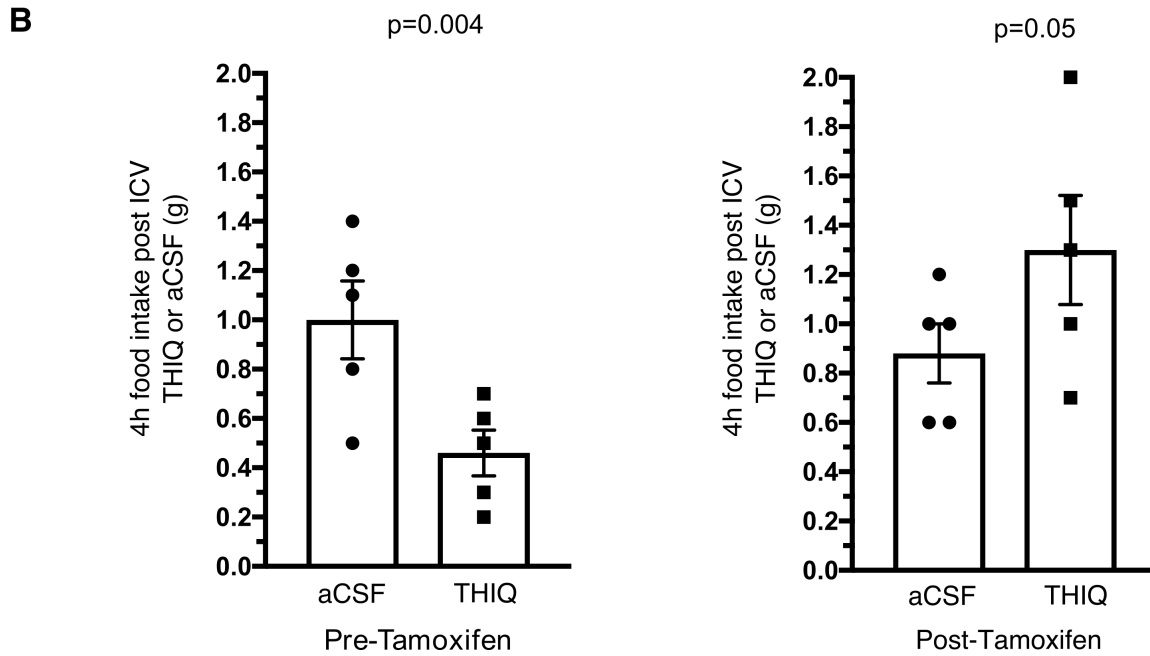
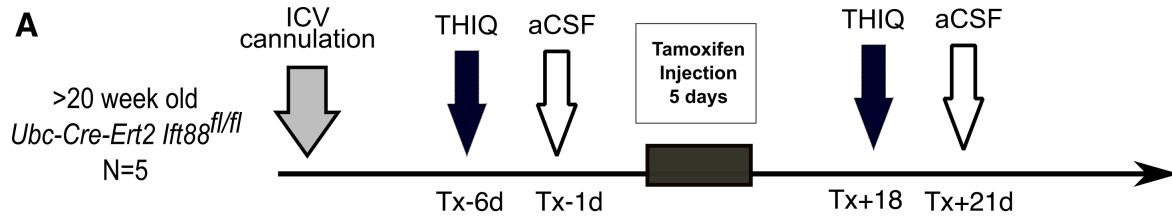


FIGURE 2.9 - SUPPLEMENTARY FIGURE 3: LOSS OF THE PRIMARY CILIUM ABOLISHES THIQ ACTIVATION OF MC4R.

A) Experimental protocol. B) Loss of the anorectic effects of ICV THIQ in tamoxifen treated *Ubc-Cre-Ert2 Ift88^{fl/fl}* mice. Data are represented as mean \pm SEM, paired t-test. n=5

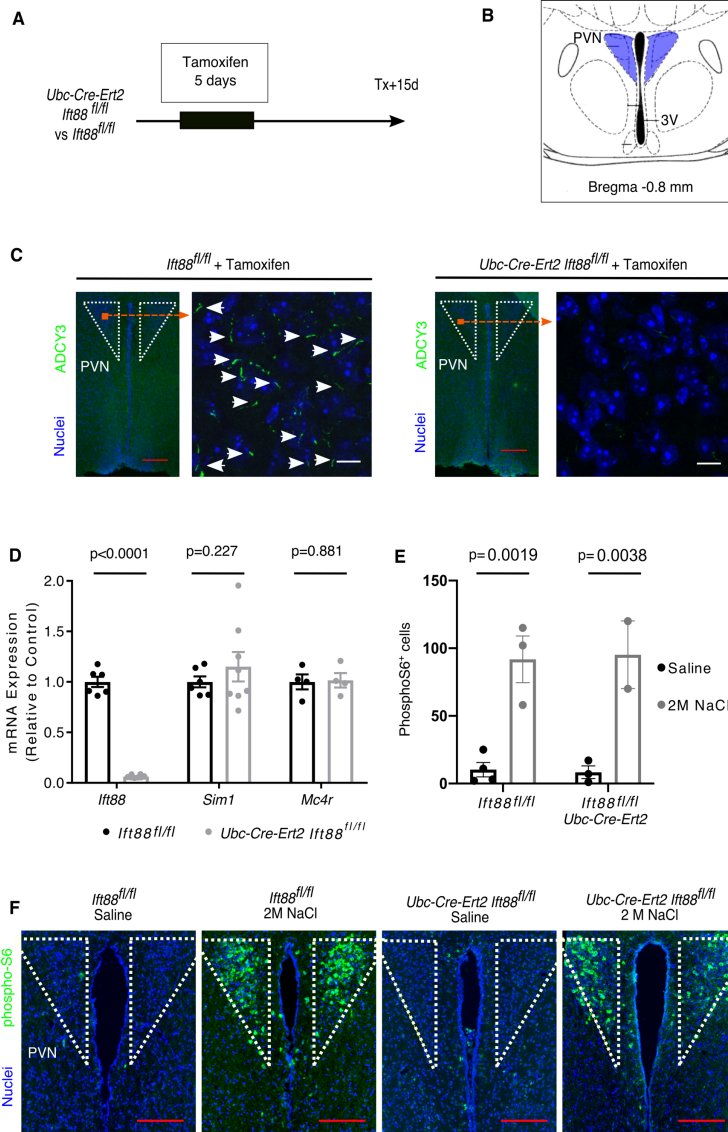


FIGURE 2.10 - SUPPLEMENTARY FIGURE 4: COMPLETE LOSS OF PVN CILIA DOES NOT AFFECT HYPOTHALAMIC *Mc4r* EXPRESSION OR GENERAL PVN NEURONAL FUNCTION.

A) Experimental protocol: 20 week old mice were treated with tamoxifen and their brains were harvested 15 days later. B) Schematic representation of hypothalamic region studied C) ADCY3-labeled primary cilia (green, arrows) are detected in neurons of the PVN of *Ift88^{fl/fl}* but not *Ubc-Cre-Ert2 Ift88^{fl/fl}* mice (repeated in at least 4 mice in each group). D) *Sim1* and *Mc4r* mRNA levels are unaffected in *Ubc-Cre-Ert2 Ift88^{fl/fl}* vs *Ift88^{fl/fl}* male mice at 15 days following tamoxifen administration, mean \pm SEM; unpaired t-test, *Ift88^{fl/fl}* vs. *Ubc-Cre-Ert2 Ift88^{fl/fl}*; p values are shown in the figure. $n=3$ vs 4 respectively for *Ift88* and *Sim1*, $n=2$ vs 2 respectively for *Mc4r* (averages of duplicates) E-F) Phospho-S6 activation assessment in the PVN of *Ift88^{fl/fl}* and *Ubc-Cre-Ert2 Ift88^{fl/fl}* 15 days after tamoxifen injection and 2 hours after either 0.3M (saline, $n=4$ and 3 respectively) or 2M NaCl injection ($n=3$ and 2 respectively). E) Quantification of the number of phospho-S6 positive cells (pS6⁺) following saline or 2M NaCl in one side of the PVN of *Ift88^{fl/fl}* and *Ubc-Cre-Ert2 Ift88^{fl/fl}* mice. F) Representative immunofluorescence staining of phospho-S6 in *Ift88^{fl/fl}* and *Ubc-Cre-Ert2 Ift88^{fl/fl}* mice following saline or 2M NaCl. Red scale bars represent 200 μ m, white scale bars represent 20 μ m. PVN: paraventricular nucleus of the hypothalamus; 3V: third ventricle.

Methods

Origin of the mouse lines used.

Mice were housed (with enrichment) in a barrier facility and maintained on a 12:12 light cycle (on: 0700-1900) at an ambient temperature of $23\pm 2^{\circ}\text{C}$ and relative humidity 50-70 %. Mice were fed with rodent diet 5058 (Lab Diet) and group-housed up to 5 or single housed after surgery. Experiments were performed with weight and sex-matched littermates.

Mice expressing tdTomato in a Cre dependent manner, *Gt(ROSA)26Sor^{tm14(CAG-tdTomato)Hze}*, and mice ubiquitously expressing Cre-Ert2, (*Tg(UBC-cre/ERT2)1Ejb, Ubc-Cre-Ert2*), were obtained from Jackson Laboratories (Bar Harbor, ME). Mice carrying the *Ift88* conditional allele (*Ift88^{tm1.1Bky, Ift88^{fl/fl}}*) were obtained from Bradley Yoder. Experimental male *Ubc-Cre-Ert2 Ift88^{fl/fl}* and control *Ift88^{fl/fl}* littermates on a mixed background were obtained by crossing *Ift88^{fl/fl}* females with *Ubc-Cre-Ert2 Ift88^{fl/fl}* males. Experimental *Mc4r^{t2aCre/t2aCre Ift88^{fl/fl}}* and control *Mc4r^{t2aCre/t2aCre Ift88^{+/+}}* littermates were obtained by crossing parents that were homozygotes for the *t2a-Cre* insertion, and heterozygotes for the *Ift88^{fl}* allele.

Generation of *MC4R^{t2aCre/t2aCre}* mice.

Was performed at the Gladstone Institute mouse transgenic core as described previously for *MC4R^{gfp/gfp}* mice¹³⁸. Briefly, Super-ovulated female FVB/N mice (4 weeks old) were mated to FVB/N stud males. Fertilized zygotes were collected from oviducts and injected with (1) Cas9 protein (50 ng/ul), (2) a donor vector (20 ng/ul) consisting of 1kb of 5' flanking sequence (i.e. the MC4R coding sequence) followed by t2aCRE and 5.5 kb of 3' flanking sequence and (3) a sgRNA (25ng/ul) of which the guide sequence (GTCTAGCAGGTATTAAGTGG) was designed to target nucleotides immediately downstream the MC4R stop codon in a short region that was not present in the donor vector into pronucleus. Injected zygotes were implanted into oviducts of pseudopregnant CD1 female mice. Pups were genotyped for insertions at the correct loci by PCR. MC4R neuron specific expression of Cre was verified by crossing mice with *Gt(ROSA)26Sor^{tm14(CAG-tdTomato)Hze}*. One full mouse brain (coronal sections) was imaged and analyzed to assess Cre expression throughout the brain (supplemental figure 1).

Generation and injections of AAVs .

AAV DJ-CMV GFP-Cre (AAV-creGFP) or AAV DJ-CMV GFP-ΔCre (AAV-nGFP), obtained from the Stanford Neuroscience Viral Core, were stereotaxically injected bilaterally (coordinates: AP=-0.8, ML=±0.2, DV=-5.5, volume= 2x0.5μL) in the brains of *Ift88^{fl/fl}* mice. Weight was measured for 1 month, after which mice were sacrificed to confirm the site of injection.

AAV DIO GPR88* plasmids were generated by replacing hChR2(H134R)-EYFP in pAAV-Ef1a-DIO-hChR2(H134R)-EYFP-WPRE-pA (obtained from K.Desseiroth, Stanford University) with GPR88(G283H)-FLAG. AAV DJ were prepared and titrated by the Stanford Neuroscience Viral Core which also provided the stock mCherry DIO-AAV (GVVC-AAV-14).

AAV DIO mCherry (0.2μL) +/- DIO GPR88 (0.8μL) were stereotaxically injected in the PVN (coordinates: AP=-0.8, ML=0.0, DV=-5.2) of *Mc4r^{t2aCre/t2aCre}* mice to anatomically and genetically restrict expression to PVN MC4R expressing neurons. Controls were either wild-type mice injected

with DIO-GPR88 + DIO-mCherry AAV or *Mc4r^{t2aCre/t2aCre}* injected solely with AAV DIO-mCherry (0.2µL) diluted in artificial cerebro-spinal fluid (aCSF, 0.8µL).

AAV DJ-hSyn-DIO-hM3Dgq-mCherry (AAV-GqDREADD), obtained from the Stanford Neuroscience Viral Core (AAV142) were stereotaxically injected bilaterally (coordinates: AP=-0.8, ML=±0.25, DV=-5.2, volume= 2x0.5µL) in the PVN of *Mc4r^{t2aCre/t2aCre} Ift88^{fl/fl}* or control mice (*Mc4r^{t2aCre/t2aCre} Ift88^{fl/+}* or *Ift88^{+/+}*). The negative control group mice (*Mc4r^{t2aCre/t2aCre} Ift88^{fl/+}* or *Ift88^{+/+}*) were injected with DIO-mCherry AAV.

Stereotaxic Surgeries.

Animals were anesthetized with an initial flow of 4% isoflurane, maintained under anesthesia using 2% isoflurane and kept at 30-37°C using a custom heating pad. The surgery was performed using aseptic and stereotaxic techniques. Briefly, the animals were put into a stereotaxic frame (KOPF Model 1900, USA), the scalp was opened, the planarity of the skull was adjusted and holes were drilled (coordinates: PVN [AP=-0.8, ML=±0.2, DV=-5.5], lateral ventricle for cannula implantation [AP=-0.3, ML=1.0, DV=-2.5]). The AAVs were injected at a rate of 0.1µL/min, and guide cannulas (PlasticsOne, 2.5mm) were implanted and secured to the skull using a tissue bonding glue (Loctite 454) and dental acrylic, and closed with a screw-on dummy cannula. Animals were given pre-operative analgesic (buprenorphine, 0.3 mg/kg) and post-operative anti-inflammatory Meloxicam (5mg/Kg) and allowed to recover at least 10 days during which time they were singly-housed and handled frequently.

Mouse metabolism studies.

Mice were single housed after AAV injection. Weight was measured weekly, or as mentioned in figures. Fat mass and lean mass were measured using EchoMRI (EchoMRI LLC, Houston, TX). Food intake was assessed either by hand or measured by CLAMS (Columbus Instruments, Columbus, OH). Energy expenditure was measured by CLAMS (Columbus Instruments, Columbus, OH). Mice were tested over 96 continuous hours, and the data from the last 48 hours were analyzed. Energy expenditure (EE) is expressed in terms of kcal per hour and calculated using the Lusk equation: $EE=(3.815+1.232\times RER)\times VO_2$, and was analyzed with CalR app software¹⁶⁰ (ANCOVA with body weight used as a covariate).

Specifically: for Figure 2 EchoMRI at 12 weeks and 24h food intake measured manually daily over 4 days; for Figure 3, Echo MRI at Tx+5, +12, +22, +27days, Food intake and energy expenditure measured by CLAMS: Tx+6-9, +13-16; +23-36; for Figure 6, EchoMRI at T0 and 3, 6 and 9 weeks post AAV injection, food intake and energy expenditure measured By CLAMS 3 weeks after AAV injection.

Acute food intake studies

Anorexigenic response to MTII. Experiments were performed as described¹⁶¹. Mice were deprived of food for 24h and injected intracerebroventricularly with either 1 µl artificial cerebro-spinal fluid (aCSF) or MTII (Genescript, Piscataway, NJ) in 1µl aCSF over a 15 sec period. For figure 4 0.5nmoles MTII were injected at Tx-2, +2, +11, +18 days, prior to weight divergence; in experiment in figure 5, 0.05nmoles MTII were injected; and 0.5 nmoles in figure 6 (randomized crossover study). Each mouse was returned to its home cage and a weighed amount of chow was placed into the cage. The remaining chow was weighed after 4 hours to determine intake. Permeability and placement

of the cannula was assessed before and after the protocol by measuring the drinking response to angiotensin II.

Anorexigenic response to THIQ. Experiments were performed as described¹⁶². Mice were deprived of food at 5PM, injected with 1 μ l aCSF or 1 μ l (32nM) THIQ (Tocris Bioscience, Bristol, UK) in aCSF at 7PM and food intake was measured 4 hours later.

Chemogenetic studies. CNO was administered at 2 mg per kg of body weight (i.p). Saline was delivered at the same volume and with same concentration of DMSO (2%). Mice were fasted for 24h prior injection and given access to food 30min after the injection. The food intake was measured as describe above 3h later.

Direct fluorescence and immunofluorescence studies of mouse hypothalamus. Mice were perfused trans-cardially with PBS followed by 4% paraformaldehyde fixation solution. Brains were dissected and post-fixed in fixation solution at 4°C overnight, soaked in 30% sucrose solution overnight, embedded in O.C.T. (Tissue-Tek, Sakura Finetek USA, INC., Torrance, CA), frozen, and cut into 20-35 μ m coronal sections, then stored at -80°C until staining.

After washing, sections were blocked for 1 hr in 50% serum 50% antibody buffer (1.125, %NaCl, 0.75%Tris base, 1%BSA,1.8 %L-Lysine, 0.04% azide), followed by incubation with primary antibody overnight at 4°C. After washing, sections were incubated with secondary antibodies for an hour at room temperature, washed and stained with Hoechst (1:5000), washed and mounted with ProlongTM Diamond antifade Mountant. Primary antibodies used: Chicken anti-GFP (Abcam, ab13970), 1:250; Rabbit anti-Adcy3 (Santa Cruz Biotechnology, sc-588), 1:500; Mouse anti-Flag M2 (Sigma, F1804), 1:500; Rabbit anti-pS6 ribosomal protein (Invitrogen, 44-923-G) 1:1000.

Secondary antibodies used: Goat anti-chicken Alexa fluor 488 (Invitrogen, A11039), 1:500; Goat anti-rabbit Alexa fluor 633 or 555 or 488 (Invitrogen, A21070, A21429, A11034), 1:500; Goat anti-mouse Alexa fluor 555 (Invitrogen, A21424), 1:500.

RNA scope

To detect single mRNA molecules, RNAScope was performed on 20 μ m frozen hypothalamic sections from a P6 *Mc4r^{t2aCre/t2aCre}* pup brain prepared as described above. The RNAScope Fluorescent Multiplex Kit V2 (Advanced Cell Diagnostics, #323100) was used according to the manufacturer's instructions. Briefly, slides were dried at -20°C for 1 hour and then at -60°C for 30minutes. They were post fixed in 4% PFA before being dehydrated in 50%, 70%, and 100% ethanol for 5 minutes. After letting the slides dry for 5minutes at room temperature, hydrogen peroxide was added to the slides for 8 minutes. Target retrieval was performed in a steamer at 100°C. Slides were first equilibrated to the steamer in distilled water, then placed in ACD's1x target retrieval agent. Slides were then allowed to dry overnight. The next day, slides were treated with protease III for 10min at room temperature. Cre-C2 (Advanced Cell Diagnostics, #312281-C2) probe and Mc4r-C3 (Advanced Cell Diagnostics, #319181-C3) probe were diluted at a 1:50 ratio with probe diluaent (Advanced Cell Diagnostics, #300041) and incubated on the slides for 2 hours at 40°C followed by 3 amplification steps. Opal 520 (Akoya Biosciences #FP1487001KT) and Opal 570 (Akoya Biosciences, #FP148800KT) fluorophores were diluted 1:1500 in TSA buffer. The Cre-C2 probe was developed with Opal 520 fluorophore and the Mc4r-C3 probe was developed with

Opal 570 fluorophore. DAPI was added to label the nuclei, and slides were mounted with Prolong Gold (Thermo Fischer Scientific).

Image capture and processing.

Confocal images were generated using a Leica SP5 (Supplementary Figure 2, 4), a Zeiss LSM 780 confocal microscope (Figure 5) or a Nikon W1 spinning disk confocal (Figure 6). RNAscope images (supplemental Figure 1) were acquired with a Leica SP8 confocal microscope.

Images were processed with Fiji. Maximal intensity Z projections are from at least 20 slices over 10-20 μm . Widefield Images of pS6 staining (Supplementary Figure 4) were generated using an Zeiss Apotome. Quantification of phospho-S6 positive cells was performed with Fiji.

Tamoxifen-induced recombination.

Ubc-Cre-Ert2-dependent recombination was induced by intra-peritoneal administration of tamoxifen (Sigma-Aldrich, St. Louis, MO) for 5 consecutive days at a dose of 10.0mg/ 40g body weight.

Osmotic stimulation.

Mice were given an IP injection of 2M NaCl (350 μl) or normal saline (0.9% NaCl, 350 μl) as control, water was removed from the cage, and mice were allowed access to food and were perfused 120 min later.

Hypothalamic RNA and Protein quantification.

Hypothalamic tissue was collected by dissection. IFT88 protein levels were assayed by immunoblot (as previously described by Reed et al. 2010). Primary antibodies used were Rabbit anti-IFT88 (Proteintech, 13967-1-AP), 1:500; Mouse anti-GAPDH (6C5) (Santa Cruz Biotechnology, 1:1000). Secondary antibodies used were Goat anti-rabbit IgG-HRP (Santa Cruz) 1:3000; Goat anti-mouse IgG-HRP (Santa Cruz) 1:3000. mRNA levels were assayed using by quantitative RT-PCR using Taqman assays (Thermo Fischer) for *Ift88* (Mm01313467_m1), *Sim1* (Mm00441391_m1), *Mc4r* (Mm00457483_s1) and β -actin (Mm00607939_s1).

Statistical analysis

Sample sizes were chosen based upon the estimated effect size drawn from previous publications (Siljee et al., 2018) and from the performed experiments. Data distribution was assumed to be normal, but this was not formally tested. Statistical analysis was performed using unpaired Student t test or repeated measures of two-way ANOVA followed by Sidak's multiple comparisons test, as indicated. All data were expressed as mean \pm SEM. A p-value ≤ 0.05 was considered as statistically significant. All data were analyzed using Prism 8.0 (GraphPad Software) or CalR app for energy expenditure data (ANCOVA with body weight included as a covariate)¹⁶⁰.

Transition

After demonstrating that MC4R's ciliary localization is necessary for its key role in regulating long term energy homeostasis, we sought to investigate the mechanisms by which MC4R is transported to cilia. Since heterozygous mutations in MC4R are sufficient to cause severe obesity, and mutations which only affect ciliary trafficking of MC4R- but not its activity or transport to the membrane- were found in patients with obesity⁵⁶, we hypothesized that genes coding for molecules necessary to transport MC4R to cilia would be candidate genes for human obesity. This leads to a simple model explaining ciliopathy-associated obesity, in which decreased localization of MC4R to the cilia of PVN neurons is the cause of impaired energy balance regulation.

While most ciliopathy-associated genes identified to date are involved in structural or functional elements of cilia themselves, and could therefore lead to obesity because of a diversity of non-cell specific effects, we sought to investigate whether MC4R would require cell-specific partners to localize to cilia.

As a proof of concept, we interrogated the function of the accessory protein MRAP2 (Melanocortin Receptor Associated Protein 2), which had previously been shown to be associated to MC4R *in vitro*, and co-expressed with MC4R in PVN neurons *in vivo*.

Chapter 3 MRAP2 regulates energy homeostasis by promoting primary cilia localization of MC4R

Adélaïde Bernard, Irene Ojeda Naharros, Florence Bourgain-Guglielmetti, Jordi Ciprin, Xinyu Yue, Sumei Zhang, Erin McDaid, Maxence Nachury, Jeremy F. Reiter, Christian Vaisse.

Published in BioRxiv, doi: <https://doi.org/10.1101/2020.11.13.382325>

Summary

The G protein-coupled receptor MC4R (Melanocortin-4 Receptor) and its associated protein MRAP2 (Melanocortin Receptor-Associated Protein 2) are both essential for the regulation of food intake and body weight in humans and mice. MC4R localizes and functions at the neuronal primary cilium, a microtubule-based organelle that senses and relays extracellular signals. Here, we demonstrate that MRAP2 is critical for the ciliary localization and weight-regulating function of MC4R. Our data reveal that GPCR localization to primary cilia can require specific accessory proteins that may not be present in heterologous cell systems. Our findings also demonstrate that targeting of MC4R to neuronal primary cilia is essential for the control of long-term energy homeostasis and suggests that genetic disruption of MC4R ciliary localization may frequently underlie inherited forms of obesity.

Introduction

The regulation of food intake and energy expenditure is dependent on the genetic, molecular and cellular integrity of the central melanocortin system, a network of hypothalamic neurons that integrate peripheral information about energy status and regulate long-term energy homeostasis, thereby preventing obesity⁴¹. This system comprises the neuropeptides α -MSH and AGRP, produced by independent populations of neurons in the arcuate nucleus which are sensitive to the adipocyte-secreted hormone leptin, as well as the receptor for these neuropeptides, the melanocortin-4 receptor (MC4R). MC4R, one of five members of the G α s-coupled Melanocortin receptor family⁴², is found in multiple brain regions but its expression in the para-ventricular nucleus of the hypothalamus (PVN) is both necessary and sufficient for the regulation of food intake and body weight^{54,163}. Underscoring the essential role of this receptor in the maintenance of energy homeostasis, heterozygous loss-of-function mutations in *MC4R* are the most common cause of monogenic obesity in humans^{47,48,52} and the *MC4R* locus displays the second strongest association with obesity amongst the common variants influencing body mass index (BMI)³⁻⁵. *Mc4r*^{+/-} and *Mc4r*^{-/-} mice recapitulate the obesity phenotypes observed in humans⁵³. The central importance of MC4R in energy homeostasis has made it a major target for the pharmacotherapy of obesity. Yet, little is known about the molecular and cellular pathways underlying the maintenance of long-term energy homeostasis by MC4R-expressing neurons.

Recently we reported that MC4R localizes and functions at the neuronal primary cilium^{56,119}, a cellular organelle that projects from the surface of most mammalian cell types and functions as an antenna to sense extracellular signals¹⁶⁴. Inherited mutations that disrupt ciliary structure or function cause ciliopathies^{134,165,166}, disorders characterized by pleiotropic clinical features which can include hyperphagia and severe obesity¹⁶⁷ such as in Alström or in Bardet-Biedl syndrome (BBS). In adult mice, genetic ablation of neuronal primary cilia also causes obesity¹⁶⁸.

MC4R physically interacts with the melanocortin receptor-associated protein MRAP2, a member of the MRAP family comprised of single-pass transmembrane proteins that interact with Melanocortin receptors¹⁶⁹ and other GPCRs^{170,171}. In non-ciliated heterologous systems, MRAP2 binds to MC4R and increases ligand sensitivity, as well as MC4R-mediated generation of cAMP¹⁷²⁻¹⁷⁴. In human, MRAP2 variants were found in patients with obesity^{172,175-177}. *Mrap2*^{-/-} mice develop severe obesity although they lack the early-onset hyperphagia of *Mc4r*^{-/-} mice¹⁷² questioning the extent to which MRAP2 qualitatively and quantitatively interacts with MC4R *in vivo*. Indeed, MRAP2 has also been suggested to interact with other GPCRs such as the Ghrelin Receptor and the Prokineticin Receptor^{170,171}.

Here we find that the central mechanism of MRAP2-associated obesity is the critical role for MRAP2 in targeting MC4R to cilia.

Results

MC4R neurons require MRAP2 to regulate energy homeostasis

Germinal deletion of MRAP2, in *Mrap2*^{-/-} mice, leads to obesity although to a lesser extent than that observed in *Mc4r*^{-/-} mice¹⁷². To determine the specific cell type that requires MRAP2 to control

energy homeostasis, we deleted MRAP2 from MC4R-expressing cells. We obtained mice bearing an *Mrap2* knockout-first (“tm1a”) allele and confirmed that, as previously reported^{169,172,173}, homozygous mutant mice (hereafter referred to as *Mrap2*^{-/-}, Figure S1a) were obese and hyperphagic at 12 weeks of age, but did not differ from their wild-type littermates at 4 weeks of age (Figure S1b,c). From these mice, we generated an *Mrap2* floxed allele (“tm1c” allele, hereafter referred to as *Mrap2*^{fl/fl}, Figure S1a). *Mrap2*^{fl/fl} mice weighed the same as their wild-type littermates (Figure S1d).

To specifically delete MRAP2 in MC4R-expressing neurons, we generated *Mc4r-t2a-Cre*¹¹⁹ *Mrap2*^{fl/fl} mice (hereafter referred to as *Mc4r*^{t2aCre/t2aCre} *Mrap2*^{fl/fl}). *Mc4r*^{t2aCre/t2aCre} *Mrap2*^{fl/fl} mice fed ad libitum regular chow developed early-onset obesity with significantly higher body weight (Figure 1a-f) and fat mass (Figure 1 k-r), associated with hyperphagia (Figure 1s-v). This phenotype was apparent at 4 weeks of age (Figure 1c,e,k,m,o,q,s,u), and was present both in females and in males (Figure 1). Together, these data demonstrate that MRAP2 is essential in MC4R-expressing neurons to regulate food intake and body weight.

MRAP2 promotes MC4R targeting to the primary cilium of IMCD3 cells

The interaction between MRAP2 and MC4R, as well as the cellular localization of MRAP2 have been previously studied in non-ciliated cells^{172–175,179}. Since MC4R localizes to the primary cilium, and MRAP2 has been reported to interact with MC4R *in vitro*¹⁷², we tested whether MRAP2 co-localizes with MC4R at the primary cilium following transfection in heterologous cells.

In transiently transfected murine Inner Medullary Collecting Duct (IMCD3) cells, we found that MRAP2 co-localized with the ciliary component, acetylated tubulin (AcTub, figure S2b), and with MC4R at the primary cilium (Figure 2a, top panel). We tested whether MRAP2 localization is a common feature to the proteins of the MRAP family. We found that a paralog of MRAP2, the Melanocortin Receptor-Associated Protein 1 (MRAP1), an essential accessory factor for the functional expression of the MC2R/ACTH receptor, did not localize to the primary cilium (Figure 2a,b, Figure S2a,b). Ciliary localization is therefore a specific feature of MRAP2.

We hypothesized that MRAP2 promotes MC4R ciliary localization, and so investigated whether MRAP2 affects MC4R localization. Remarkably, we found that MRAP2 increased MC4R enrichment at the primary cilium, whereas MRAP1 had no effect (Figure 2a,b top panel). Therefore, MRAP2, but not MRAP1, enriches MC4R at primary cilia.

Finally, we assessed the specificity of the interaction between MRAP2 and MC4R by systematically testing the ciliary enrichment of all five Melanocortin receptor family members in the presence or absence of MPRAPs (n=30, Figure 2b,c). Although MRAP2 promoted the ciliary localization of other Melanocortin receptors, the greatest effect was observed on MC4R (Figure 2b,c). MRAP1 did not affect ciliary enrichment of any of the receptors (Figure 2b). Thus, MRAP2 specifically promotes MC4R localization to the primary cilia.

MRAP2 colocalizes with MC4R at the primary cilium of hypothalamic neurons *in vivo*

To determine whether MRAP2 localizes to the primary cilia *in vivo*, we used a transgenic reporter mouse model in which primary cilia are labelled with GFP (*Arl13b-GFP^{tg}*)¹⁸⁰. MRAP2 subcellular localization was assessed by immunofluorescence, which revealed that MRAP2 localizes at the primary cilium in the PVN of these mice (Figure 3a-c). The specificity of the anti-MRAP2 antibody was confirmed by staining hypothalamic sections from *Mrap2^{-/-}* mice (Figure S3).

To further determine whether MRAP2 colocalizes with MC4R at primary cilia, we used a mouse line in which GFP was fused to the C-terminus of MC4R at the endogenous locus⁵⁶ (hereafter referred to as *Mc4r^{gfp}*) allowing for the assessment of the sub-cellular localization of the endogenous MC4R. In the PVN of *Mc4r^{gfp}* mice, most MC4R-GFP localized at primary cilia (Figure S4) and, remarkably, MRAP2 localized exclusively to the cilium of these cells (Figure 3f).

MC4R localization to primary cilia requires MRAP2

Since MRAP2 enhances MC4R localization at primary cilia *in vitro*, and MC4R co-localizes with MRAP2 at primary cilia *in vivo*, we tested whether loss of MRAP2 compromises MC4R localization at primary cilia *in vivo*. We generated *Mrap2^{+/+} Mc4r^{gfp}* and *Mrap2^{-/-} Mc4r^{gfp}* mice to compare the ciliary localization of MC4R-GFP in the presence and absence of MRAP2.

In the PVN of *Mrap2^{+/+}* mice, MC4R-GFP mainly localized to cilia (Figure 4a). Remarkably, in *Mrap2^{-/-}* mice, MC4R-GFP mainly localized to neuronal cell bodies, and was rarely found at primary cilia (Figure 4b). The normalized intensity of MC4R-GFP at cilia (defined by ADCY3 immunostaining) was decreased in *Mrap2* mutants compared to wildtype (Figure 4c, $p < 0.0001$) and MC4R was no longer enriched in cilia in the absence of MRAP2 (Figure 4d, $p < 0.0001$). Thus, MRAP2 is necessary for MC4R enrichment at primary cilia both *in vitro* and *in vivo*.

Since whole-body deletion of *Mrap2* could lead to developmental defects potentially accounting for MC4R inability to localize to cilia, we investigated whether acute deletion of *Mrap2* could result in the disruption of MC4R ciliary localization. To test this hypothesis, we removed MRAP2 from the PVN of adult mice. Specifically, by injecting *Mrap2^{fl/fl} Mc4r^{gfp}* mice unilaterally with an Adeno Associated Virus (AAV) encoding mCherry-IRES-Cre, *Mrap2* was deleted from the infected PVN by cre-mediated recombination, and the contralateral uninfected PVN served as an internal control (Figure 5b). The brains were harvested 3 weeks following the AAV injections and analyzed. Concordant with our prediction, immunofluorescence staining revealed that MRAP2 was absent from cilia of mCherry-expressing cells, whereas MRAP2 localized to cilia of the contralateral control PVN ($n=4$, Figure 5b,c). Cilia, identified by ADCY3 staining, were present in the infected PVN (Figure 5d), confirming that MRAP2 is dispensable for PVN primary cilia maintenance. Remarkably, MC4R localized to cilia in control PVNs, but not in the PVNs from which MRAP2 had been removed (Figure 5d), confirming MRAP2 is essential for MC4R ciliary localization.

To test whether MRAP2 contributes to the ciliary localization of other GPCRs, we assessed the localization of the Somatostatin Receptor 3 (SSTR3) in the presence or absence of MRAP2. SSTR3 is a cilia-localized GPCR which is also expressed in the PVN¹⁸¹, including a subset of MRAP2-expressing neurons (Figure S5d,e). Interestingly, the absence of MRAP2 did not affect ciliary localization of SSTR3 (Figure S6). We conclude that MRAP2 is specifically required for MC4R localization at the primary cilium *in vivo*.

Discussion

Ablating primary cilium by conditionally knocking out *Ift88* in adult mice leads to obesity, either when deleted ubiquitously, specifically in neurons, or only in the PVN, directly implicating PVN cilia in the control of feeding behavior^{119,168}.

The composition of the primary ciliary membrane is different from that of the surrounding plasma membrane, as it is enriched for proteins involved in specific forms of signaling¹⁸². We previously identified MC4R as one of a select subset of GPCRs that localizes to cilia. Moreover, antagonizing Gs signaling specifically at the primary cilium of MC4R-expressing PVN neurons also leads to obesity¹¹⁹, suggesting that not only does MC4R localize to cilia, but it functions in cilia to mediate energy homeostasis. Importantly, human obesity-associated *MC4R* mutations affecting its third intracellular loop (a domain previously implicated in the ciliary localization of other GPCRs¹⁸³) impair MC4R ciliary localization without affecting its trafficking to the cell membrane or its ability to couple to G proteins⁵⁶. In the present study, we demonstrate that a ciliary GPCR accessory protein, MRAP2, restrains feeding by acting in MC4R-expressing neurons to direct its associated GPCR, MC4R, to cilia. These studies providing multiple concordant lines of evidence to demonstrate that ciliary localization is critical for MC4R function in humans and mice. As MC4R and MRAP2 are essential for suppressing feeding behavior and MC4R fails to localize to primary cilia in *Mrap2*^{-/-} mice, we propose that the failure of MC4R to localize to cilia accounts for the obesity observed in MRAP2-deficient mice and humans.

Previous *in vitro* studies in unciliated cells have reported conflicting effects of MRAP2 on MC4R function: one study reported that MRAP2 does not affect MC4R activity¹⁷⁹, another suggested that MRAP2 may inhibit MC4R activity¹⁷³, and others that MRAP2 increases its response to ligand^{172,174}. MRAP2 was also reported to either positively or negatively regulate MC4R activity depending on their relative concentrations¹⁷⁵. Similarly, MRAP2 has been reported to either decrease¹⁷³ or modestly increase¹⁷⁴ MC4R cell-surface expression. It will be of interest to repeat these assays in ciliated cells.

The ciliary targeting of class A GPCRs such as SSTR3, D1R, MCHR1 and HTR6 depends on interactors such as Tubby family members and the IFT-A complex^{104,181,184,185}. In contrast, the dependence of MC4R on MRAP2 for ciliary trafficking reveals a more specific requirement. For example, we found that, although MRAP2 and SSTR3 co-localize at primary cilia of some PVN neurons, SSTR3 does not require MRAP2 for ciliary localization. Therefore, MRAP2 may be a ciliary trafficking chaperone for MC4R, rather than a component of the general ciliary trafficking machinery. Ciliary accessory proteins such as MRAP2 may represent a site of regulation for the ciliary localization and function of their associated receptors.

Although MRAP2 is not required generally for ciliary GPCR localization, it may associate with other GPCRs beyond MC4R, including GHSR1a¹⁷¹ and PKR1¹⁷⁰. It will be interesting to assess whether other MRAP2-associated receptors localize to cilia in MRAP2-dependent ways. Association of MRAP2 with receptors other than MC4R could also explain the differences in weight phenotypes caused by removing *Mrap2* globally and specifically in MC4R-expressing neurons. Specifically, we found that inactivating *Mrap2* specifically in MC4R-expressing neurons causes, like *Mc4R* loss-of-function, early onset hyperphagia and obesity, whereas germline inactivation of *Mrap2* caused a

milder phenotype, with late onset hyperphagia and obesity^{172,178}. Therefore, it will be interesting to assess whether MRAP2 promotes the ciliary function of orexigenic receptors.

The role of primary cilia in metabolism^{56,167,186–188} has motivated screens in heterologous cell culture systems to identify ciliary GPCRs that control energy homeostasis. Previously described ciliary GPCRs include the Melanin-Concentrating Hormone Receptor 1 (MCHR1)¹⁸³ and the Neuropeptide Y Receptor 2 (NPY2R)^{189,190}. However, the necessity of an accessory protein like MRAP2 for ciliary trafficking of specific GPCRs was not considered, suggesting that these screens may have missed a number of ciliary GPCRs, including MC4R^{189,190}. Whether other ciliary GPCRs use accessory proteins for ciliary trafficking is an open question, but is hinted at by studies demonstrating that proteins, such as Rhodopsin, localize robustly to cilia in their native cell types, but less well in heterologous ciliated cells¹⁹¹.

Our study revealed that MRAP2 is required for MC4R localization to and function at primary cilia and its resulting function, and is therefore necessary to regulate long-term energy homeostasis. The emerging connection between primary cilia and energy homeostasis^{56,167,186–188} suggests that mutations in other genes necessary for the ciliary localization and function of MC4R will be candidate causes for human obesity.

Figures

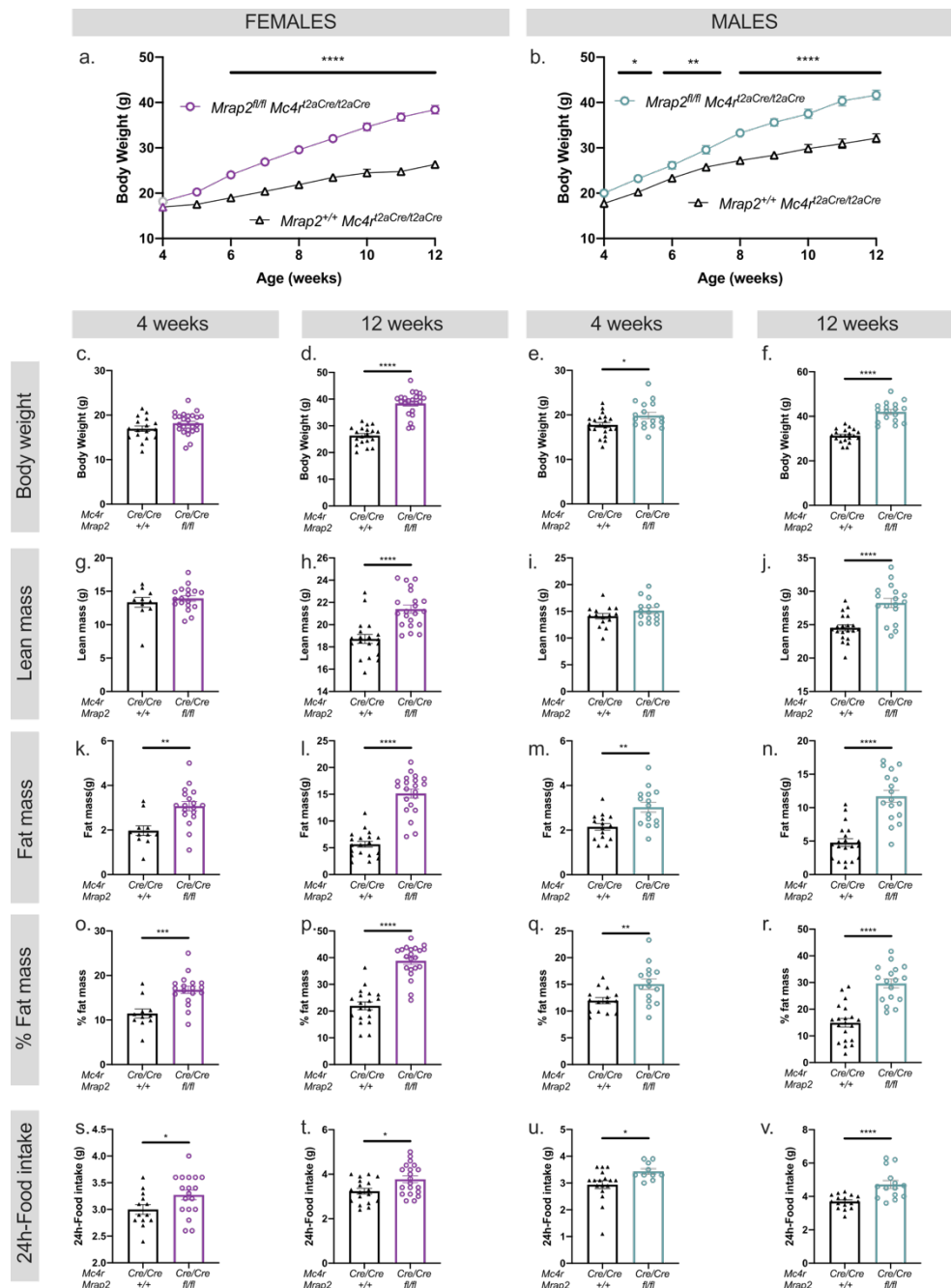


FIGURE 3.1 MRAP2 FUNCTIONS IN MC4R-EXPRESSING CELLS TO REGULATE FOOD INTAKE AND RESTRAIN BODY WEIGHT.

Body weight curve of $Mc4R^{t2aCre/t2aCre} Mrap2^{fl/fl}$ vs $Mc4R^{t2aCre/t2aCre} Mrap2^{+/+}$ female (**a**) and male (**b**) mice. Respective body composition at 4 and 12 weeks of $Mc4R^{t2aCre/t2aCre} Mrap2^{fl/fl}$ vs $Mc4R^{t2aCre/t2aCre} Mrap2^{+/+}$ females (body weight [**c,d**], lean mass [**g,h**], fat mass [**k,l**], percent fat mass [**o,p**]) and males (body weight [**e,f**], lean mass [**i,j**], fat mass [**m,n**], percent fat mass [**q,r**]). 24h-food intake at 4 and 12 weeks of $Mc4R^{t2aCre/t2aCre} Mrap2^{fl/fl}$ vs $Mc4R^{t2aCre/t2aCre} Mrap2^{+/+}$ females (**s,t**) and males (**u,v**). n=11 to n=24 mice per group were used, individual values are displayed. Data are represented as mean \pm SEM, *p<0.05, **p<0.01, ***p<0.001, ****p<0.0001, Student's unpaired t-test (column analysis); mixed-effects model (REML) and Sidak's multiple comparisons tests (weight curves).

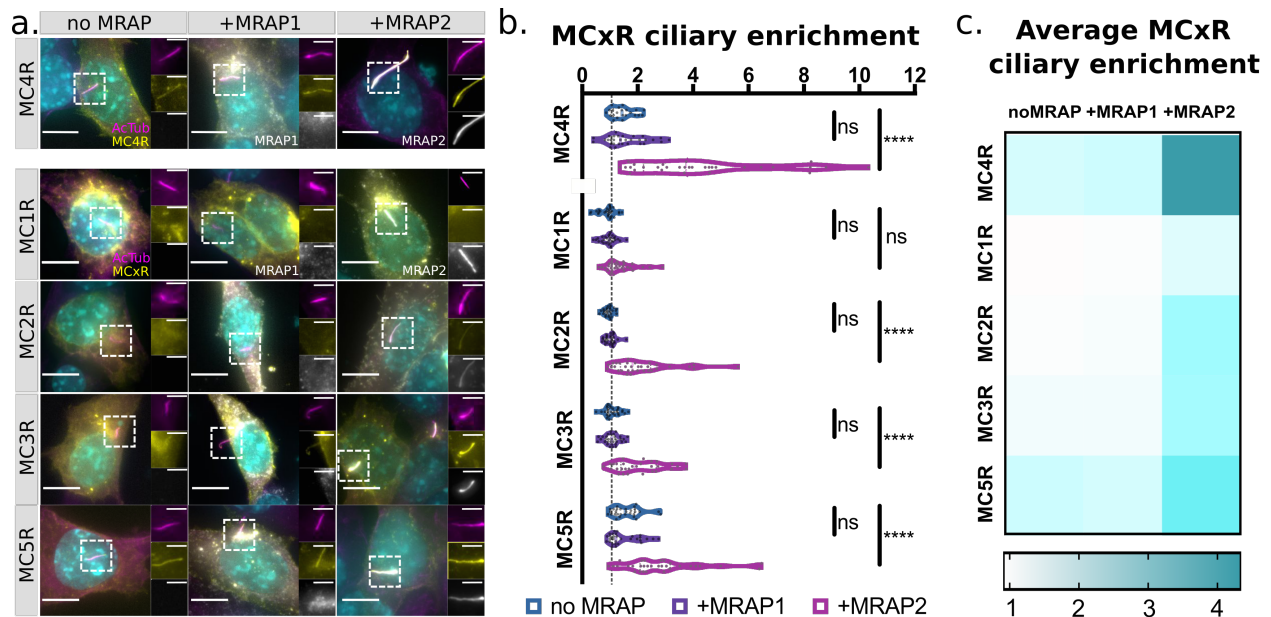


FIGURE 3.2 MRAP2 LOCALIZES MC4R TO THE IMCD3 PRIMARY CILIUM

a Representative widefield micrographs of IMCD3 cells transiently transfected with GFP-tagged Melanocortin receptors alone (left), or co-transfected with MRAP1-FLAG (center) or MRAP2-FLAG (right). Cells are stained for cilia (AcTub, magenta), GFP-tagged melanocortin receptors (yellow), MRAP1- or MRAP2-FLAG (white) and nuclei (Hoechst 33342, cyan). MC4R-GFP and MRAP2-FLAG colocalize at the primary cilium (top panel). Scale bars represent 5 μm for low magnification images and 2 μm for the inserts. **b** Melanocortin receptor enrichment at the cilium when transfected without MRAP (blue), with MRAP1 (purple) or with MRAP2 (magenta). MRAP2 expression increases ciliary localization of MC2R, MC3R, MC4R and MC5R, but not MC1R. MRAP1 co-expression has no effect on ciliary localization. **c** Heatmap displaying mean enrichment at the cilium when MCRs are transfected without MRAP (column 1), with MRAP1 (column 2) or MRAP2 (column 3). MRAP2 highly enriches MC4R localization at the cilium compared to other MCRs.

30-34 ciliated cells per condition were imaged and analyzed. Ciliary and cell body intensity of Melanocortin receptor and MRAP was measured using Fiji. Enrichment at the cilium is expressed as (integrated density at the cilium)/(integrated density in the cell body). Enrichment >1 indicates higher localization of GFP-tagged melanocortin receptor or MRAP at the primary cilium than at the cell body. Data are represented as violin plots. **** $p < 0.0001$, ordinary one-way ANOVA with Sidak's multiple comparisons test.

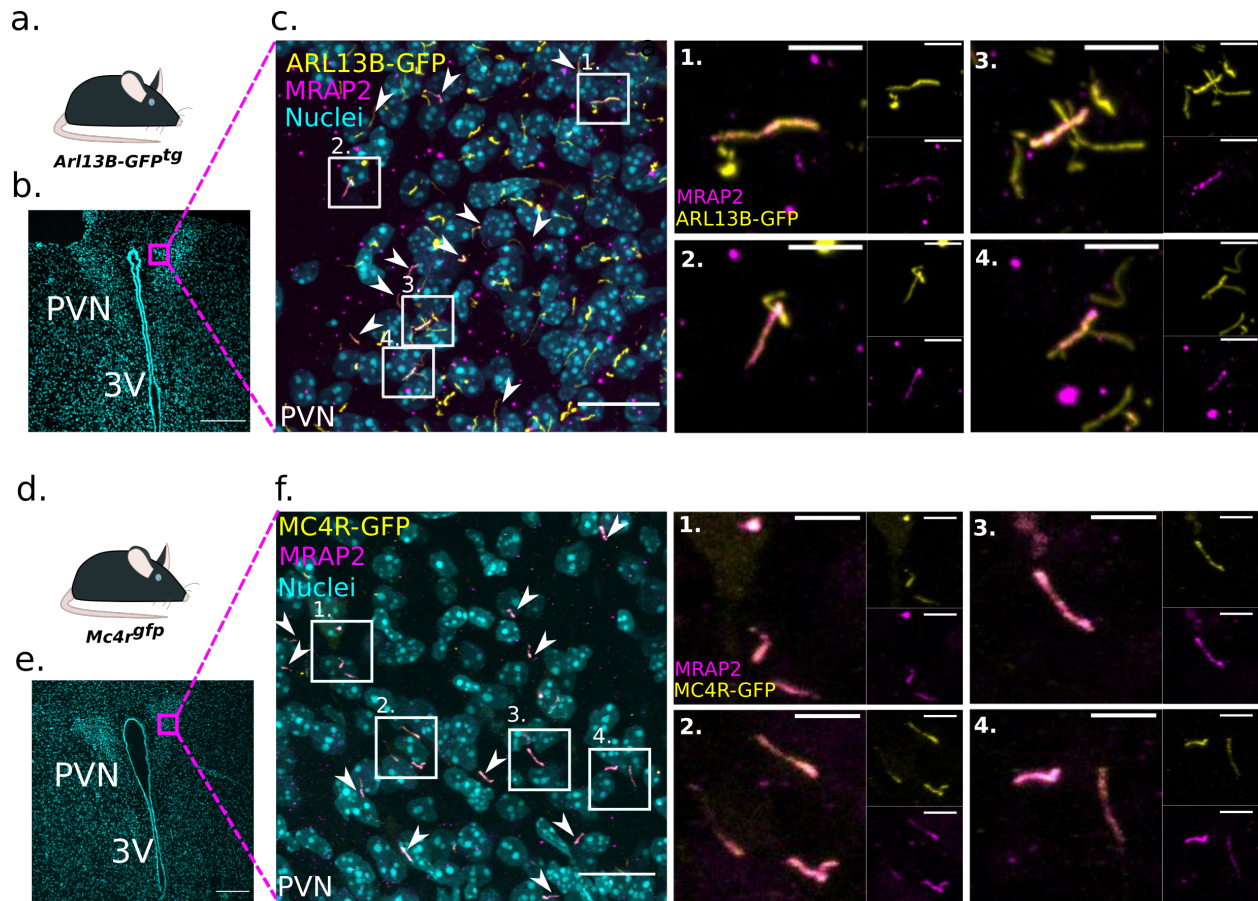


FIGURE 3.3 MRAP2 COLOCALIZES WITH MC4R AT THE PRIMARY CILIA IN VIVO.

a-c MRAP2 localizes to primary cilia in vivo. a Mice expressing a transgene encoding for a ciliary GFP (Arl13-GFP) were used in this experiment. b Representative low magnification image of the PVN, nuclei (Hoescht, cyan). Magenta square indicates higher magnification image depicted in c. Scale bar, 200 μm . c Immunofluorescence image of cilia (Arl13b-GFPtg, yellow), MRAP2 (magenta) and nuclei (Hoechst, cyan) in the mouse PVN, showing that MRAP2 localizes to primary cilia (arrows). d-f MRAP2 colocalizes with MC4R in vivo (arrows and boxes). d Mouse line expressing a GFP tag in frame at the C-terminus of the endogenous Mc4r locus. e Representative low magnification image of the PVN, nuclei (Hoescht, cyan). Magenta square indicates higher magnification image depicted in f. Scale bar, 200 μm . f Immunofluorescence image of MC4R-GFP (yellow), MRAP2 (Magenta) and nuclei (Hoechst, cyan) in the mouse PVN. Indicated boxed regions are shown to the right at higher magnification. Scale bars, 20 μm for low powered images and 5 μm for high powered images. 3V: third ventricle, PVN: paraventricular nucleus of the hypothalamus SCH: suprachiasmatic nucleus.

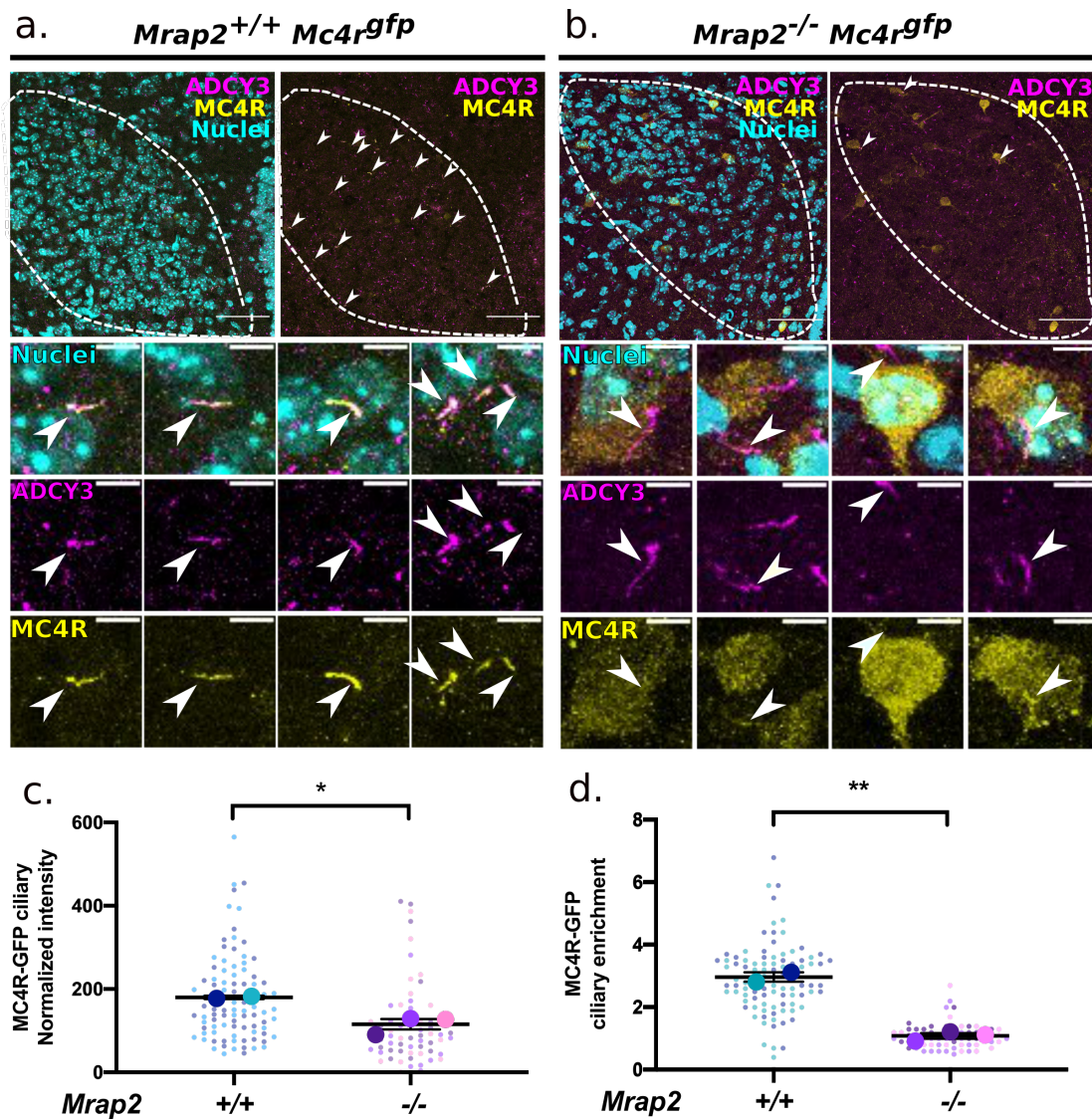


FIGURE 3.4 MRAP2 IS REQUIRED FOR MC4R LOCALIZATION TO THE PRIMARY CILIA

a,b Immunofluorescence images of MC4R-GFP (yellow), cilia (ADCY3, magenta) and nuclei (Hoechst, cyan). Top panels: dashed lines delineate the PVNs. Scale bar, 50 μ m. Bottom panels: High magnification images. Scalebar, 5 μ m. Arrowheads indicate MC4R-GFP⁺ cilia. **c** Quantitation of MC4R-GFP fluorescence intensity at the primary cilium (in arbitrary units). MC4R-GFP ciliary localization is decreased in the absence of MRAP2. **d** Quantitation of MC4R-GFP enrichment at the primary cilium as (integrated density at the cilium)/(integrated density in an equal area of the cell body). Enrichment >1 indicates higher localization of MC4R-GFP at the primary cilium than at the cell body. MC4R-GFP localization was quantified from two PVNs per P6 *Mc4r*^{gfp} *Mrap2*^{+/+} (n=2) and *Mc4r*^{gfp} *Mrap2*^{-/-} (n=3) mice. Data are represented as mean \pm SEM, *p<0.05, **p<0.01, Student's t test.

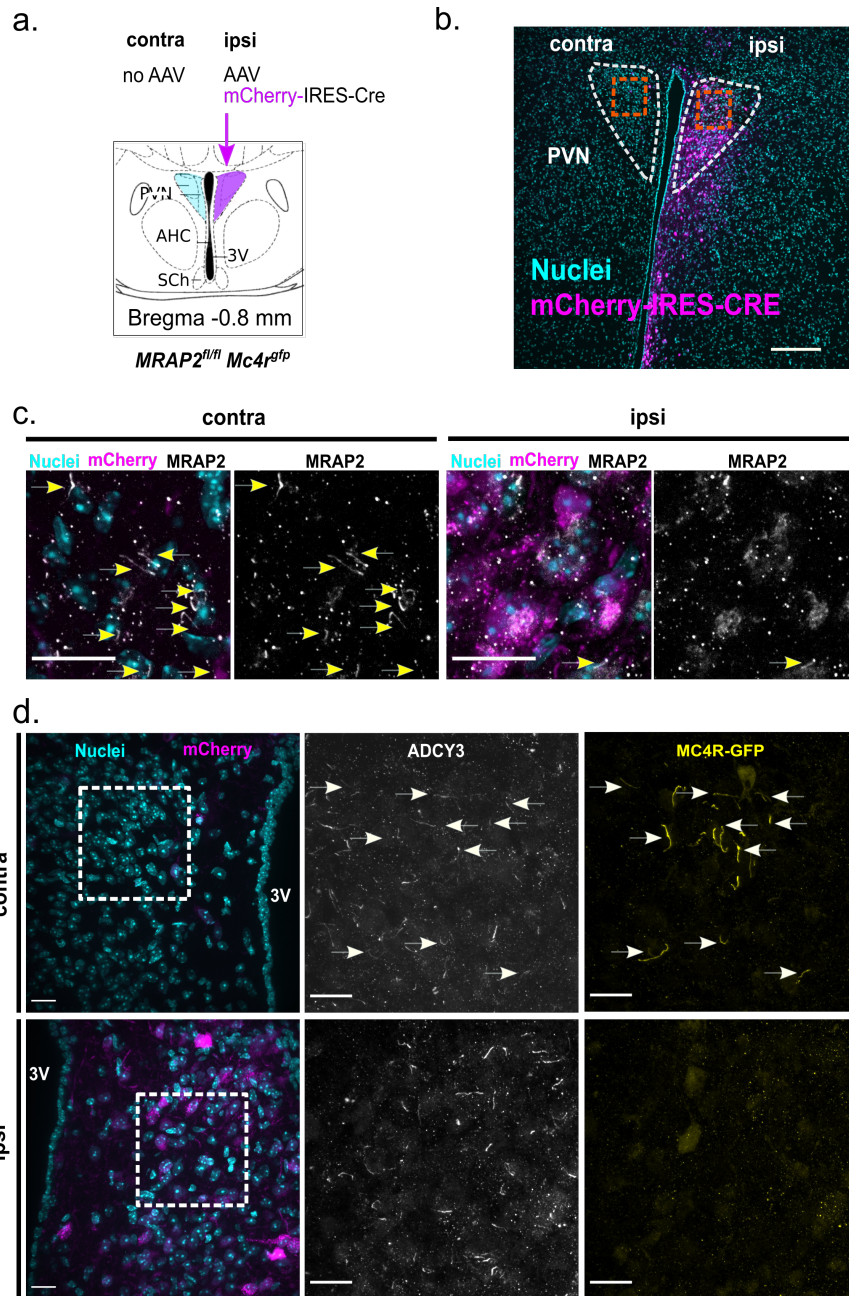


FIGURE 3.5 MRAP2 IS REQUIRED IN THE ADULT PVN FOR MC4R CILIARY LOCALIZATION

a Experimental design. *Mrap2^{fl/fl} Mc4rgfp* mice were injected unilaterally with AAV encoding mCherry-IRES-Cre (n=4 8-week-old females) and analyzed 3 weeks following injection. b Representative low magnification image of PVN, mCherry (magenta) and nuclei (Hoescht, cyan). Orange squares indicate higher magnification images depicted in c. Scale bar, 200 μ m. c Higher magnification images of inserts from b. Immunofluorescent staining of MRAP2 (white) of the control contralateral and experimental, ipsilateral PVN with mCherry (magenta) and nuclei (Hoescht, cyan). Arrows indicate MRAP2+ cilia, absent from mCherry-expressing cells. Scale bar, 50 μ m. d Immunofluorescent staining of control, contralateral PVN and experimental, ipsilateral PVN for, on the left, mCherry (magenta) and nuclei (Hoescht, cyan), in the middle, ADCY3 (white) and, on the right, MC4R-GFP (yellow). White squares indicate regions imaged for higher magnification images in the middle and right. ADCY3 is not altered by loss of MRAP2 while MC4R-GFP localization to neuronal primary cilia is abrogated by loss of MRAP2. Arrows indicate MC4R+ cilia. Scale bars, 20 μ m.

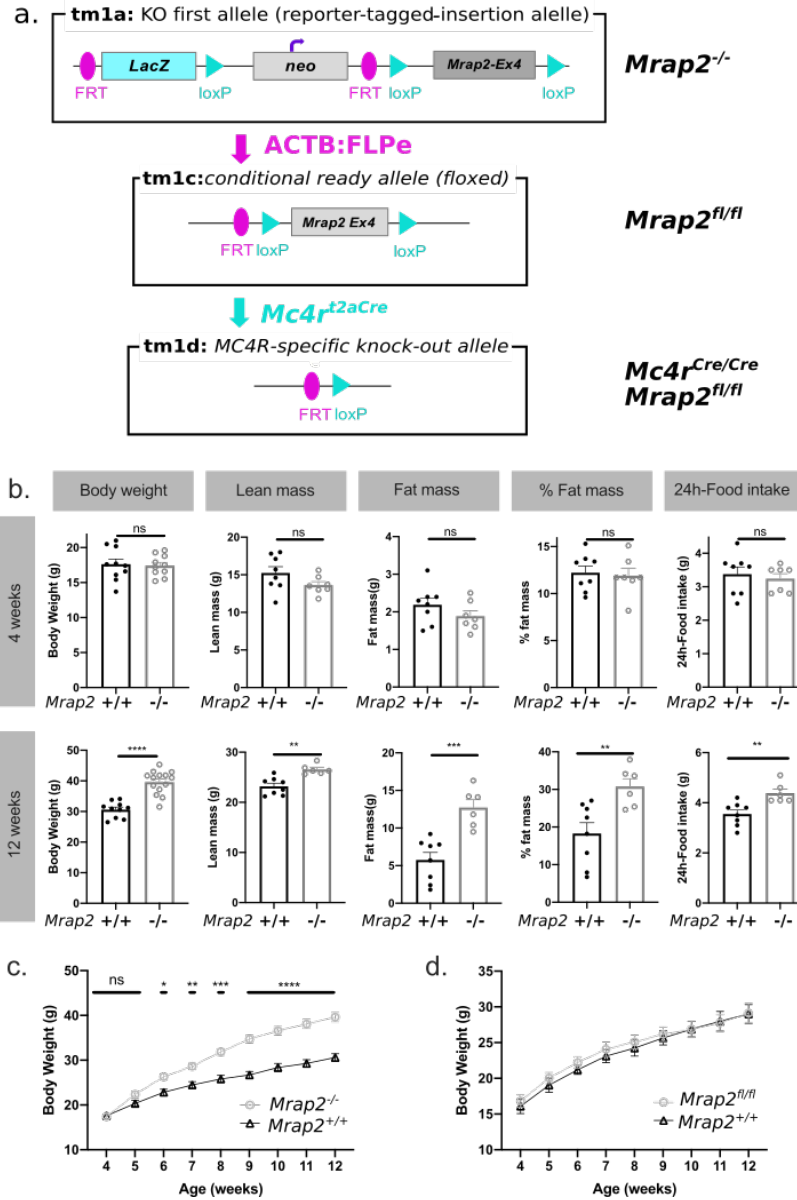
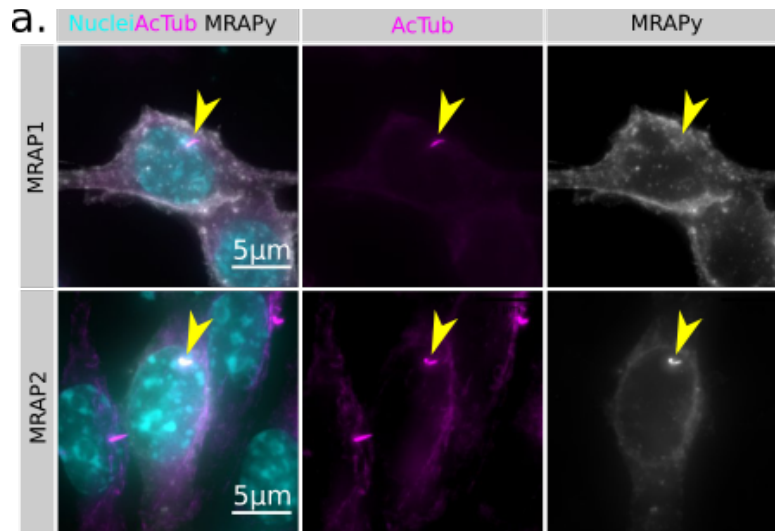


FIGURE 3.6 FIGURE S1: PHENOTYPICAL CHARACTERIZATION OF MICE BEARING EUCOMM MRAP2 TM1A AND TM1C ALLELES.

a EUCOMM allele nomenclature and specific crosses. EUCOMM *Mrap2* knockout-First allele (“tm1a”) mice carry an *frt*-flanked β -gal gene and neo cassette preventing widespread expression of the *Mrap2* gene (EUCOMM tm1a allele or *Mrap2^{-/-}*). When mice harboring this allele are crossed into an actin-flip background (ACTB:FLPe), the *frt*-flanked cassette is excised and *Mrap2* wild-type function is restored (EUCOMM tm1c allele or *Mrap2^{fl/fl}*). After Flip-mediated excision, a loxP-flanked Exon 4 remains, which allows for *Mc4r* cell-specific deletion when crossed to *Mc4r-t2a-CRE* knock-in mice (*Mc4r^{t2aCre/t2aCre} Mrap2^{fl/fl}*). **b** Body composition and 24h-food intake at 4 and 12 weeks of age (top and bottom panel respectively) of male mice homozygous for the EUCOMM *Mrap2^{tm1a}* allele (*Mrap2* whole body knockout, *Mrap2^{-/-}*; n=14) compared to their wildtype littermates (*Mrap2^{+/+}*; n=10). **c** Body weight curve of *Mrap2^{-/-}* (n=14) compared to wildtype *Mrap2^{+/+}* littermates (n=10). **d** Body weight curve of male mice homozygous for the EUCOMM *Mrap2^{tm1c}* allele (*Mrap2* floxed allele, *Mrap2^{fl/fl}*; n=7), compared to their wildtype littermates (*Mrap2^{+/+}*; n=10). Data are represented as mean \pm SEM, *p<0.05, **p<0.01, ***p<0.001, ****p<0.0001, Student’s unpaired t-test (column analysis); Mixed-effects model (REML) and Sidak’s multiple comparisons tests (weight curves).



b. MRAPy and MCxR ciliary enrichment

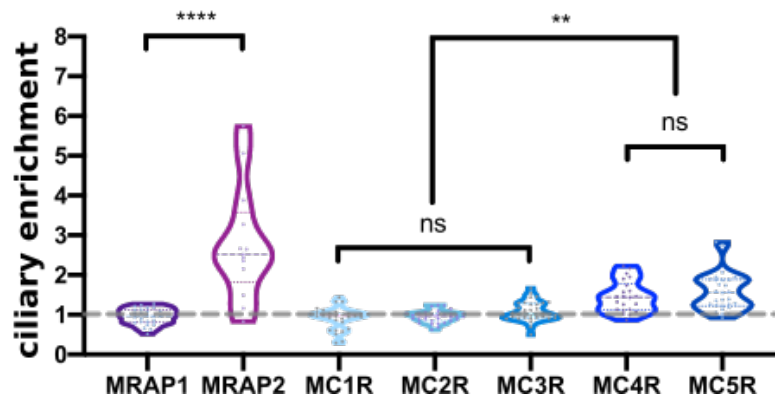


FIGURE 3.7 SUPPLEMENTARY FIGURE 2: CILIARY ENRICHMENT OF MELANOCORTIN RECEPTORS, MRAP1 AND MRAP2.

a MRAP2 (lower panel) is enriched at the primary cilium when transfected in IMCD3 cells without any Melanocortin Receptor, while MRAP1 (upper panel) does not. Yellow arrows point at primary cilium of transfected cells. Scale bar 5 μm. **b** Quantification of the enrichment at the primary cilia of IMCD3 cells transfected with MRAPs and MCRs alone. 30-34 ciliated cells per condition were imaged and analyzed. Ciliary and cell body intensity of MCxR and MRAPy was measured with Fiji. Enrichment at the cilium is expressed as (integrated density at the cilium)/ (integrated density in the cell body). Enrichment >1 indicates higher localization of the protein at the cilium than at the cell body. Data are represented as violin plots, *p<0.05, ***p<0.001, ****p<0.0001, ordinary one-way ANOVA with Sidak's multiple comparisons test.

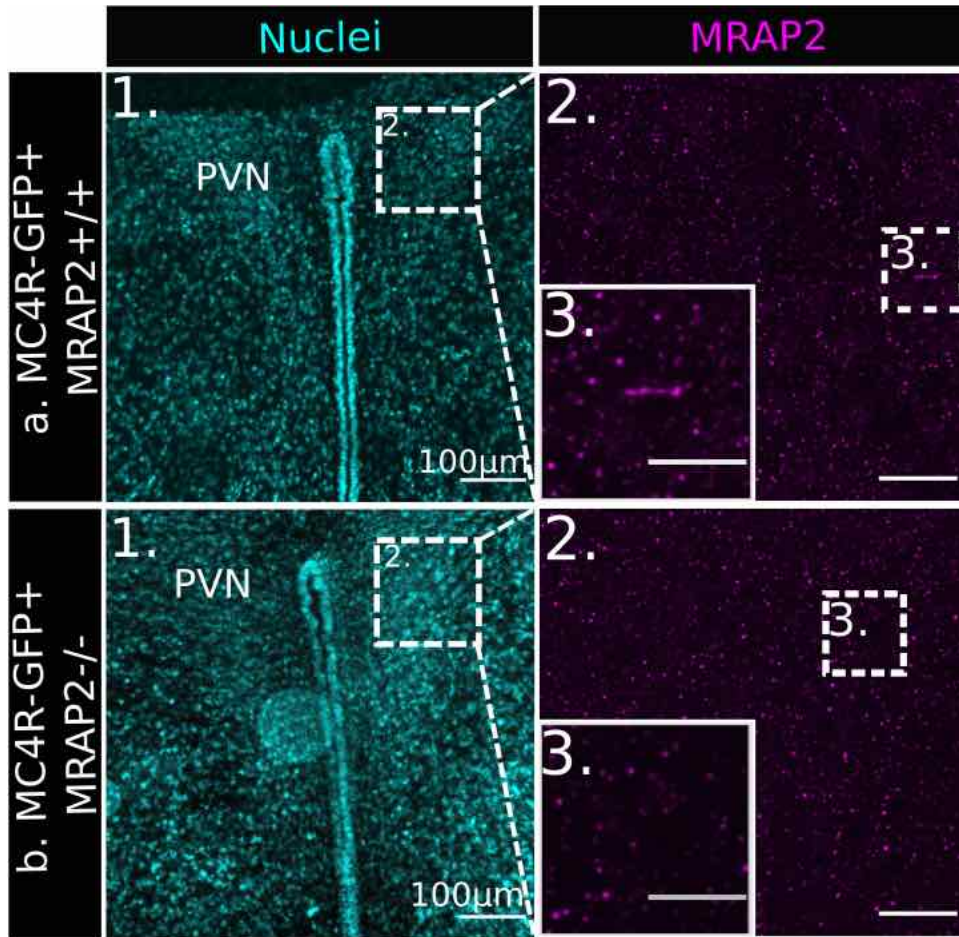


FIGURE 3.8 SUPPLEMENTARY FIGURE3: SPECIFICITY OF MRAP2 ANTIBODY: NO SIGNAL OBSERVED IN MRAP2 KNOCK-OUT HYPOTHALAMIC SECTIONS.

a In wild-type sections, cilia expressing MRAP2 can be found. **b** In *MRAP2* knockout sections, MRAP2 is not detectable. **1)** low magnification of the Paraventricular nucleus (PVN), nuclei stained with Hoechst (cyan), scale bar=100µm. **2)** Insert from 1), scale bar=20 µm. **3)** Insert from 2), scale bar=10µm.

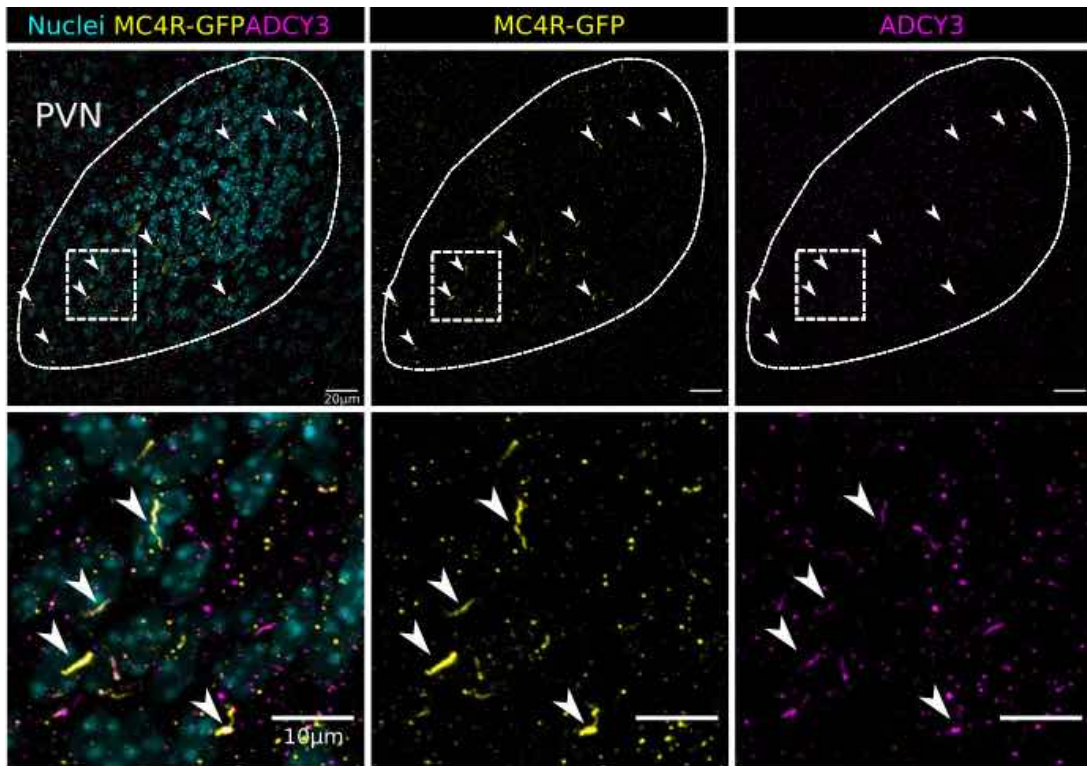


FIGURE 3.9 SUPPLEMENTARY FIGURE 4: MC4R LOCALIZES AT THE PRIMARY CILIUM IN P6 PUPS.

MC4R-GFP (Yellow) colocalizes with the specific neuronal primary cilia marker ADCY3 (magenta) in the PVN of P6 pups. Scale bars: 20 μm (top) and 10 μm (bottom).

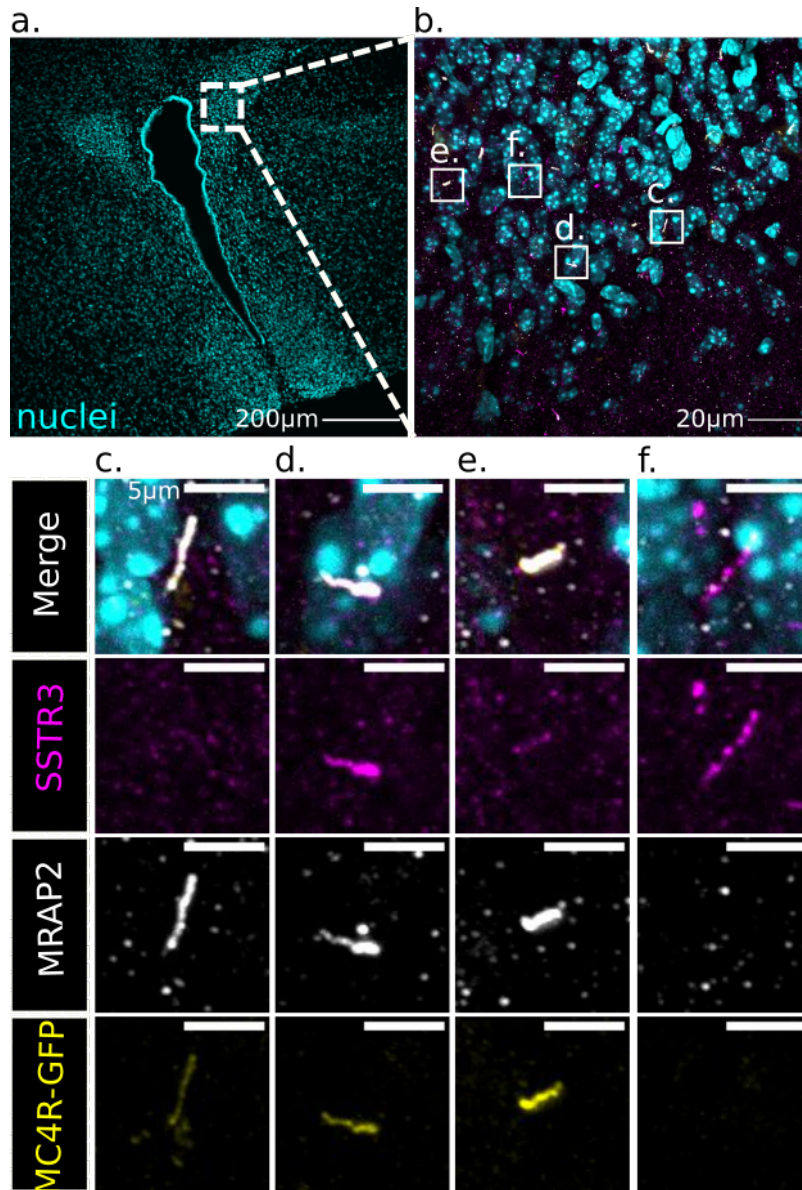


FIGURE 3.10 SUPPLEMENTARY FIGURE 5: MRAP2 CO-LOCALIZES WITH SSTR3 AND MC4R-GFP IN A SUBSET OF NEURONS IN THE PVN.

a Low magnification image showing the position of the insert in **b**. Scale bar, 200 μm **b** Insert from **a**. Scale bar, 20 μm . **c** Primary cilium double positive for MC4R-GFP and MRAP2, but not SSTR3. **d** and **e** Primary cilia triple positive for MC4R-GFP, MRAP2 and SSTR3. **f** Primary cilium positive for SSTR3 only.

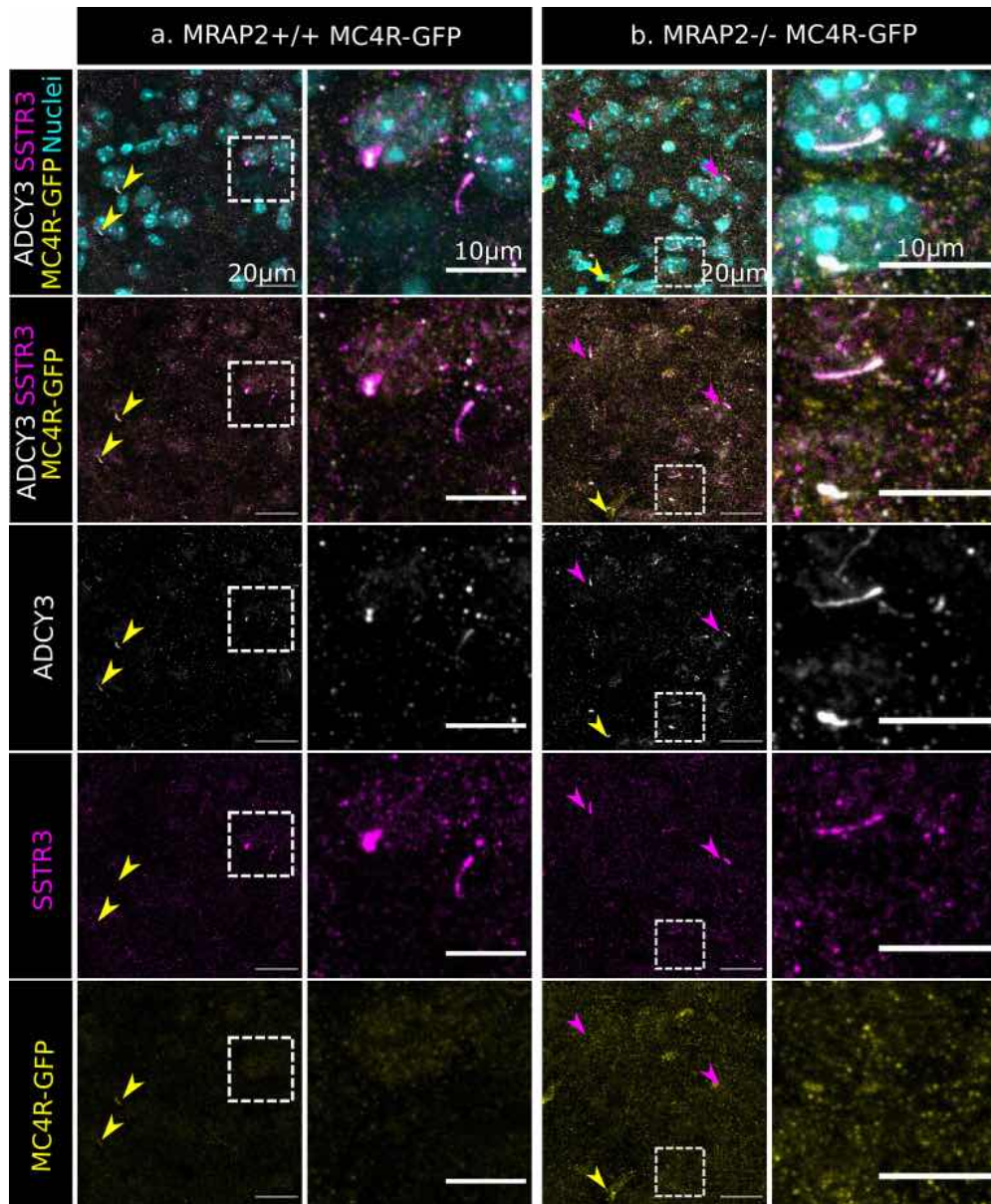


FIGURE 3.11 SUPPLEMENTARY FIGURE 6: MRAP2 DELETION DOES NOT IMPACT SSTR3 CILIARY LOCALIZATION.

Immunofluorescence imaging of the PVN of a MRAP2 wild type (**a**) and a MRAP2 knockout mouse (**b**), showing co-localization of SSTR3 (magenta) with ADCY3 (white) at the neuronal primary cilium. Yellow arrows point at MC4R-GFP+ cilia, while magenta arrows point at SSTR3 positive cilia. Second and fourth columns are inserts of first and second columns showing SSTR3+ cilia in both MRAP2 wild type and mutant mice, respectively

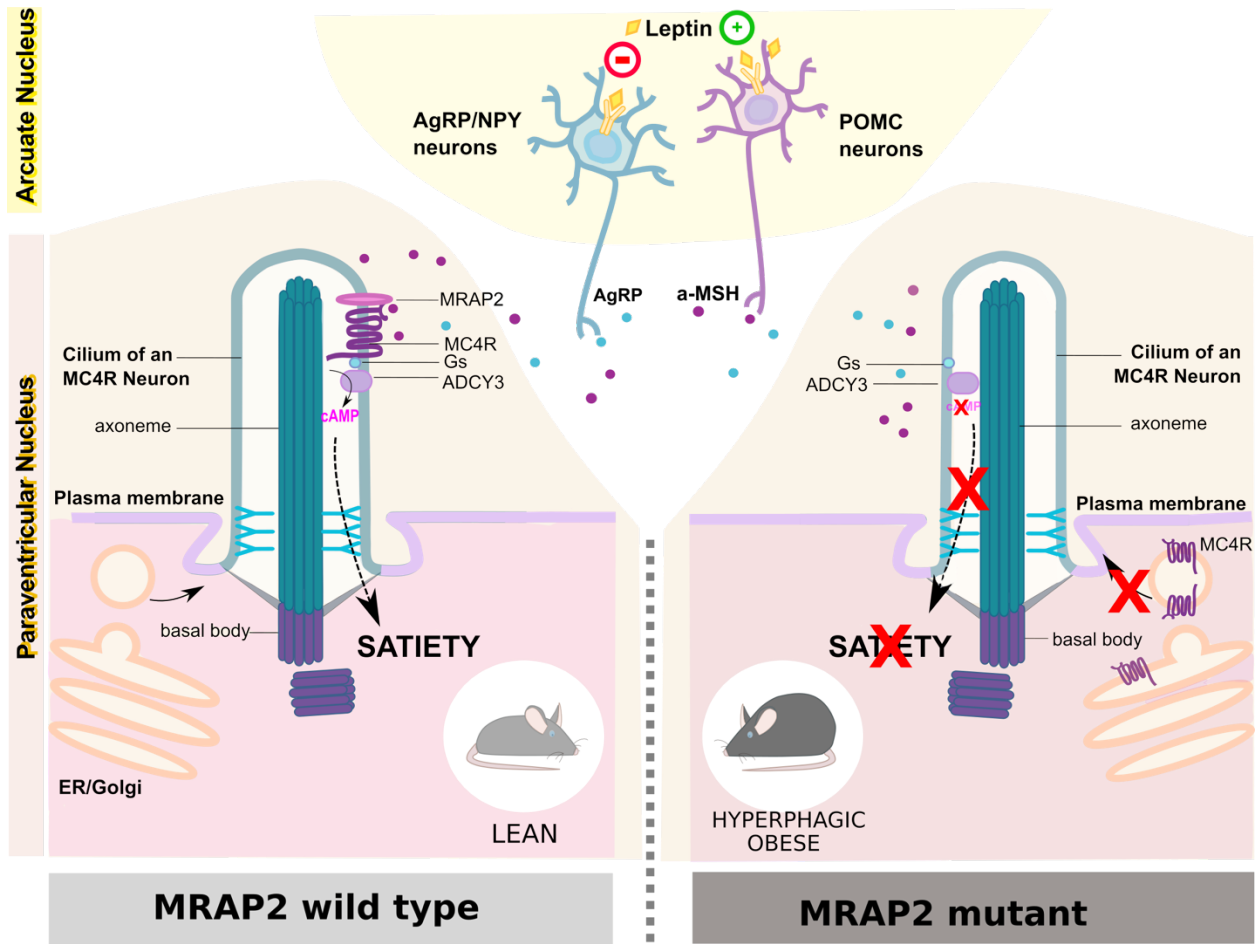


FIGURE 3.12 GRAPHICAL ABSTRACT

HIGHLIGHTS

MRAP2 specifically enhances localization of MC4R to primary cilia in heterologous cells

MRAP2 is required for MC4R localization to the neuronal primary cilia *in vivo*

MC4R expressing neurons require MRAP2 to regulate food intake and body weight

Methods

Cell culture and Transfections

Expression plasmids

MC1R-GFP, MC2R-GFP, MC3R-GFP and MC5R-GFP expression constructs were constructed as previously described for MC4R-GFP⁴³. Plasmids encoding MRAP1-FLAG and MRAP2-FLAG were obtained from Dr. Hinkle¹⁷⁹.

Ciliary expression of MCRs and MRAPs in cultured cells

IMCD3 cells were transfected using X-tremeGENE™ 9 DNA Transfection Reagent (06365809001, Roche). The transfection reagent was diluted in OptiMEM (Life Technologies) and incubated at room temperature for 5 min. Then, the mixture was added to the diluted plasmids in a 6:1 ratio (6 µl transfection reagent to 1 µg DNA). 50,000 cells in suspension were added to the transfection mixture after 20 min incubation at room temperature. Transfected cells were switched to starvation media after 24 h and fixed after 16 h. Double plasmid transfections were done by diluting equal mass of each vector.

Cell imaging

50,000 cells were seeded for transfection on acid-washed 12 mm #1.5 cover glass (Fisherbrand) in a 24-well plate. Starved cells were fixed in phosphate buffered saline (PBS) containing 4% paraformaldehyde (Electron Microscopy Sciences) for 15 min at room temperature and permeabilized in ice-cold 100% methanol (Fisher Scientific) for 5 min. Cells were then further permeabilized in PBS containing 0.1% Triton X-100 (BP151-500, Thermo Fisher Scientific), 5% normal donkey serum (017-000-121, Jackson Immunoresearch Labs), and 3% bovine serum albumin (BP1605-100, Thermo Fisher Scientific) for 30 min. Permeabilized cells were incubated with the specified primary antibodies (mouse monoclonal anti-acetylated tubulin T6793, Sigma-Aldrich; and mouse monoclonal anti-FLAG M2 antibody, F1804, Sigma-Aldrich) for 1 h washed with PBS, and incubated with dye-coupled secondary antibodies (Jackson Immunoresearch Labs) for 30 min. Cells were then washed with PBS, stained with Hoechst DNA dye, and washed with PBS before mounting with Fluoromount G (Electron Microscopy Sciences).

Cells were imaged in a widefield fluorescence DeltaVision microscope (Applied Precision) equipped with a PlanApo 60x/1.40NA objective lens (Olympus), a pco.edge 4.2 sCMOS camera, a solid state illumination module (Insight) and a Quad polycroic (Chroma). Z stacks with 0.2 µm separation between planes were acquired using SoftWoRx. The illumination settings were: 140 µW 390 nm wavelength for 0.15 s to image Hoechst, 222 µW 475 nm wavelength for 0.3 s to image Alexa Fluor 488-stained MCRs, 123 µW 543 nm wavelength for 0.3 s to image Cy3-stained acetylated tubulin and 115 µW 632 nm wavelength for 0.15 s to image Cy5-stained FLAG-labelled MRAPs. Images were flat field-corrected, background subtracted and maximally projected using Fiji. Ciliary intensity measurements were also taken in Fiji.

In vivo experiments

Animals

Mice were housed in a barrier facility and maintained on a 12:12 light cycle (on: 0700-1900) at an ambient temperature of 23±2°C and relative humidity 50-70%. Mice were fed with rodent diet

5058 (Lab Diet) and group-housed up to 5. Experiments were performed with weight matched littermates.

All animal procedures were approved by the Institutional Animal Care and Use Committee of the University of California, San Francisco.

Mouse line	Description	Origin
Mc4r ^{tm1(egfp)Vai} ("Mc4r ^{gfp} ")	An EGFP tag inserted in frame at the C-terminus of the endogenous <i>Mc4r</i> locus.	Vaisse lab, Previously described ⁵⁶
Mc4rtm2(cre)Vai ("Mc4r ^{t2aCre} ")	A -t2a-CRE sequence inserted in frame at the C-terminus of the endogenous <i>Mc4r</i> locus.	Vaisse lab, previously described ¹¹⁹
C57BL/6-Mrap2 ^{tm1a(EUCOMM)Wtsi/JsbgJ}	<i>Mrap2</i> EUCOMM: <i>Mrap2</i> KO mice have a <i>frt</i> -flanked β -gal gene and neo cassette preventing widespread expression of MRAP2. Exon 4 is flanked by <i>loxP</i> sites	Jackson Laboratories (Bar Harbor, ME)
Arl13B-GFP ^{tg}	This transgenic strain ubiquitously expresses a GFP-tagged version of the ciliary protein ARL13B, under the control of the CAG promoter.	Markus Delling, UCSF ¹⁸⁰
Tg(ACTFLPe)9205Dym	This transgenic strain expresses a <i>FLP1</i> recombinase gene under the direction of the human ACTB promoter	Jackson Laboratories (Bar Harbor, ME)
Mrap2 ^{tm1c} (Mrap2 ^{fl})	MRAP2 floxed allele	Obtained by crossing <i>Mrap2</i> ^{tm1a/+} mice were crossed with mice expressing actin-FLpE
Mc4r ^{t2aCre/t2aCre} Mrap2 ^{tm1c/tm1c} (Mc4r ^{t2aCre/t2aCre} Mrap2 ^{fl/fl})	Deletion of MRAP2 specifically in MC4R-expressing neurons	Obtained by crossing <i>Mrap2</i> ^{tm1c} mice with <i>Mc4r</i> ^{t2a-reE} mice

EUCOMM MRAP2 mice

EUCOMM MRAP2 knockout-First allele (“tm1a”) mice carry an frt-flanked β -gal gene and neo cassette preventing widespread expression of the *Mrap2* gene (EUCOMM tm1a allele or *Mrap2*^{-/-}). When mice harboring this allele are crossed into an actin-flip background, the frt-flanked cassette is excised and MRAP2 wild-type function is restored (EUCOMM tm1c allele or *Mrap2*^{fl/fl}). After Flip-mediated excision, a loxP-flanked Exon 4 remains, which allows for MC4R cell-specific deletion when crossed to *Mc4r*-t2a-CRE knock-in mice (*Mc4rt2aCre/t2aCre Mrap2*^{fl/fl}).

Stereotaxic AAV-injection Surgeries.

8 weeks old *Mrap2*^{fl/fl} *Mc4r*^{gfp} females (n=4) were injected unilaterally with pAAV-Ef1a-mCherry-IRES-CRE (Addgene, catalog #55632-AAV8).

Animals were anesthetized with an initial flow of 4% isoflurane, maintained under anesthesia using 2% isoflurane and kept at 30-37°C using a custom heating pad. The surgery was performed using aseptic and stereotaxic techniques. Briefly, the animals were put into a stereotaxic frame (KOPF Model 1900, USA), the scalp was opened, the planarity of the skull was adjusted and a hole was drilled (PVN coordinates: AP=-0.8, ML=-0.2, DV=-5.3). A volume of 300 nl was injected at a rate of 0.1 μ L/min. Animals were given pre-operative analgesic (buprenorphine, 0.3 mg/kg) and post-operative anti-inflammatory Meloxicam (5 mg/Kg) and allowed to recover at least 10 days during which time they were single-housed and handled frequently. The mice were calorie-restricted at 75% for 2 weeks prior to perfusion.

Brain imaging

Mice were perfused trans-cardially with PBS followed by 4% paraformaldehyde fixation solution. Brains were dissected and post-fixed in fixation solution at 4°C overnight, soaked in 30% sucrose solution overnight, embedded in O.C.T. (Tissue-Tek, Sakura Finetek USA, INC., Torrance, CA), frozen, and cut into 20-35 μ m coronal sections, then stored at -80°C until staining.

After washing, sections were blocked for 1 h in 50% serum 50% antibody buffer (1.125% NaCl, 0.75% Tris base, 1% BSA, 1.8 % L-Lysine, 0.04% sodium azide), followed by incubation with primary antibody overnight at 4°C. After washing, sections were incubated with secondary antibodies for 1 h at room temperature, washed and stained with Hoechst (1:5000), washed and mounted with Prolong™ Diamond antifade Mountant.

Primary antibodies	
Chicken anti-GFP (abcam, ab13970)	1:250
Rabbit anti-Adcy3 (Santa Cruz Biotechnology, sc-588)	1:500
Rabbit anti-MRAP2 (Proteintech, 17259-1-AP)	1:200
Goat anti-SSTR3 (M-18), (Santa Cruz Biotechnology, sc-11617)	1:200
Secondary antibodies	
Goat anti-chicken Alexa Fluor 488 (Invitrogen)	1:500

Goat anti-rabbit Alexa Fluor 633 or 555 (Invitrogen)	1:500
Donkey anti-chicken Alexa Fluor 488 (Invitrogen)	1:500
Donkey anti-rabbit Alexa Fluor 647 (Invitrogen)	1:500
Donkey anti-goat Alexa Fluor 555 (Invitrogen)	1:500

In figure 5, the immunofluorescence stainings were performed on brain sections from mice that were calorie-restricted for a week at 75% of baseline food intake on regular chow and fasted for 24 h prior to perfusion. In figure S3 (validation of MRAP2 antibody), the staining for MRAP2 and GFP was performed on brain sections from P6 mice expressing MC4R-GFP, either wild type or knock out for MRAP2 (MRAP2 1a/1a).

Microscopy

Microscope	Figure
Leica SP5 (Z-stack, 0.5 μm steps)	Assessment of MC4R-GFP at the cilium of MRAP2 wt vs KO
Leica SP8 with resonant scanner	Colocalization of MC4R-GFP and MRAP2 in P6 mice
Nikon W1 wide field-of-view spinning disk confocal with Andor Zyla sCMOS camera, (Z-stack, 0.26 μm steps)	SSTR3 imaging, MRAP2 IF in MC4R-GFP adults

Image processing

Images were processed with Fiji. Maximal intensity Z projections are from at least 20 slices over 15-20 μm . Quantified slices were matched for the number of slices projected and settings.

Quantification of ciliary localization in cultured cells and hypothalamus sections

Matched Z-stack maximum projections were analyzed in Fiji. Relative ciliary enrichment was calculated as follows: each primary cilium was manually defined by a segmented line following ADCY3+ signal, and the pixel intensity in other channels was measured in that defined area (integrated density, IntDen). Ciliary intensity of MC4R-GFP was then calculated as the IntDen of MC4R-GFP in the cilium, subtracting adjacent background (measured as IntDen of same defined area nearby the cilium). To calculate relative cilia enrichment, the IntDen (cilium) was divided by the Intden (cell body), measured in the closest cell body (as defined by the presence of a Hoechst positive nucleus). Enrichment >1 therefore indicates higher localization of the receptor at the primary cilium compared to cell body.

Mouse Metabolism Studies

For experiments presented in Figure 1, mice were weaned at 4 weeks of age, single-housed and their food intake was measured manually every 24 h for 4 consecutive days and averaged. Food intake data was excluded if the mouse lost a significant amount of weight because of single housing stress. The animals were then housed in groups of five, and their weight was measured weekly until 12 weeks of age. Food intake was again assessed as described at 12 weeks of age. Body composition was assessed by EchoMRI™ at 4 and 12 weeks of age.

Statistics

Sample sizes were chosen based upon the estimated effect size drawn from previous publications and from the performed experiments. Data distribution were assumed to be normal, but this was not formally tested. All tests used are indicated in the figures. We analyzed all data using Prism 7.0 (GraphPad Software). (^{ns} $p > 0.05$; * $P \leq 0.05$; ** $P \leq 0.01$; *** $P \leq 0.001$; **** $P \leq 0.0001$).

Data availability

The data that support the findings of this study are available from the corresponding author upon request

Chapter 4 : Final discussion and Conclusions

Challenges in the Identification of players in primary-cilia regulated energy homeostasis

The first hint implying a role for neuronal primary cilia in energy homeostasis derives from the fact that targeted deletion of primary cilia from neurons led to an obese phenotype comparable to adult ubiquitous deletion⁹⁸. Although some region-specific ablation experiments highlighted the medio-basal hypothalamus as an important region, only a small number of studies attempted to identify which other regions within and outside the hypothalamus are key for cilia-regulated energy homeostasis. With this work, we established that the primary cilia of PVN MC4R neurons are essential for the regulation of food intake and body weight.

In addition to region-specific ablation experiments, it will be key to identify sparse neuronal populations involved in the control of energy balance through primary cilia. However, there are several caveats that will need to be addressed. First, most cell-specific Cre-recombinase drivers are expressed early on during development, and little is known about the effect of ciliary deletion on neuronal development and projection extension. Thus, it will be critical to develop inducible systems that allow for dissociation between developmental and adult homeostatic effects. Second, a lot of neuronal markers overlap within different populations. It will therefore be necessary to combine different genetic and pharmacological techniques to determine which populations truly rely on primary cilia to control energy homeostasis.

The increasing interest in understanding how primary cilia control energy homeostasis motivated different *in vitro* screens aimed at identifying new ciliary receptors involved in body weight control^{192,193}. One newly identified candidate was the Neuropeptide Y (NPY) Receptor NPY2R. Although NPY is an orexigenic peptide, one of these studies showed that deletion of primary cilia in NPY2R-expressing cells leads to obesity¹⁹². NPY2R ciliary enrichment was also decreased in *Bbs* mutant models^{193,194}. Importantly, while these screens identified known ciliary receptors and discovered some new ones, like the prolactin-releasing hormone or neuromedin U receptor 1, they failed to identify some confirmed ciliary GPCRs, like for example MC4R. This highlights the technical caveats of working with *in vitro* systems that don't recapitulate physiological conditions. However, these experiments support that mis-localization of GPCRs to primary cilia may be responsible for hyperphagia-induced obesity.

If MC4R localization at the primary cilium is instrumental for its weight-regulating function, then genes encoding proteins necessary for its transport to the cilium could be considered as candidate genes for human obesity. This hypothesis supports a simple model in which every ciliopathy-associated gene impacting MC4R ciliary localization will cause obesity. As a proof of concept, we demonstrated that the accessory protein MRAP2 is necessary for MC4R trafficking to primary cilia *in vivo*, and that *Mrap2* deletion leads to decreased MC4R ciliary enrichment and obesity. It is interesting to note that all previous *in vitro* published data on MC4R-MRAP2 interaction were collected from non-ciliated heterologous over-expressing systems. Importantly, the necessity of accessory proteins for the localization of receptors to cilia has not been taken into account in previous screens aimed at discovering ciliary GPCRs, which could therefore explain why some known ciliary GPCRs, like MC4R, were not identified. Next-generation screens should be designed

to identify partner proteins necessary to traffic receptors to cilia. This will be instrumental in drawing a cilium-interactome which might help unveil new therapeutic targets in the quest to fight obesity.

On the other hand, whether impaired ciliary localization of MC4R is one of the mechanisms by which ciliopathies like BBS or Alström syndrome cause obesity is not known. It will be interesting to determine whether BBS proteins, ALMS1 or other proteins like TUBBY are critical for MC4R localization to PVN cilia. Future experiments could include crossing our *Mc4r^{gfp}* mouse model to different ciliopathy mouse models to assess MC4R ciliary localization. The development of targeted approaches using AAVs will also allow for cell-, region-, and time-specific studies. Combining these techniques with the power of CRISPRCas9 modulation technology will lead to powerful tools to dissect the role of different ciliopathy-associated genes *in vivo*.

Towards understanding ciliary mechanisms regulating energy homeostasis in neurons

Maintaining energy balance requires the coordination of short-term feeding decisions to sustain the long-term goal of matching food intake to energy expenditure to maintain a stable body weight. While short-term regulation of feeding is known to rely on transient stimuli that are transformed into fast chemo-electrical signaling at neuronal synapses, long-term assessment of energy stores depends on leptin (Figure 1). These two sets of afferent signals need to be integrated by the neurons in the central Leptin-melanocortin system, implying that signaling needs to be compartmentalized.

Arcuate nucleus POMC and AgRP neurons are sensitive to both short- and long-term signals. Recent data showed that the activity of these neurons is modified within seconds of seeing food, even before consuming it. Hunger AgRP neurons have also recently been shown to be sensitive to intragastric caloric content, in a caloric-dependent manner¹⁹⁵. Interestingly, leptin has no acute effect on the dynamics of these circuits or their sensory regulation, but was shown to modulate their output in the long term, and is required for the inhibition of feeding¹⁹⁵.

Short-term chemogenetic and optogenetic activation of AgRP neurons leads to voracious feeding and inhibition of MC4R neurons through GABAergic input^{55,158,195}. In contrast, only sustained activation of ARC POMC neurons has an effect of food intake, and was shown to be MC4R-dependent¹⁹⁶. These data suggest that AgRP neurons can communicate energy status to MC4R neurons in two different time scales (short-term through GABA signaling, and long-term through AgRP itself), while POMC neurons convey long-term information through the release of α -MSH.

In mice, artificial chemo-electrical activation or inhibition of the MC4R neurons leads to acute anorexia or hyperphagia, respectively⁵⁵. MC4R neurons are therefore a key component of short-term regulation of energy balance. However, the activity of MC4R itself depends on the extracellular ratio of α -MSH and AgRP, which reflect slow variation in adiposity levels. It has thus been a challenge to understand how MC4R neurons can integrate this stable, long-term information with the ever-changing real-time information about feeding status.

Since cilia transmit non-synaptic information, it will be essential to determine how ligands are released from pre-ciliary neurons and how far they can diffuse in the extracellular environment to be detected by their target receptors in cilia. For example, little is known about concentrations and turnover of α -MSH and AgRP in the PVN, as well as how they are affected by physiological changes. At the subcellular level, how primary cilia impact the activity of neurons responsible for controlling energy homeostasis remains largely unexplored. MC4R is a Gs-coupled GPCR, meaning its activation leads to local increase of levels of cAMP through the activation of ADCY3. Recent data demonstrated that ciliary concentration of cAMP is uncoupled from intracellular cAMP and can convey different messages to the cell^{197,198}. However, this has not been studied in neurons or in the context of energy homeostasis. While we showed that inhibiting Gs signaling specifically at the primary cilia of MC4R neurons leads to hyperphagia and obesity¹¹⁹, how ciliary cAMP is differentially encoded in neurons in the context of energy balance is not known.

Whether MC4R activation at the primary cilia leads to transcriptional changes, perturbations in calcium homeostasis or changes in neuronal excitability remains to be elucidated, but some hypotheses can be drawn from previously published data. First, in the hippocampus, MC4R activation has been shown to enhance the abundance of AMPA receptors in synapses¹⁹⁹. In the PVN, activation of the GLP-1 receptor (GLP-1R) has been shown to augment excitatory synaptic strength in corticotropin-releasing hormone (CRH) neurons, by promoting a protein kinase A (PKA)-dependent signaling cascade leading to the trafficking of AMPA receptors to the plasma membrane²⁰⁰. Lastly, in brain slices, α -MSH has been shown to significantly increase the AMPAR/NMDAR ratios, and increase the amplitude of spontaneous EPSCs (sEPSC), while the amplitude of sEPSC is reduced in POMC knock out animals²⁰¹. Together, these results seem to point towards a possible cAMP/PKA downstream signaling cascade that could change the excitability of MC4R neurons. Whether ciliary cAMP is able to induce such changes will need to be investigated. Understanding these mechanisms will hopefully unravel how cilia dysfunction leads to obesity, and how healthy MC4R neurons are capable of integrating information at different timescales (Figure 2).

Interaction between diet, obesity and primary cilia homeostasis

Obesity can also result from the over-consumption of palatable and calorically dense food. A limited number of studies have looked at the interaction between diet, obesity and primary cilia homeostasis. Particularly, it was recently shown that mice fed a high fat diet had an increased proportion of shorter cilia in the arcuate nucleus (ARC) and in the ventromedial hypothalamus (VMH) compared to lean controls. However, the same was observed in the hypothalamus of leptin-deficient mice. Interestingly, in this model, cilia length could be rescued by injections of recombinant leptin⁶¹. It is not clear whether diet itself or the resulting obesity are responsible for the changes in cilia morphology. It is also not known whether high fat diet impacts ciliary localization and function of receptors regulating energy balance. Future studies will need to address these questions as well as whether cilia length impacts ciliary signaling cascades involved in the regulation of energy homeostasis.

Reward-induced overeating has emerged as one of the mechanisms contributing to the development of obesity following high fat diet challenge. Recent data demonstrated that dopaminergic signaling within the suprachiasmatic nucleus (SCN), the central circadian clock, results in overconsumption of food during the light cycle, which is defined as hedonic feeding^{202,203}. Notably, this phenotype was dependent on the dopamine receptors D1 (DRD1), which is a Gs-coupled ciliary GPCR. Interestingly, DRD1 ciliary localization is increased in neurons of *Bbs4* knock out mice²⁰³. These recent findings provide a link between primary cilia and non-homeostatic feeding behaviors leading to obesity.

Neuronal primary cilia and human obesity

Targeted treatment options for genetic obesity are unfortunately exceptional and are only available for specific and very rare disorders. The first effective treatment for monogenic obesity was conducted in 1997, when two children were diagnosed with leptin deficiency and treated with recombinant leptin. However, leptin-deficiency is extremely rare, and has only been reported in a few families^{204,205}.

Nevertheless, in most cases, obesity isn't related to leptin deficiency, but rather to leptin resistance. Although patients with obesity usually present with hyperleptinemia, leptin is no longer recognized by the central anorexigenic centers in the brain, and therefore, leptin treatment does not improve body weight in these subjects. To date, the mechanisms underlying leptin resistance still remain unclear, but several possibilities have been postulated: failure of circulating leptin to cross the blood-brain-barrier, inhibition of the neuronal leptin signaling cascade, and "defensive" decrease in the expression of leptin receptor and desensitization of cellular downstream pathways are some of the current hypotheses being explored^{206,207}. More recently, the primary cilium has been implicated as one of the possible elements whose dysfunction could lead to leptin resistance. Understanding how leptin resistance results from and can further accentuate obesity is an essential step in designing therapies to treat obesity and its derived co-morbidities.

Recent success targeting the leptin-melanocortin system opened a new field in the search for therapies targeting genetic obesity. Since 2016, the use of Setmelanotide, an MC4R synthetic agonist, showed promising results in patients with POMC and Leptin Receptor deficiencies, achieving sustainable reduction of hunger and substantial weight loss^{208,209}. Setmelanotide also led to weight loss in a phase 1b clinical trial in obese heterozygote *MC4R* variant carrier patients²¹⁰. In mouse models of obesity, Setmelanotide was shown to lead to weight loss in heterozygous *Mc4r* knockout, but notably, also in diet-induced obese wild-type animals²¹⁰.

Interestingly, intra-cerebroventricular administration of an artificial MC4R agonist seems to reduce food intake and body weight in *Bbs* knockout mice¹⁰¹, and a more recent study showed that setmelanotide reduces food intake and body weight in a mouse model of Alström syndrome²¹¹. These studies concluded that the obesity in BBS is due to a defect in signaling upstream of MC4R, that can therefore be rescued by activating MC4R. However, another hypothesis could be that MC4R function is altered in these ciliopathy models, but somehow these modified agonists are able to rescue MC4R function in a way its endogenous ligands can't. While more studies will be necessary to understand how these agonists interact with MC4R, Setmelanotide is currently

the target of phase 2 and phase 3 trials for the treatment of ciliopathies including Bardet-Biedl and Alstrom syndrome ²¹².

While new promising drugs are currently being tested, as of today, bariatric surgery remains the only effective treatment against morbid obesity, as it results in a significant and sustained weight loss, remission of obesity-related comorbidities and improvement of quality of life ²¹³. While there is growing evidence that bariatric surgery is effective in patients suffering from genetic obesity linked to *MC4R* heterozygous deficiency, subjects with homozygous *MC4R* mutations do not seem to respond ^{214–218}. Accordingly, since *Mc4r* knock-out mice did not achieve weight loss following gastric bypass surgery, it was suggested that MC4R might be necessary to benefit from the effects of bariatric surgery ^{215,218}. Only a few studies and case reports have investigated the effects of bariatric surgery in patients with ciliopathies. Some promising results have been achieved after gastric-bypass and sleeve gastrectomy in two patients suffering from morbid obesity related to BBS. Three years after surgery, patients had respectively a total weight loss of 30 and 32 % and both showed resolutions or improvement of obesity-related comorbidities ^{219,220}. However, since very few studies assessing the effects of bariatric surgery in patients with monogenic obesity, including ciliopathies, have been reported, it is difficult to draw substantial conclusions about the efficacy of these procedures in these populations. Therefore, future research will need to address to what extent the benefits from bariatric surgery depend on the leptin-melanocortin system or the primary cilia.

Final conclusion

To conclude, primary cilia are undeniably instrumental in the control of energy metabolism, and there is strong evidence pointing at their role in relaying information in the central leptin melanocortin system.

The present work highlights MC4R as a central player controlling long-term energy homeostasis at the intersection between the leptin-melanocortin system and his role as a ciliary GPCR.

To date, there is no medical treatment for obesity, and patients suffering from ciliopathies can only be treated with supportive therapies. Understanding how primary cilia sense and relay information about energy status will be crucial to unravel promising and innovative targeted therapies for the future.

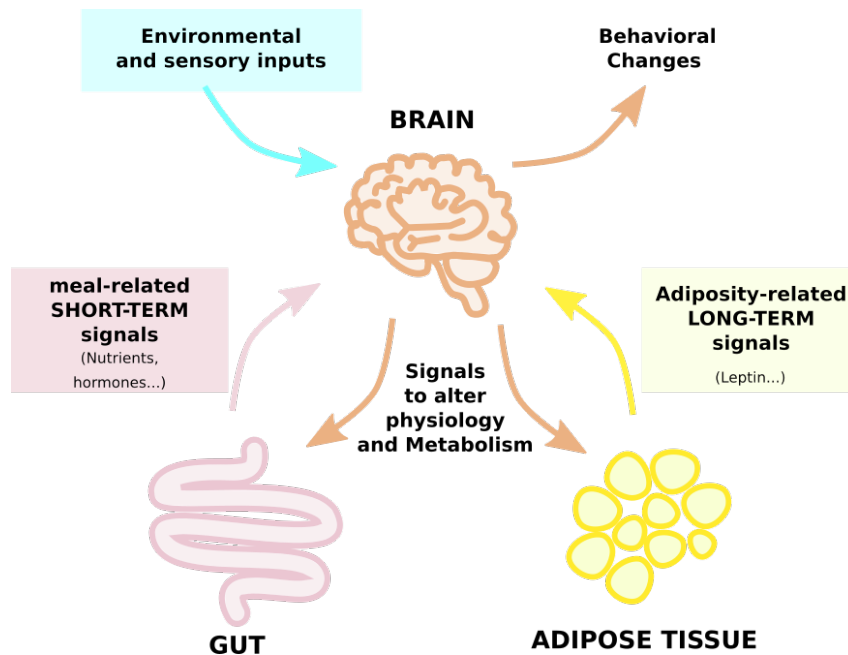


FIGURE 4.1 THE GUT-FAT-BRAIN AXIS.

Short-term regulation of feeding relies on transient stimuli (meal-related signals and environmental and sensory input) that are transformed into fast chemo-electrical signaling at neuronal synapses. Long-term assessment of energy stores depends on secreted factors like leptin that act chronically on their central receptors. These two sets of afferent signals are integrated by the brain in order to dictate behavioral changes and adjustments to physiology and metabolism.

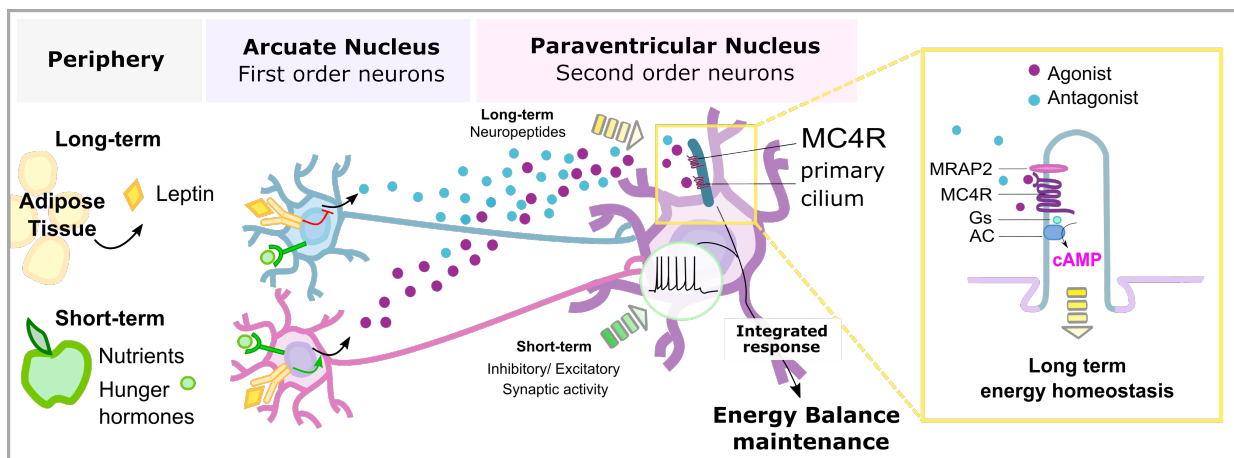


FIGURE 4.2: MODEL FOR THE INTEGRATION OF SHORT- AND LONG-TERM ENERGY HOMEOSTASIS SIGNALS IN MC4R NEURONS.

MC4R neurons receive information in different time scales. Long-term information reflecting energy stores in the periphery are transmitted by leptin to ARC POMC and AgRP neurons, and transformed into a pool of neuropeptides (a-MSH and AgRP) that signal at the ciliary MC4R. The activation level of MC4R dictates the levels of ciliary cAMP, which in turn modulate the neuronal response to short term stimuli reflecting changes in immediate nutritional status and sensory cues to, in turn, lead to an integrated response intended to maintain long-term energy homeostasis.

Chapter 5 References

1. Jensen, M. D. *et al.* 2013 AHA/ACC/TOS Guideline for the Management of Overweight and Obesity in Adults. *Circulation* **129**, S102–S138 (2014).
2. Ashrafi, K. *Obesity and the regulation of fat metabolism. WormBook: The Online Review of C. elegans Biology [Internet]* (WormBook, 2007).
3. Benzinou, M. *et al.* Common nonsynonymous variants in PCSK1 confer risk of obesity. *Nature Genetics* (2008) doi:10.1038/ng.177.
4. Loos, R. J. F. *et al.* Common variants near MC4R are associated with fat mass, weight and risk of obesity. *Nat. Genet.* **40**, 768–775 (2008).
5. Willer, C. J. *et al.* Six new loci associated with body mass index highlight a neuronal influence on body weight regulation. *Nat. Genet.* **41**, 25–34 (2009).
6. Loos, R. J. F. & Yeo, G. S. H. The bigger picture of FTO: the first GWAS-identified obesity gene. *Nat Rev Endocrinol* **10**, 51–61 (2014).
7. Coleman, D. L. A historical perspective on leptin. *Nat Med* **16**, 1097–1099 (2010).
8. Zhang, Y. *et al.* Positional cloning of the mouse obese gene and its human homologue. *Nature* **372**, 425–432 (1994).
9. Tartaglia, L. A. *et al.* Identification and expression cloning of a leptin receptor, OB-R. *Cell* **83**, 1263–1271 (1995).
10. Chen, H. *et al.* Evidence That the Diabetes Gene Encodes the Leptin Receptor: Identification of a Mutation in the Leptin Receptor Gene in db/db Mice. *Cell* **84**, 491–495 (1996).
11. Friedman, J. M. & Halaas, J. L. Leptin and the regulation of body weight in mammals. *Nature* **395**, 763–770 (1998).
12. Montague, C. T. *et al.* Congenital leptin deficiency is associated with severe early-onset obesity in humans. *Nature* **387**, 903–908 (1997).
13. Farooqi, I. S. *et al.* Effects of Recombinant Leptin Therapy in a Child with Congenital Leptin Deficiency. *New England Journal of Medicine* **341**, 879–884 (1999).
14. Elmquist, J. K., Bjørbaek, C., Ahima, R. S., Flier, J. S. & Saper, C. B. Distributions of leptin receptor mRNA isoforms in the rat brain. *J. Comp. Neurol.* **395**, 535–547 (1998).
15. Myers Jr., M. G., Münzberg, H., Leininger, G. M. & Leshan, R. L. The Geometry of Leptin Action in the Brain: More Complicated Than a Simple ARC. *Cell Metabolism* **9**, 117–123 (2009).
16. Frühbeck, G. Intracellular signalling pathways activated by leptin. *Biochem. J.* **393**, 7–20 (2006).
17. Hübschle, T. *et al.* Leptin-Induced Nuclear Translocation of STAT3 Immunoreactivity in Hypothalamic Nuclei Involved in Body Weight Regulation. *J. Neurosci.* **21**, 2413–2424 (2001).
18. Frontini, A. *et al.* Leptin-dependent STAT3 phosphorylation in postnatal mouse hypothalamus. *Brain Res.* **1215**, 105–115 (2008).
19. Robertson, S. A., Leininger, G. M. & Myers, M. G. Molecular and Neural Mediators of Leptin Action. *Physiol Behav* **94**, 637–642 (2008).
20. Schwartz, M. W. *et al.* Leptin increases hypothalamic pro-opiomelanocortin mRNA expression in the rostral arcuate nucleus. *Diabetes* **46**, 2119–2123 (1997).

21. Baskin, D. G. *et al.* Leptin Receptor Long-form Splice-variant Protein Expression in Neuron Cell Bodies of the Brain and Co-localization with Neuropeptide Y mRNA in the Arcuate Nucleus. *J Histochem Cytochem* **47**, 353–362 (1999).
22. Fry, M. & Ferguson, A. V. The sensory circumventricular organs: Brain targets for circulating signals controlling ingestive behavior. *Physiology & Behavior* **91**, 413–423 (2007).
23. Myers, M. G., Cowley, M. A. & Münzberg, H. Mechanisms of leptin action and leptin resistance. *Annu. Rev. Physiol.* **70**, 537–556 (2008).
24. Cowley, M. A. *et al.* Leptin activates anorexigenic POMC neurons through a neural network in the arcuate nucleus. *Nature* **411**, 480–484 (2001).
25. Barsh, G. S. & Schwartz, M. W. Genetic approaches to studying energy balance: perception and integration. *Nat Rev Genet* **3**, 589–600 (2002).
26. Krude, H. *et al.* Severe early-onset obesity, adrenal insufficiency and red hair pigmentation caused by POMC mutations in humans. *Nat. Genet.* **19**, 155–157 (1998).
27. Yaswen, L., Diehl, N., Brennan, M. B. & Hochgeschwender, U. Obesity in the mouse model of pro-opiomelanocortin deficiency responds to peripheral melanocortin. *Nat. Med.* **5**, 1066–1070 (1999).
28. Balthasar, N. *et al.* Leptin receptor signaling in POMC neurons is required for normal body weight homeostasis. *Neuron* **42**, 983–991 (2004).
29. Lam, D. D. *et al.* Conditional expression of Pomc in the Lepr-positive subpopulation of POMC neurons is sufficient for normal energy homeostasis and metabolism. *Endocrinology* **156**, 1292–1302 (2015).
30. Vergoni, A. V., Poggioli, R. & Bertolini, A. Corticotropin inhibits food intake in rats. *Neuropeptides* **7**, 153–158 (1986).
31. Poggioli, R., Vergoni, A. V. & Bertolini, A. ACTH-(1-24) and alpha-MSH antagonize feeding behavior stimulated by kappa opiate agonists. *Peptides* **7**, 843–848 (1986).
32. Corander, M. P., Rimmington, D., Challis, B. G., O’Rahilly, S. & Coll, A. P. Loss of Agouti-Related Peptide Does Not Significantly Impact the Phenotype of Murine POMC Deficiency. *Endocrinology* **152**, 1819–1828 (2011).
33. Morrison, C. D., Morton, G. J., Niswender, K. D., Gelling, R. W. & Schwartz, M. W. Leptin inhibits hypothalamic Npy and Agrp gene expression via a mechanism that requires phosphatidylinositol 3-OH-kinase signaling. *Am. J. Physiol. Endocrinol. Metab.* **289**, E1051-1057 (2005).
34. Qian, S. *et al.* Neither Agouti-Related Protein nor Neuropeptide Y Is Critically Required for the Regulation of Energy Homeostasis in Mice. *Mol. Cell. Biol.* **22**, 5027–5035 (2002).
35. Palmiter, R. D., Erickson, J. C., Hollopeter, G., Baraban, S. C. & Schwartz, M. W. Life without neuropeptide Y. *Recent Prog. Horm. Res.* **53**, 163–199 (1998).
36. Wortley, K. E. *et al.* Agouti-related protein-deficient mice display an age-related lean phenotype. *Cell Metab.* **2**, 421–427 (2005).
37. Luquet, S., Perez, F. A., Hnasko, T. S. & Palmiter, R. D. NPY/AgRP Neurons Are Essential for Feeding in Adult Mice but Can Be Ablated in Neonates. *Science* **310**, 683–685 (2005).
38. Wu, Q., Howell, M. P., Cowley, M. A. & Palmiter, R. D. Starvation after AgRP neuron ablation is independent of melanocortin signaling. *Proc. Natl. Acad. Sci. U.S.A.* **105**, 2687–2692 (2008).
39. Wu, Q., Boyle, M. P. & Palmiter, R. D. Loss of GABAergic signaling by AgRP neurons to the parabrachial nucleus leads to starvation. *Cell* **137**, 1225–1234 (2009).

40. Krashes, M. J. *et al.* Rapid, reversible activation of AgRP neurons drives feeding behavior in mice. *J Clin Invest* **121**, 1424–1428 (2011).
41. Krashes, M. J., Lowell, B. B. & Garfield, A. S. Melanocortin-4 receptor-regulated energy homeostasis. *Nat. Neurosci.* **19**, 206–219 (2016).
42. Abdel-Malek, Z. A. Melanocortin receptors: their functions and regulation by physiological agonists and antagonists. *Cell. Mol. Life Sci.* **58**, 434–441 (2001).
43. Ersoy, B. A. *et al.* Mechanism of N-terminal modulation of activity at the melanocortin-4 receptor GPCR. *Nat. Chem. Biol.* **8**, 725–730 (2012).
44. Joseph, C. G. *et al.* Gamma2-Melanocyte Stimulation Hormone (γ 2-MSH) Truncation Studies Results in the Cautionary Note that γ 2-MSH is Not Selective for the Mouse MC3R over the Mouse MC5R. *Peptides* **31**, 2304–2313 (2010).
45. Low, M. J. Agnostic about in Vivo Inverse Agonism of Agouti-Related Peptide. *Endocrinology* **152**, 1731–1733 (2011).
46. Yang, Y. Structure, function and regulation of the melanocortin receptors. *Eur J Pharmacol* **660**, 125–130 (2011).
47. Vaisse, C. *et al.* Melanocortin-4 receptor mutations are a frequent and heterogeneous cause of morbid obesity. *J Clin Invest* **106**, 253–262 (2000).
48. Vaisse, C., Clement, K., Guy-Grand, B. & Froguel, P. A frameshift mutation in human MC4R is associated with a dominant form of obesity. *Nat Genet* **20**, 113–114 (1998).
49. Gu, W. *et al.* Identification and functional analysis of novel human melanocortin-4 receptor variants. *Diabetes* **48**, 635–9 (1999).
50. Dubern, B. *et al.* Mutational analysis of melanocortin-4 receptor, agouti-related protein, and alpha-melanocyte-stimulating hormone genes in severely obese children. *J. Pediatr.* **139**, 204–209 (2001).
51. Bromberg, Y., Overton, J., Vaisse, C., Leibel, R. L. & Rost, B. In silico mutagenesis: a case study of the melanocortin 4 receptor. *FASEB J.* **23**, 3059–3069 (2009).
52. Lubrano-Berthelie, C. *et al.* Melanocortin 4 receptor mutations in a large cohort of severely obese adults: prevalence, functional classification, genotype-phenotype relationship, and lack of association with binge eating. *J. Clin. Endocrinol. Metab.* **91**, 1811–1818 (2006).
53. Huszar, D. *et al.* Targeted disruption of the melanocortin-4 receptor results in obesity in mice. *Cell* **88**, 131–141 (1997).
54. Shah, B. P. *et al.* MC4R-expressing glutamatergic neurons in the paraventricular hypothalamus regulate feeding and are synaptically connected to the parabrachial nucleus. *Proc. Natl. Acad. Sci. U.S.A.* **111**, 13193–13198 (2014).
55. Garfield, A. S. *et al.* A neural basis for melanocortin-4 receptor-regulated appetite. *Nat. Neurosci.* (2015) doi:10.1038/nn.4011.
56. Siljee, J. E. *et al.* Subcellular localization of MC4R with ADCY3 at neuronal primary cilia underlies a common pathway for genetic predisposition to obesity. *Nature Genetics* **50**, 180 (2018).
57. Goetz, S. C. & Anderson, K. V. The Primary Cilium: A Signaling Center During Vertebrate Development. *Nat Rev Genet* **11**, 331–344 (2010).
58. Fry, A. M., Leaper, M. J. & Bayliss, R. The primary cilium: guardian of organ development and homeostasis. *Organogenesis* **10**, 62–68 (2014).

59. Reiter, J. F. & Leroux, M. R. Genes and molecular pathways underpinning ciliopathies. *Nat. Rev. Mol. Cell Biol.* **18**, 533–547 (2017).
60. Pala, R., Alomari, N. & Nauli, S. M. Primary Cilium-Dependent Signaling Mechanisms. *Int J Mol Sci* **18**, (2017).
61. Han, Y. M. *et al.* Leptin-promoted cilia assembly is critical for normal energy balance. *J Clin Invest* **124**, 2193–2197 (2014).
62. Kim, S. & Dynlacht, B. D. Assembling a primary cilium. *Curr Opin Cell Biol* **25**, 506–511 (2013).
63. Fisch, C. & Dupuis-Williams, P. Ultrastructure of cilia and flagella - back to the future! *Biol. Cell* **103**, 249–270 (2011).
64. Reiter, J. F., Blacque, O. E. & Leroux, M. R. The base of the cilium: roles for transition fibres and the transition zone in ciliary formation, maintenance and compartmentalization. *EMBO Rep.* **13**, 608–618 (2012).
65. Song, D. K., Choi, J. H. & Kim, M. S. Primary Cilia as a Signaling Platform for Control of Energy Metabolism. *Diabetes Metab J* **42**, 117–127 (2018).
66. Delling, M., DeCaen, P. G., Doerner, J. F. & Febvay, S. Primary cilia are specialized calcium signaling organelles. 26 (2014).
67. Nishimura, Y., Kasahara, K., Shiromizu, T., Watanabe, M. & Inagaki, M. Primary Cilia as Signaling Hubs in Health and Disease. *Adv Sci (Weinh)* **6**, 1801138 (2019).
68. Dyson, J. M. *et al.* INPP5E regulates phosphoinositide-dependent cilia transition zone function. *J Cell Biol* **216**, 247–263 (2017).
69. Jacoby, M. *et al.* INPP5E mutations cause primary cilium signaling defects, ciliary instability and ciliopathies in human and mouse. *Nat. Genet.* **41**, 1027–1031 (2009).
70. Nakatsu, F. A Phosphoinositide Code for Primary Cilia. *Developmental Cell* **34**, 379–380 (2015).
71. Prevo, B., Scholey, J. M. & Peterman, E. J. G. Intraflagellar transport: mechanisms of motor action, cooperation, and cargo delivery. *FEBS J.* **284**, 2905–2931 (2017).
72. Ye, F., Nager, A. R. & Nachury, M. V. BBSome trains remove activated GPCRs from cilia by enabling passage through the transition zone. *J. Cell Biol.* **217**, 1847–1868 (2018).
73. Nachury, M. V. The molecular machines that traffic signaling receptors into and out of cilia. *Current Opinion in Cell Biology* **51**, 124–131 (2018).
74. Nachury, M. V. How do cilia organize signalling cascades? *Philos Trans R Soc Lond B Biol Sci* **369**, (2014).
75. Hilgendorf, K. I., Johnson, C. T. & Jackson, P. K. The primary cilium as a cellular receiver: organizing ciliary GPCR signaling. *Curr. Opin. Cell Biol.* **39**, 84–92 (2016).
76. Schou, K. B., Pedersen, L. B. & Christensen, S. T. Ins and outs of GPCR signaling in primary cilia. *EMBO Rep.* **16**, 1099–1113 (2015).
77. Hamamoto, A. *et al.* Modulation of primary cilia length by melanin-concentrating hormone receptor 1. *Cell. Signal.* **28**, 572–584 (2016).
78. Siljee, J. E. *et al.* Subcellular localization of MC4R with ADCY3 at neuronal primary cilia underlies a common pathway for genetic predisposition to obesity. *Nature Genetics* **50**, 180 (2018).
79. Besharse, J. C., Hollyfield, J. G. & Rayborn, M. E. Photoreceptor outer segments: accelerated membrane renewal in rods after exposure to light. *Science* **196**, 536–538 (1977).

80. Calvert, P. D. *et al.* Membrane protein diffusion sets the speed of rod phototransduction. *Nature* **411**, 90–94 (2001).
81. Kuhlmann, K. *et al.* The membrane proteome of sensory cilia to the depth of olfactory receptors. *Mol. Cell Proteomics* **13**, 1828–1843 (2014).
82. Nakamura, T. & Gold, G. H. A cyclic nucleotide-gated conductance in olfactory receptor cilia. *Nature* **325**, 442–444 (1987).
83. Breer, H. Sense of smell: recognition and transduction of olfactory signals. *Biochem. Soc. Trans.* **31**, 113–116 (2003).
84. AbouAlaiwi, W. A. *et al.* Ciliary Polycystin-2 Is a Mechanosensitive Calcium Channel Involved in Nitric Oxide Signaling Cascades. *Circ Res* **104**, 860–869 (2009).
85. Nauli, S. M. *et al.* Endothelial Cilia Are Fluid Shear Sensors That Regulate Calcium Signaling and Nitric Oxide Production Through Polycystin-1. *Circulation* **117**, 1161–1171 (2008).
86. Jin, X. *et al.* Cilioplasm is a cellular compartment for calcium signaling in response to mechanical and chemical stimuli. *Cell. Mol. Life Sci.* **71**, 2165–2178 (2014).
87. Lee, K. L. *et al.* The primary cilium functions as a mechanical and calcium signaling nexus. *Cilia* **4**, (2015).
88. Rydholm, S. *et al.* Mechanical properties of primary cilia regulate the response to fluid flow. *Am. J. Physiol. Renal Physiol.* **298**, F1096–1102 (2010).
89. Mykytyn, K. & Askwith, C. G-Protein-Coupled Receptor Signaling in Cilia. *Cold Spring Harb Perspect Biol* **9**, (2017).
90. Jiang, J. & Hui, C.-C. Hedgehog signaling in development and cancer. *Dev. Cell* **15**, 801–812 (2008).
91. Oh, E. C. & Katsanis, N. Cilia in vertebrate development and disease. *Development* **139**, 443–448 (2012).
92. Oh, E. C., Vasanth, S. & Katsanis, N. Metabolic Regulation and Energy Homeostasis through the Primary Cilium. *Cell Metabolism* **21**, 21–31 (2015).
93. Lee, H., Song, J., Jung, J. H. & Ko, H. W. Primary cilia in energy balance signaling and metabolic disorder. *BMB Rep* **48**, 647–654 (2015).
94. Alstrom, C. H., Hallgren, B., Nilsson, L. B. & Asander, H. Retinal degeneration combined with obesity, diabetes mellitus and neurogenous deafness: a specific syndrome (not hitherto described) distinct from the Laurence-Moon-Bardet-Biedl syndrome: a clinical, endocrinological and genetic examination based on a large pedigree. *Acta Psychiatr Neurol Scand Suppl* **129**, 1–35 (1959).
95. Heydet, D. *et al.* A truncating mutation of *Alms1* reduces the number of hypothalamic neuronal cilia in obese mice. *Dev Neurobiol* **73**, 1–13 (2013).
96. Thomas, S. *et al.* Identification of a novel *ARL13B* variant in a Joubert syndrome-affected patient with retinal impairment and obesity. *Eur J Hum Genet* **23**, 621–627 (2015).
97. Jenkins, D. *et al.* *RAB23* mutations in Carpenter syndrome imply an unexpected role for hedgehog signaling in cranial-suture development and obesity. *Am. J. Hum. Genet.* **80**, 1162–1170 (2007).
98. Davenport, J. R. *et al.* Conditional disruption of intraflagellar transport in adult mice leads to hyperphagia-induced obesity and slow onset cystic kidney disease. *Curr Biol* **17**, 1586–1594 (2007).

99. Sun, J. S. *et al.* Ventromedial hypothalamic primary cilia control energy and skeletal homeostasis. *J Clin Invest* **131**, (2021).
100. Lee, C. H. *et al.* Primary cilia mediate early life programming of adiposity through lysosomal regulation in the developing mouse hypothalamus. *Nature Communications* **11**, 5772 (2020).
101. Seo, S. *et al.* Requirement of Bardet-Biedl syndrome proteins for leptin receptor signaling. *Hum. Mol. Genet.* **18**, 1323–1331 (2009).
102. Guo, D.-F. *et al.* The BBSome Controls Energy Homeostasis by Mediating the Transport of the Leptin Receptor to the Plasma Membrane. *PLoS Genet* **12**, (2016).
103. Berbari, N. F. *et al.* Leptin resistance is a secondary consequence of the obesity in ciliopathy mutant mice. *PNAS* **110**, 7796–7801 (2013).
104. Berbari, N. F., Lewis, J. S., Bishop, G. A., Askwith, C. C. & Mykityn, K. Bardet-Biedl syndrome proteins are required for the localization of G protein-coupled receptors to primary cilia. *Proceedings of the National Academy of Sciences of the United States of America* **105**, 4242–6 (2008).
105. Hernandez-Hernandez, V. *et al.* Bardet–Biedl syndrome proteins control the cilia length through regulation of actin polymerization. *Hum Mol Genet* **22**, 3858–3868 (2013).
106. Nager, A. R. *et al.* An Actin Network Dispatches Ciliary GPCRs into Extracellular Vesicles to Modulate Signaling. *Cell* **168**, 252–263.e14 (2017).
107. Shah, B. P. *et al.* MC4R-expressing glutamatergic neurons in the paraventricular hypothalamus regulate feeding and are synaptically connected to the parabrachial nucleus. *Proc. Natl. Acad. Sci. U.S.A.* **111**, 13193–13198 (2014).
108. Vaisse, C., Reiter, J. F. & Berbari, N. F. Cilia and Obesity. *Cold Spring Harb Perspect Biol* **9**, (2017).
109. Grarup, N. *et al.* Loss-of-function variants in ADCY3 increase risk of obesity and type 2 diabetes. *Nat. Genet.* **50**, 172–174 (2018).
110. Saeed, S. *et al.* Loss-of-function mutations in ADCY3 cause monogenic severe obesity. *Nat. Genet.* **50**, 175–179 (2018).
111. Wang, Z. *et al.* Adult type 3 adenylyl cyclase-deficient mice are obese. *PloS one* **4**, e6979 (2009).
112. Cao, H., Chen, X., Yang, Y. & Storm, D. Disruption of Type 3 Adenylyl Cyclase Expression in the Hypothalamus Leads to Obesity. *Integrative Obesity and Diabetes* **2**, 225–228 (2016).
113. Stratigopoulos, G. *et al.* Hypomorphism for RPGRIP1L, a ciliary gene vicinal to the FTO locus, causes increased adiposity in mice. *Cell Metab* **19**, 767–779 (2014).
114. Heukers, R., De Groof, T. W. M. & Smit, M. J. Nanobodies detecting and modulating GPCRs outside in and inside out. *Current Opinion in Cell Biology* **57**, 115–122 (2019).
115. Dummer, A., Poelma, C., DeRuiter, M. C., Goumans, M.-J. T. H. & Hierck, B. P. Measuring the primary cilium length: improved method for unbiased high-throughput analysis. *Cilia* **5**, 7 (2016).
116. Han, Y. M. *et al.* Leptin-promoted cilia assembly is critical for normal energy balance. *J Clin Invest* **124**, 2193–2197 (2014).
117. Guo, L., Münzberg, H., Stuart, R., Nillni, E. & Bjørbaek, C. N-acetylation of hypothalamic - melanocyte-stimulating hormone and regulation by leptin. *Proceedings of the National Academy of Sciences of the United States of America* **101**, 11797–802 (2004).

118. Liu, H. *et al.* Transgenic mice expressing green fluorescent protein under the control of the melanocortin-4 receptor promoter. *J. Neurosci.* **23**, 7143–7154 (2003).
119. Wang, Y. *et al.* Melanocortin 4 receptor signals at the neuronal primary cilium to control food intake and body weight. *J Clin Invest* **131**, (2021).
120. Hall, K. D. *et al.* Energy balance and its components: implications for body weight regulation. *Am J Clin Nutr* **95**, 989–994 (2012).
121. Frederich, R. C. *et al.* Expression of ob mRNA and its encoded protein in rodents. Impact of nutrition and obesity. *J Clin Invest* **96**, 1658–1663 (1995).
122. Mizuno, T. M. & Mobbs, C. V. Hypothalamic agouti-related protein messenger ribonucleic acid is inhibited by leptin and stimulated by fasting. *Endocrinology* **140**, 814–817 (1999).
123. Cui, H. *et al.* Neuroanatomy of melanocortin-4 receptor pathway in the lateral hypothalamic area. *J Comp Neurol* **520**, 4168–4183 (2012).
124. Nager, A. R. *et al.* An actin network dispatches ciliary GPCRs into extracellular vesicles to modulate signaling. *Cell* **168**, 252–263.e14 (2017).
125. Ekstrand, M. I. *et al.* Molecular profiling of neurons based on connectivity. *Cell* **157**, 1230–1242 (2014).
126. Maier, M. T. *et al.* Regulation of Hepatic Lipid Accumulation and Distribution by Agouti-Related Protein in Male Mice. *Endocrinology* **159**, 2408–2420 (2018).
127. Singla, V. & Reiter, J. F. The primary cilium as the cell’s antenna: signaling at a sensory organelle. *Science* **313**, 629–633 (2006).
128. Reiter, J. F. & Leroux, M. R. Genes and molecular pathways underpinning ciliopathies. *Nat. Rev. Mol. Cell Biol.* **18**, 533–547 (2017).
129. Saeed, S. *et al.* Loss-of-function mutations in ADCY3 cause monogenic severe obesity. *Nat. Genet.* **50**, 175–179 (2018).
130. Shalata, A. *et al.* Morbid obesity resulting from inactivation of the ciliary protein CEP19 in humans and mice. *American journal of human genetics* **93**, 1061–71 (2013).
131. Wang, Z. *et al.* Adult type 3 adenylyl cyclase-deficient mice are obese. *PloS one* **4**, e6979 (2009).
132. Acs, P. *et al.* A novel form of ciliopathy underlies hyperphagia and obesity in Ankrd26 knockout mice. *Brain Struct Funct* **220**, 1511–1528 (2015).
133. Vaisse, C., Reiter, J. F. & Berbari, N. F. Cilia and Obesity. *Cold Spring Harb Perspect Biol* **9**, (2017).
134. Hildebrandt, F., Benzing, T. & Katsanis, N. Ciliopathies. *N Engl J Med* **364**, 1533–43 (2011).
135. Wong, S. Y. & Reiter, J. F. The primary cilium at the crossroads of mammalian hedgehog signaling. *Curr. Top. Dev. Biol.* **85**, 225–260 (2008).
136. Bangs, F. & Anderson, K. V. Primary Cilia and Mammalian Hedgehog Signaling. *Cold Spring Harb Perspect Biol* **9**, (2017).
137. Davenport, J. *et al.* Disruption of Intraflagellar Transport in Adult Mice Leads to Obesity and Slow-Onset Cystic Kidney Disease. *Current Biology* **17**, 1586–1594 (2007).
138. Siljee, J. E. *et al.* Subcellular localization of MC4R with ADCY3 at neuronal primary cilia underlies a common pathway for genetic predisposition to obesity. *Nat. Genet.* **50**, 180–185 (2018).
139. Loos, R. J. F. *et al.* Common variants near MC4R are associated with fat mass, weight and risk of obesity. *Nat. Genet.* **40**, 768–775 (2008).

140. Lubrano-Berthelier, C. *et al.* Melanocortin 4 receptor mutations in a large cohort of severely obese adults: prevalence, functional classification, genotype-phenotype relationship, and lack of association with binge eating. *J. Clin. Endocrinol. Metab.* **91**, 1811–1818 (2006).
141. Vaisse, C., Clement, K., Guy-Grand, B. & Froguel, P. A frameshift mutation in human MC4R is associated with a dominant form of obesity. *Nat. Genet.* **20**, 113–114 (1998).
142. Vaisse, C. *et al.* Melanocortin-4 receptor mutations are a frequent and heterogeneous cause of morbid obesity. *J. Clin. Invest.* **106**, 253–262 (2000).
143. Huszar, D. *et al.* Targeted disruption of the melanocortin-4 receptor results in obesity in mice. *Cell* **88**, 131–141 (1997).
144. Shah, B. P. *et al.* MC4R-expressing glutamatergic neurons in the paraventricular hypothalamus regulate feeding and are synaptically connected to the parabrachial nucleus. *Proc. Natl. Acad. Sci. U.S.A.* **111**, 13193–13198 (2014).
145. Pan, W. W. & Myers, M. G. Leptin and the maintenance of elevated body weight. *Nature Reviews Neuroscience* **19**, 95–105 (2018).
146. Haycraft, C. J. *et al.* Intraflagellar transport is essential for endochondral bone formation. *Development* **134**, 307–316 (2007).
147. Garfield, A. S. *et al.* A neural basis for melanocortin-4 receptor-regulated appetite. *Nature neuroscience* **18**, 863–71 (2015).
148. Balthasar, N. *et al.* Divergence of melanocortin pathways in the control of food intake and energy expenditure. *Cell* **123**, 493–505 (2005).
149. Knight, Z. A. *et al.* Molecular Profiling of Activated Neurons by Phosphorylated Ribosome Capture. *Cell* **151**, (2012).
150. Kishi, T. *et al.* Expression of melanocortin 4 receptor mRNA in the central nervous system of the rat. *Journal of Comparative Neurology* **457**, 213–235 (2003).
151. Ersoy, B. A. *et al.* Mechanism of N-terminal modulation of activity at the melanocortin-4 receptor GPCR. *Nat. Chem. Biol.* **8**, 725–730 (2012).
152. Marley, A., Choy, R. W.-Y. & von Zastrow, M. GPR88 reveals a discrete function of primary cilia as selective insulators of GPCR cross-talk. *PLoS ONE* **8**, e70857 (2013).
153. Guo, D.-F. *et al.* The BBSome Controls Energy Homeostasis by Mediating the Transport of the Leptin Receptor to the Plasma Membrane. *PLoS Genet* **12**, e1005890 (2016).
154. Rahmouni, K. *et al.* Leptin resistance contributes to obesity and hypertension in mouse models of Bardet-Biedl syndrome. *The Journal of Clinical Investigation* **118**, 1458–67 (2008).
155. Barbari, N. F. *et al.* Leptin resistance is a secondary consequence of the obesity in ciliopathy mutant mice. *PNAS* **110**, 7796–7801 (2013).
156. Ghosh, S. & Bouchard, C. Convergence between biological, behavioural and genetic determinants of obesity. *Nature Reviews Genetics* **18**, 731–748 (2017).
157. Stratigopoulos, G. *et al.* Hypomorphism of *Fto* and *Rpgrip1l* causes obesity in mice. *J Clin Invest* **126**, 1897–1910 (2016).
158. Chen, Y. *et al.* Sustained NPY signaling enables AgRP neurons to drive feeding. *eLife* **8**, e46348 (2019).
159. Krashes, M. J., Shah, B. P., Koda, S. & Lowell, B. B. Rapid versus delayed stimulation of feeding by the endogenously released AgRP neuron mediators GABA, NPY, and AgRP. *Cell Metab* **18**, 588–595 (2013).

160. Mina, A. I. *et al.* CalR: A Web-Based Analysis Tool for Indirect Calorimetry Experiments. *Cell Metab.* **28**, 656-666.e1 (2018).
161. Rowland, N. E., Schaub, J. W., Robertson, K. L., Andreasen, A. & Haskell-Luevano, C. Effect of MTII on food intake and brain c-Fos in melanocortin-3, melanocortin-4, and double MC3 and MC4 receptor knockout mice. *Peptides* **31**, 2314–2317 (2010).
162. Cepoi, D. *et al.* Assessment of a small molecule melanocortin-4 receptor-specific agonist on energy homeostasis. *Brain Res.* **1000**, 64–71 (2004).
163. Balthasar, N. *et al.* Divergence of melanocortin pathways in the control of food intake and energy expenditure. *Cell* **123**, 493–505 (2005).
164. Goetz, S. C. & Anderson, K. V. The primary cilium: a signalling centre during vertebrate development. *Nature reviews. Genetics* **11**, 331–44 (2010).
165. Reiter, J. F. & Leroux, M. R. Genes and molecular pathways underpinning ciliopathies. *Nat. Rev. Mol. Cell Biol.* **18**, 533–547 (2017).
166. Green, J. A. & Mykityn, K. Neuronal ciliary signaling in homeostasis and disease. *Cellular and molecular life sciences : CMLS* **67**, 3287–97 (2010).
167. Vaisse, C., Reiter, J. F. & Berbari, N. F. Cilia and Obesity. *Cold Spring Harb Perspect Biol* **9**, (2017).
168. Davenport, J. *et al.* Disruption of Intraflagellar Transport in Adult Mice Leads to Obesity and Slow-Onset Cystic Kidney Disease. *Current Biology* **17**, 1586–1594 (2007).
169. Rouault, A. A. J., Srinivasan, D. K., Yin, T. C., Lee, A. A. & Sebag, J. A. Melanocortin Receptor Accessory Proteins (MRAPs): Functions in the melanocortin system and beyond. *Biochimica et Biophysica Acta (BBA) - Molecular Basis of Disease* **1863**, 2462–2467 (2017).
170. Chaly, A. L., Srisai, D., Gardner, E. E. & Sebag, J. A. The Melanocortin Receptor Accessory Protein 2 promotes food intake through inhibition of the Prokineticin Receptor-1. *eLife* **5**,
171. Srisai, D. *et al.* MRAP2 regulates ghrelin receptor signaling and hunger sensing. *Nature Communications* **8**, 713 (2017).
172. Asai, M. *et al.* Loss of function of the melanocortin 2 receptor accessory protein 2 is associated with mammalian obesity. *Science* **341**, 275–8 (2013).
173. Chan, L. F. *et al.* MRAP and MRAP2 are bidirectional regulators of the melanocortin receptor family. *Proceedings of the National Academy of Sciences of the United States of America* **106**, 6146–51 (2009).
174. Sebag, J. A., Zhang, C., Hinkle, P. M., Bradshaw, A. M. & Cone, R. D. Developmental control of the melanocortin-4 receptor by MRAP2 proteins in zebrafish. *Science* **341**, 278–81 (2013).
175. Schonnop, L. *et al.* Decreased melanocortin-4 receptor function conferred by an infrequent variant at the human melanocortin receptor accessory protein 2 gene. *Obesity (Silver Spring)* **24**, 1976–1982 (2016).
176. Geets, E. *et al.* Copy number variation (CNV) analysis and mutation analysis of the 6q14.1-6q16.3 genes SIM1 and MRAP2 in Prader Willi like patients. *Mol. Genet. Metab.* **117**, 383–388 (2016).
177. Baron, M. *et al.* Loss-of-function mutations in MRAP2 are pathogenic in hyperphagic obesity with hyperglycemia and hypertension. *Nat. Med.* **25**, 1733–1738 (2019).
178. Novoselova, T. V. *et al.* Loss of Mrap2 is associated with Sim1 deficiency and increased circulating cholesterol. *J. Endocrinol.* **230**, 13–26 (2016).

179. Sebag, J. A. & Hinkle, P. M. Regulation of G protein-coupled receptor signaling: specific dominant-negative effects of melanocortin 2 receptor accessory protein 2. *Sci Signal* **3**, ra28 (2010).
180. Delling, M., DeCaen, P. G., Doerner, J. F. & Febvay, S. Primary cilia are specialized calcium signaling organelles. *26* (2014).
181. Handel, M. *et al.* Selective targeting of somatostatin receptor 3 to neuronal cilia. *Neuroscience* **89**, 909–26 (1999).
182. Berbari, N. F., O'Connor, A. K., Haycraft, C. J. & Yoder, B. K. The primary cilium as a complex signaling center. *Curr. Biol.* **19**, R526-535 (2009).
183. Berbari, N. F., Johnson, A. D., Lewis, J. S., Askwith, C. C. & Mykityn, K. Identification of ciliary localization sequences within the third intracellular loop of G protein-coupled receptors. *Mol. Biol. Cell* **19**, 1540–1547 (2008).
184. Sun, X. *et al.* Tubby is required for trafficking G protein-coupled receptors to neuronal cilia. *Cilia* **1**, 21 (2012).
185. Mukhopadhyay, S. *et al.* TULP3 bridges the IFT-A complex and membrane phosphoinositides to promote trafficking of G protein-coupled receptors into primary cilia. *Genes Dev.* **24**, 2180–2193 (2010).
186. Saeed, S. *et al.* Loss-of-function mutations in ADCY3 cause monogenic severe obesity. *Nat. Genet.* **50**, 175–179 (2018).
187. Oh, E. C., Vasanth, S. & Katsanis, N. Metabolic Regulation and Energy Homeostasis through the Primary Cilium. *Cell Metabolism* **21**, 21–31 (2015).
188. Song, D. K., Choi, J. H. & Kim, M. S. Primary Cilia as a Signaling Platform for Control of Energy Metabolism. *Diabetes Metab J* **42**, 117–127 (2018).
189. Loktev, A. V. & Jackson, P. K. Neuropeptide Y family receptors traffic via the Bardet-Biedl syndrome pathway to signal in neuronal primary cilia. *Cell reports* **5**, 1316–29 (2013).
190. Omori, Y. *et al.* Identification of G Protein-Coupled Receptors (GPCRs) in Primary Cilia and Their Possible Involvement in Body Weight Control. *PLoS One* **10**, (2015).
191. Geneva, I. I., Tan, H. Y. & Calvert, P. D. Untangling ciliary access and enrichment of two rhodopsin-like receptors using quantitative fluorescence microscopy reveals cell-specific sorting pathways. *Mol Biol Cell* **28**, 554–566 (2017).
192. Omori, Y. *et al.* Identification of G Protein-Coupled Receptors (GPCRs) in Primary Cilia and Their Possible Involvement in Body Weight Control. *PLoS One* **10**, (2015).
193. Loktev, A. V. & Jackson, P. K. Neuropeptide Y family receptors traffic via the Bardet-Biedl syndrome pathway to signal in neuronal primary cilia. *Cell reports* **5**, 1316–29 (2013).
194. Guo, D.-F. *et al.* The BBSome in POMC and AgRP Neurons Is Necessary for Body Weight Regulation and Sorting of Metabolic Receptors. *Diabetes* **68**, 1591–1603 (2019).
195. Beutler, L. R. *et al.* Dynamics of gut-brain communication underlying hunger. *Neuron* **96**, 461-475.e5 (2017).
196. Aponte, Y., Atasoy, D. & Sternson, S. M. AGRP neurons are sufficient to orchestrate feeding behavior rapidly and without training. *Nat. Neurosci.* **14**, 351–355 (2011).
197. Jiang, J. Y., Falcone, J. L., Curci, S. & Hofer, A. M. Direct visualization of cAMP signaling in primary cilia reveals up-regulation of ciliary GPCR activity following Hedgehog activation. *PNAS* **116**, 12066–12071 (2019).

198. Sherpa, R. T. *et al.* Sensory primary cilium is a responsive cAMP microdomain in renal epithelia. *Sci Rep* **9**, 6523 (2019).
199. Shen, Y., Fu, W.-Y., Cheng, E. Y. L., Fu, A. K. Y. & Ip, N. Y. Melanocortin-4 Receptor Regulates Hippocampal Synaptic Plasticity through a Protein Kinase A-Dependent Mechanism. *J. Neurosci.* **33**, 464–472 (2013).
200. Liu, J. *et al.* Enhanced AMPA Receptor Trafficking Mediates the Anorexigenic Effect of Endogenous Glucagon-like Peptide-1 in the Paraventricular Hypothalamus. *Neuron* **96**, 897–909.e5 (2017).
201. Fenselau, H. *et al.* A rapidly acting glutamatergic ARC→PVH satiety circuit postsynaptically regulated by alpha-MSH. *Nature neuroscience* **20**, 42–51 (2017).
202. Grippo, R. M. *et al.* Dopamine Signaling in the Suprachiasmatic Nucleus Enables Weight Gain Associated with Hedonic Feeding. *Curr. Biol.* **30**, 196–208.e8 (2020).
203. Domire, J. *et al.* Dopamine Receptor 1 Localizes to Neuronal Cilia in a Dynamic Process that Requires the Bardet-Biedl Syndrome Proteins. *Cellular and molecular life sciences : CMLS* **68**, 2951–60 (2010).
204. Farooqi, I. S. *et al.* Effects of recombinant leptin therapy in a child with congenital leptin deficiency. *N. Engl. J. Med.* **341**, 879–884 (1999).
205. Paz-Filho, G., Mastronardi, C., Delibasi, T., Wong, M.-L. & Licinio, J. Congenital leptin deficiency: diagnosis and effects of leptin replacement therapy. *Arq Bras Endocrinol Metabol* **54**, 690–697 (2010).
206. Sáinz, N., Barrenetxe, J., Moreno-Aliaga, M. J. & Martínez, J. A. Leptin resistance and diet-induced obesity: central and peripheral actions of leptin. *Metab. Clin. Exp.* **64**, 35–46 (2015).
207. Paz-Filho, G., Mastronardi, C. A. & Licinio, J. Leptin treatment: facts and expectations. *Metab. Clin. Exp.* **64**, 146–156 (2015).
208. Kühnen, P. *et al.* Proopiomelanocortin Deficiency Treated with a Melanocortin-4 Receptor Agonist. *N. Engl. J. Med.* **375**, 240–246 (2016).
209. Clément, K. *et al.* MC4R agonism promotes durable weight loss in patients with leptin receptor deficiency. *Nature Medicine* **24**, 551–555 (2018).
210. Collet, T.-H. *et al.* Evaluation of a melanocortin-4 receptor (MC4R) agonist (Setmelanotide) in MC4R deficiency. *Mol Metab* **6**, 1321–1329 (2017).
211. Stephenson, E., McAllan, L., Stayton, A. & Han, J. *MON-LB019 Setmelanotide (RM-493) Reduces Food Intake and Rapidly Induces Weight Loss in a Mouse Model of Alström Syndrome.* *Journal of the Endocrine Society* vol. 3 (2019).
212. Setmelanotide Phase 2 Treatment Trial in Patients With Rare Genetic Disorders of Obesity - Full Text View - ClinicalTrials.gov. <https://clinicaltrials.gov/ct2/show/NCT03013543>.
213. Sjöström, L. *et al.* Lifestyle, diabetes, and cardiovascular risk factors 10 years after bariatric surgery. *N. Engl. J. Med.* **351**, 2683–2693 (2004).
214. Aslan, I. R. *et al.* Weight loss after Roux-en-Y gastric bypass in obese patients heterozygous for MC4R mutations. *Obes Surg* **21**, 930–934 (2011).
215. Hatoum, I. J. *et al.* Melanocortin-4 receptor signaling is required for weight loss after gastric bypass surgery. *J. Clin. Endocrinol. Metab.* **97**, E1023–1031 (2012).
216. Valette, M. *et al.* Melanocortin-4 receptor mutations and polymorphisms do not affect weight loss after bariatric surgery. *PLoS ONE* **7**, e48221 (2012).

217. Aslan, I. R. *et al.* Bariatric surgery in a patient with complete MC4R deficiency. *Int J Obes (Lond)* **35**, 457–461 (2011).
218. Zechner, J. F. *et al.* Weight-Independent Effects of Roux-en-Y Gastric Bypass on Glucose Homeostasis via Melanocortin-4 Receptors in Mice and Humans. *Gastroenterology* **144**, (2013).
219. Daskalakis, M., Till, H., Kiess, W. & Weiner, R. A. Roux-en-Y gastric bypass in an adolescent patient with Bardet-Biedl syndrome, a monogenic obesity disorder. *Obes Surg* **20**, 121–125 (2010).
220. Boscolo, M., Féry, F. & Cnop, M. Beneficial Outcomes of Sleeve Gastrectomy in a Morbidly Obese Patient With Bardet-Biedl Syndrome. *J Endocr Soc* **1**, 317–322 (2017).